ABSTRACT

Shedd, Justin M. - Remote Sensing Procedures to Update Forested Geospatial Datasets after a Landscape Altering Event

The creation of accurate geospatial datasets like vegetation and fire fuel loads is a time consuming effort and these datasets are routinely used by resource managers. Therefore the accuracy of these datasets is vital. Vegetation and fire fuel load datasets often represent a dynamic landscape and landscape altering events such as a wildland fire or a hurricane can drastically change that landscape. The goal of this research is to investigate the use of automated change detection techniques that can not only indicate areas of change but also quantify the magnitude of change that occurred as well.

Hurricane Isabel did extensive damage to the forest landscapes of central Virginia in September of 2003, specifically Petersburg National Battlefield. The Rocky Top Fire occurred in July of 2002 in Shenandoah National Park, resulting in a mosaic pattern of burns, covering roughly 1500 acres.

The objective of this research was to test the use of remote sensing procedures to update vegetation and fire fuel load spatial datasets. First, using digital orthorectified photomosaics, the automated feature extraction technique Visual Learning System's Feature Analyst, was employed to delineate forest damage following Hurricane Isabel. Second, the satellite based remote sensing technique Normalized Burn Ratio, was utilized to delineate and quantify burn severity on vegetation after the Rocky Top Fire. A third objective was to estimate fire behavior differences between the existing pre-event and the remotely sensed

post-event fuel load datasets using the FARSITE model, thereby cataloging the potential need for vegetation and fuel load updates.

The results of this research show that, 1) VLS Feature Analyst is an excellent indicator of downed woody debris, 2) the Normalized Burn Ratio is the best technique available for indicating and quantifying the effects of a wildland fire on the landscape, 3) changes in assigned Fuel Models, especially in the Logging Slash group, affect FARSITE outcomes, and 4) Fuel Models should be assigned based on expected fire behavior, not on the total fuel loading.

Remote Sensing Procedures to Update Forested Geospatial Datasets after a Landscape Altering Event

by

Justin McEachern Shedd

A thesis submitted to the Graduate Faculty of

North Carolina State University

In partial fulfillment of the

Requirements for the degree of

Master of Science

In

Natural Resource

Raleigh, NC

2006

Approved by:

_____	_____
Dr. Heather Cheshire	Dr. Stacy Nelson

_____

Chair of Advisory Committee
Dr. Hugh A. Devine

DEDICATION

This work is dedicated to my parents for their expectations and my wife, Melissa, for helping me achieve them.

BIOGRAPHY

The author grew up in Virginia Beach, Virginia and is a graduate of UNC-Chapel Hill with a bachelor's degree in Geography. After graduation he worked at several National Parks across the United States; working as a seasonal park ranger for the U.S. National Park Service in Utah, Oregon, Wyoming and North Carolina, specifically at Arches, Crater Lake, and Grand Teton National Parks, and the Blue Ridge Parkway. His strong interest in natural resource issues, remote sensing and knowledge of Geographic Information Systems led him back to North Carolina State University, specifically the Center for Earth Observation. Awarded a Teaching and Research Assistantship has afforded him numerous opportunities; from the development of assignments and web-pages to the various National Park Service projects, in turn preparing him for a future GIS career.

ACKNOWLEDGMENTS

I would like to thank my committee members Dr. Hugh Devine, Dr. Heather Cheshire, and Dr. Stacy Nelson for not only helping me through my arduous journey that has culminated in my thesis, but for their dedication to teaching. Their knowledge and personal interest has been evident in the several classes I have taken. I would like to extend a thank you to several former and current employees of the Center for Earth Observation: Linda Babcock, Kris Callahan, Beth Eastman, Bill Millinor, and Bill Slocumb as well as several students; specifically Barry Hester, Dr. Frank Koch and believe it or not Tom Colson.

Furthermore, thank you Melissa Foder and especially KellyAnn Gorman of Shenandoah National Park, as you were an excellent source of fire-related information and insight. Thank you Tim Blumenschine and Larry Newkirk of Petersburg National Battlefield for answering all my questions and being my tour guide.

To my field crew: Kris, Millinor and Jill Stephens, without you I'd still be counting and identifying twigs and Dan Hurlbert, for letting me use your house, it helped immensely – Thank You.

Finally, thank you mom and dad, and Melissa for your encouragement and help that was there 24/7.

TABLE OF CONTENTS

LIST OF FIGURES

LIST OF TABLES

1 Introduction:

Historically, wildland fire has played a significant role in the Eastern United States. Native Americans (prior to 1600s) are believed to have burned grasslands and forests to encourage wild game and desired crops (Frost 1998). Likewise, early European settlers (1800s) actively burned to clear land for crops and livestock (Pyne 1982). More recently, after decades of successful suppression, wildland fires nationally have been reduced in frequency but have increased in severity and size (National Interagency Fire Center Website, http://www.nifc.gov). In addition, as described by Cohen and Sutherland (1997), residential and business development has been increasing in areas adjacent to forested regions, giving rise to considerable threats to both lives and property in the Wildland Urban Interface (WUI). The WUI creates an environment in which a fire can spread easily between vegetation fuels and structures. The build-up of forest fuel loads, from a lack of wildland fire, coupled with the encroachment of the WUI has led to more costly and deadly fires.

National Park Service fire management plans, call for the pre-suppression management of forest fuels (http://www.nps.gov/fire/fire/fir_wildland.html). Proper management (pre-suppression and suppression) of forest fuels requires explicit knowledge about their type, continuity, and spatial distribution. Geospatial datasets, specifically vegetation and fuel loads, enable land management officers to plan and implement various tactics to reduce the overall fuel load as well as allowing for the allocation of vital resources in the event of a wildland fire.

While the actual tools for fighting wildland fire have not changed, the emergence of Geographic Information Systems (GIS) has equipped fire fighters with better

knowledge of the situation they will be encountering. However, a GIS is useful only with accurate data. Forest fuels do not cause a fire to start; they do however have dramatic effects on the characteristics of a fire. Fuels are dynamic, always in a state of flux, due to influences of moisture and rates of decay, as well as changes in fuel loading and arrangement (Pyne 1996). Therefore, the accuracy of the geospatial datasets that describe these fuels is vital and the need to update them, especially after a landscape altering event such as a hurricane or a wildland fire, is imperative.

Landscape altering events generally only affect portions of a landscape. The goal of change detection is to delineate and quantify only those areas that have undergone change. Examples of these types of events include burned and unburned areas after a wildland fire (Kushla and Ripple, 1998) and canopy gaps that occur after an ice storm (Jackson et al., 2000). Numerous change detection techniques exist to delineate these changes (Lu et al., 2004). Choosing the appropriate technique depends on the type of data available and the land manager's objectives (Bobbe et al., 2001). Only after areas undergoing change have been delineated and quantified can the resulting classification be used to update the vegetation and fuel load spatial datasets. These updated geospatial datasets will ensure that land management officers can make informed decisions with the best available data.

2 Literature Review:

The following literature review examines various aspects of updating geospatial datasets after a landscape-altering event has occurred. Forest fuels and their importance in the ecosystem and on wildland fire are discussed, along with various methods of measuring and mapping fuel loads. Studies of mapped wind-induced damage occurring in forested landscapes are also reviewed. In addition, automated feature extraction and pixel based classification methods and studies utilizing various remote sensing data transformation methods to record fuel load and vegetation change after a wildland fire are compared.

2.1 Forest Fuels

2.1.1 Fuel Description

Fuels are the organic matter (leaves, twigs, needles, bark, cones, etc.) available for fire ignition and combustion. Fuel types and amounts play an important role in the ignition, rate of spread, and severity associated with wildland fires (Brown 1974, Pyne 1996, and Anderson 1982). Fuel types are defined by physical characteristics, such as loading, size, and bulk density of the live and dead biomass that contribute to the spread and intensity of a wildland fire. Fuel loading is defined as the amount of dead and alive fuel present expressed quantitatively in terms of weight of fuel per unit area (National Interagency Fire Center website, http://www.nifc.org). Fuels are also characterized by their location within a wildland setting, generally referred to as fuelbed or fuel complex. Fuelbeds are characterized into three layers: ground fuels (decomposing vegetation), surface fuels (live and dead vegetation above the duff but below canopy trees), and canopy fuels (large trees and shrubs comprising the forest canopy). Dead fuels are

further divided into several categories: fine woody debris (sticks less than 3 inches in diameter), coarse woody debris (sticks greater than 3 inches in diameter), duff (layer of distinguishable organic matter on top of soil), and litter (loose leaves, twigs and pine cones on top of duff). Live fuels consist of biomass such as grasses, shrubs, saplings and trees.

Fuels are also described as hour fuels, e.g., 1-, 10-, 100-, and 1000-hour fuels. The moisture content of a fuel is regulated by environmental conditions such as air temperature, humidity, and windspeed (Burgan and Rothermel, 1986). The hour classification represents the time required for a fuel's moisture content to reach equilibrium (with current atmospheric conditions) and is determined by the fuel's diameter. 1-Hour fuels measure less than 0.25 inches in diameter, 10-Hour Fuels are 0.25 to 1 inch in diameter, 100-Hour fuels are 1 to 3 inches in diameter and 1000-Hour fuels account for any downed woody debris over 3 inches in diameter (Burgan and Rothermel, 1986, Brown 1974, and Anderson 1982).

Of the fuel types mentioned above, 1000-Hour fuel or coarse woody debris (CWD) is most relevant to this study, as CWD increases the "resistance-to-control" factor, making it harder for hand crews and equipment to reach and combat a wildfire (Brown and Davis 1973). Brown et al. (2003) outlined the important dynamics of increases in CWD in an area. CWD is vital to all aspects of an ecosystem: wildlife, terrestrial and aquatic, soil development and regeneration. CWD has little influence on the ignitability and spread of a surface fire, but contributes to the development of more severe fires. Partially decayed CWD, coupled with high winds, can result in an increased risk of fire spotting e.g., where the fire front is advanced under windy conditions ahead of

the main fire. Identifying and mapping areas with an abundance of CWD is important because it enables land managers to quickly access and mitigate potentially high fire risk areas. Therefore, the existence of an accurate spatial data layer representing fuel loads is one of the most important pieces of information utilized by a land manager.

2.1.2 Fuel Mapping

Early fuel mapping focus was on the rate of spread of a fire versus the initial attack response to the fire, with other projects focusing on how difficult a fire would be to suppress (Sandberg et al., 2001). Both of these approaches had little to do with characterizing the actual fuel type or load, but instead focused on mapping the fire's threat (to an area) or time till complete suppression. Early wildland fire research focused on fire fighter movement (personnel and equipment) and their ability to suppress the advancing front of a fire. As wildland fire research increased, knowledge of fuel characteristics and behavior has increased, enabling the creation of maps indicting the different forest fuels.

Fuel maps are vital to fire management at various spatial scales. Coarse-scaled fuel maps relate to a variety of themes, such as assessing the national fire danger level and national ecosystem health assessments. For example, the US Forest Service completed a coarse scale wildland fire map of the conterminous US, by overlaying several spatial data layers (e.g. vegetation, soil, aspect, parcel ownership, watersheds, elevation) to determine an area's 'rate of departure' from its historic natural fire regime. This dataset was then used by regional land managers to allocate appropriate funding to different areas. The resolution of this project was one kilometer (Schmidt et al., 2002).

Regional or state level fuel maps allow researchers and planners to focus their efforts on reducing threats to homes in the Wildland Urban Interface. For example, Colorado State Forest Service, in their Wildland Urban Interface Hazard – Risk Assessment Project, created maps to indicate hazards determined by overlaying natural resource (slope, fuels, aspect, etc.) and infrastructure (roads, population, homes, etc.) data layers (http://www.colostate.edu/Depts/CSFS/). The state of California's Fire and Resource Protection Division of the Forestry and Fire Protection Department had a similar project that involved overlaying a weighted fuels data layer and other environmental data layers to construct an at-risk data layer (http://frap.cdf.ca.gov/projects/wui/). Both of these projects had a spatial resolution of one mile, designed for fire hazard comparisons between counties and areas of the state, not to determine wildand fire threats to individual homes.

Landscape or large-scaled fuel maps enable local land managers to map fuels of locations of interest at a smaller resolution. At Yosemite National Park, researchers used Landsat satellite imagery to delineate different types of forest fuels to give park fire management personnel a valuable tool for combating wildland fires (Van Wagtendonk and Root, 2000).

Fuel mapping techniques are as varied as well, but four main approaches dominate: field reconnaissance, direct mapping, biophysical modeling, and indirect mapping (Keane, et al., 2001). Field reconnaissance requires numerous field measurements and is the most accurate but time consuming technique. However, with increased costs and extensive amount of time needed, coupled with the availability of

remotely sensed data, field reconnaissance is not used often today, but it was essential to early fuel mapping projects.

Direct mapping refers to the mapping of fuels using remotely sensed data, such as satellite imagery or aerial photography. Predominantly utilized in national and regional scaled fuel mapping projects, direct mapping projects utilize Leaf Area Index (LAI) (Jordan, 1969) or the Normalized Differenced Vegetation Index (NDVI) technique (Rouse et al., 1973). LAI refers to the measuring of the visible and near infrared energy reflected by vegetation. LAI provides information on the structure of the plant canopy, as well as expressing how much surface area is covered by green foliage relative to total land surface area. NDVI is calculated from the visible and near-infrared (NIR) light reflected by vegetation.

The biophysical modeling approach uses direct and indirect environmental gradients, such as climate, topography and landuse history, to map fuels. Biophysical modeling employs ecosystem models that quantify those gradients across a particular landscape (Keane, et al., 2001). At Glacier National Park a biophysical model using different topographic and vegetation layers was used to create a fuelbed spatial dataset (Kessell, 1979). While extensive amounts of data and statistical analyses are required, the resulting classification can be updated as conditions change. However, these datasets tend to express the potential vegetation of an area, not the actual vegetation found (Keane et al, 2001).

Indirect mapping of fuels refers to the use of remotely sensed data collected for one purpose that is then used to create another closely related but different geospatial

dataset. With most satellite sensors designed to discriminate different vegetation types, this approach is popular because of its accuracy and "two-for-one" mapping approach. Two datasets (vegetation and fuels) are created from a single purchase of remotely sensed data, making this approach cost effective and timely. This is the approach that North Carolina State University's Center for Earth Observation (NCSU-CEO) followed when creating vegetation and fuel load spatial datasets for the North East Region of the National Park Service (NPS). Following a procedure developed by Millinor (2001) vegetation datasets were delineated from aerial photomosaics. Smith (2003) developed a crosswalk that allowed for the creation of a fuel load (based on the original 13 fuel models) spatial dataset relative to the type of vegetation mapped.

2.1.3 Measuring Fuels

Just as there are several approaches to mapping fuel loads; there are several methods upon which forest fuels are actually measured or quantified. The following section will discuss methods of measuring forest fuels as well as introduce the use of fuel load models that are data inputs into fire behavior computer models that simulate fire spread.

James K. Brown (1974) created a handbook for inventorying downed woody material along two 50-foot transects. The handbook provides the user with a guideline to establish sampling plots, rules of inclusion/exclusion of woody material, necessary field equipment, and additional information to be used in calculating the amount of fuel loading. After collecting required field measurements (1-, 10-, 100- and 1000-hour fuels) the values are calculated with the results representing the amount of fuel loading for each

size class in tons per acre. The National Park Service (NPS) uses this method of data collection when monitoring vegetation and pre- and post-burn fire plots.

Qualitative fuel measures are done to record the fuel complex (arrangement and load type) of the plot; rather than a quantifiable measure of vegetation (Burgan and Rothermel 1984). Burgan and Rothermel developed an extensive list of field measurements in order to capture an accurate representation of the vegetation and fuel complex found in the plot. Information such as: grass type and height, shrub type and height, and tree type and height are collected along with other non-tallied observations based on categories (e.g. waxy or oily leaves, litter source, litter compactness, bulk density, grass type, etc.). Numerous studies have used these qualitative measurements when creating custom fuel models for use in fire behavior models.

The difficulties of fuel bed data collection led to the development of standard fuel characterizations or fire fuel models (Rothermel 1972, Albini 1976, and Scott and Burgan 2005) and guides to facilitate assigning these fuel models (Anderson 1982, Scott and Burgan 2005).

2.1.4 Fuel Models

Hal E. Anderson (1982) created a guide to assist natural resource managers in predicting fire behavior through the use of photographic illustrations. This guide was developed based on the 13 fuel models calculated by Rothermel (1972) and Albini (1976) to estimate fire behavior predictions. (Rothermel developed 11 fuel models with Albini later adding two more fuel models to represent “dormant brush” and “southern rough”, Fuel Models 6 and 7 respectfully). The 13 fire fuel models are grouped into four main

categories: Grass (Fuel Model 1, 2, and 3), Shrub (Fuel Model 4, 5, 6, and 7), Timber (Fuel Model 8, 9, and 10) and Logging Slash (Fuel Model 11, 12, and 13). Each category has different parameters (fuel particle size and load) that affect a fire's rate of spread and intensity. Furthermore, within each category fuel models have additional parameters (surface area to volume, moisture of extinction, heat content, and others) that determine the characteristics of the simulated fire. For each of the fuel models an example photograph is provided as well as a brief description of the typical parameter values.

For this research the differences in the fuel models of the Timber and Logging Slash Groups are of particular interest. Timber Group Fuel Models (8, 9, and 10) characterize slow-burning surface fires that occur in closed canopy hardwood and coniferous forests. Fuel Model 8 represents a landscape where a slow spreading, low intensity fire is found. Fuel Model 9 represents a faster spreading, low intensity surface fire. Fuel Model 10 represents a landscape with increased available fuels which creates the potential for fires of higher intensity with longer flame lengths. The Logging Slash Fuel Models (11, 12, and 13) characterize a landscape where large quantities of downed woody debris exist, including CWD. The difference between these fuel models is the fire's rate of spread. Fuel Model 11 represents a slower spreading fire affected by the lack of a continuous fuelbed. Fuel Model 12 represents a rapidly spreading and very intense fire that is often fueled by smaller woody debris and dead herbaceous matter. Fuel Model 13 represents an area completely covered by woody debris, large and small; where a fire could quickly spread and gain in intensity because of the mixture of fuels.

The 13 original fire models were inherently "western-centric" and designed for predicting spread rate and intensity of active fires at the peak of fire season, however they

were rather inaccurate for other purposes such as, prescribed fire, wildland fire use during off-peak seasons and conditions, and simulating the effects of fuel treatments on fire behavior. Joe Scott and Robert Burgan (2005) developed 49 "new" fuel models along with a guide, similar to Anderson's, to assist in assigning fuel models to landscapes. These new fuel models offer a marked improvement for fire behavior predictions outside peak fire season and in other areas of the United States other than the west.

The Fuel Characteristic Classification (FCC) system developed by the Fire and Environmental Research Applications team of the United States Department of Agriculture, Forest Service Pacific Northwest Research Team provides a more in-depth characterization of fuelbeds (http://www.fs.fed.us/pnw/fera/fccs/). The FCC system uses fuelbed descriptions or "prototypes" which are based on; the quality of the fuel present and the abundance of fuels. Additional factors affecting the fuel complex, such as: vegetation form, structure class, and agent of change (e.g. disease, insect infestation) are input parameters used to create individual prototypes. All of these factors go into calculating total fuel loading and other parameters used by fire behavior models (Harrington, 2005). Unfortunately the FCC system has not yet developed its own fire behavior model (expected completion winter 2005) and has not been incorporated into any fire behavior model in current use.

The original 13 fire fuel models will be utilized for the purposes of this research as these are the fuel models currently used by the NPS for their fire management planning.

2.1.5 Fire Behavior Models

There are several fire behavior models that rely on Rothermel's fire spread model (Rothermel 1972). One such fire behavior model is FARSITE (Fire Area Simulator). Developed by Dr. Mark Finney, FARSITE is used by many federal land management agencies including the NPS. FARSITE is often used in a decision support system allowing land managers to make informed decisions based on the best available information. As required by the NPS, each park must have a fire management plan; this plan provides specific details and operational procedures in case of a wildland forest fire. FARSITE is based on Huygen's Principle that states that rate and spread directions of the fire are based on elliptical transformations (Finney 1998, 2004). These ellipses, representing fire spread, are determined by wind speed, slope of the landscape and characteristics of the fuelbed. One of several input data layers required by FARSITE is a data layer that represents the fire fuel models. Currently the original 13 fuel models, the new 49 fuel models, and custom made fuel models can be input into FARSITE. Five spatial data layers are required by FARSITE in order to create a simulation; slope, aspect, elevation, fuel model, and canopy cover. Of those data inputs, fuel model is highly subjective, as it is determined by one or several professionals, and not necessarily by field measurements.

FARSITE will be used to validate the resulting classifications of the methodologies followed in this research because it is used by the NPS for their fire management planning.

2.2 Remote Sensing

2.2.1 Remotely Sensed Imagery

As mentioned earlier, indirect mapping using remotely sensed imagery is a cost-effective and timely approach to classifying vegetation; from which fire fuel model datasets can be created. The use of remotely sensed imagery and the various remote sensing techniques used to create geospatial datasets has increased dramatically over the recent decades (Blaschke 2000). Competition between an increasing number of government and private satellites has lead to the reduction in cost, and increase in resolution of satellite imagery. Furthermore, the reduction in production time and cost coupled with an increase in spatial resolution, has led to the dramatic increase in the use of digital aerial photography as well (McGarigle, 1997 http://www.govtech.net).

2.2.1a Satellite Imagery

Depending on the requirements and desired outputs of a project there may be several types of imagery available. The Landsat Thematic Mapper (TM) sensor despite its relatively low spatial resolution (30mx30m) collects seven bands of spectral data. Landsat TM imagery has been used in countless change detection studies in both multi-image and single image analyses (Lu 2004). With four of the seven bands recording in the infrared range, Landsat TM imagery is an excellent discriminator of vegetation (Lillesand et al., 2004).

With the deployment of satellite platforms such as Ikonos and Quickbird, very high resolution satellite imagery (sub-meter panchromatic and three meter multi-spectral resolution) is now available to decision makers in the public, academia, and private sectors. While many issues related to the delineation of features and locational

accuracies have been solved, new problems have arisen, for example, the occurrence of a mixed pixel or "mixel." A mixel denotes a pixel in which multiple classification (road, grass, forest) classes are contained. Merely increasing the spatial resolution of an image does not solve this problem; it creates new mixed pixels (Blaschke, 2000). Another issue is an inability to classify or map features easily discernable to the naked eye. The spatial resolution of aerial and satellite imagery has become so great that the importance of measuring a single pixel has given way to the power of detecting groups of pixels.

In past studies, researchers focused on pixel by pixel analysis of an image to delineate or highlight a real world feature that was large in size, such as a shoreline or land cover type (White and Asmar, 1999). With the availability of high resolution remotely sensed data not only can large features like shorelines and landcover be delineated more accurately, but smaller features like homes (Al-Khudhairy, 2005) and streams (Zhang, 2000) can be delineated. Data classification techniques utilizing high resolution imagery focus on indicating features based on spatial patterns rather than on classifying a pixel by a range of spectral values.

2.2.1b Digital Aerial Photography

Aerial photomosaics, more specifically ortho-photomosaics serve many purposes, from backgrounds when overlaying vector GIS data to a means of providing land managers with a way of delineating real-world features. Until recently the process of creating aerial photomosaics was done digitally, while the capture of the aerial photography was not. The advent of digitally acquired aerial photographs has decreased the production time and the overall cost of a project (Leberl and Gruber, 2003).

Digital photography relies on electronics rather than chemistry to capture and process images. The greatest benefit of digitally acquired aerial photographs is the quick turn around time and lower cost, all the while maintaining the overall quality of the image. Overall, the benefits (adjustable footprint of picture, immediate viewing of imagery allowing for instant quality control, simultaneously capture of true color and false color imagery, reduction in turn around time and production cost, etc.), (McGarigle, 1997 http://govtech.net) of digital aerial photography make it a valid choice of remotely sensed imagery for use in indicating areas of change.

2.3 Change Detection

In addition to the increase in available remotely sensed data like digital aerial photography and Landsat TM satellite data, the number of data enhancements or transformations used to classify these images has increased as well. Indicating features or areas of interest is important when maintaining the accuracy of spatial datasets. Automated Feature Extraction (AFE), specifically its ability to indicate areas of change by mapping real-world features like downed trees, with the resulting classifications being used to create updated geospatial datasets, will be discussed in the following section. In addition, change detection provides the foundation for a better understanding of interactions between human and natural resource processes. This is especially of interest to land managers along the Eastern US as human development encroaches on forested landscapes. Not only does human development pose an increased risk to wildland fire, but landscapes altered by wildland fire need to be monitored to ensure further environmental degradation does not occur. The following section discusses the use of

several data transformations that can not only indicate but quantify change resulting from a wildland fire.

2.3.1a Kauth Thomas Data Transformation

Wildland forest fires modify biophysical properties in vegetation and in the various soil horizons (Patterson and Yool, 1998). Remote sensing data expresses these changes in terms of brightness, greenness, and wetness; which can be detected by the Kauth-Thomas or Tasseled Cap data transformation (Jenson, 2000). Initially created utilizing the Landsat Multi-Spectral Scanner (MSS) 4 band sensor (Kauth and Thomas, 1976), Tasseled Cap was modified for Landsat TM data utilizing 6 bands of spectral data (Crist and Cicone, 1984). Tasseled Cap data transformation rotates the spectral data so that they are shown in three dimensions representing brightness, greenness and wetness. The brightness indicator is a sum of all six TM bands. Greenness contrasts the sum of the visible and NIR bands. Wetness contrasts the sum of the visible and NIR by the sum of the longer wavelength bands.

Tasseled Cap was originally designed for use in agricultural applications, but has more recently been used to detect fire-induced changes in moisture contents of soil and vegetation (Patterson and Yool, 1998). Patterson and Yool studied vegetation reduction caused by the Rattlesnake Fire in Arizona in 1994, in which Landsat MSS data was analyzed using the Tasseled Cap and Principal Components (PC) methods. While the PC and Tasseled Cap methods produced similar classifications, the Tasseled Cap's ability to discern differences in soil and vegetation moisture levels led to a more accurate classification of the fire's severity. Tasseled Cap can be used to detect a fire's severity

not upon only vegetation, but across the entire landscape. Soils are typically only blackened during cooler less intense fires, thus changing their brightness level (Pyne et al 1996). Canopy fires are typically associated with more severe burn events. With the overstory effectively removed, moisture in the form of humidity once captured by the forest canopy is no longer present. Fires of higher severity alter soil properties causing them to become water repelling (hydrophobic), causing environmental degradation in the form of mass wasting. Furthermore, in a study that mapped different levels of burn severity, the Tasseled Cap classification, when compared to the Intensity Hue Saturation (IHS) data transformation, was more accurate in its ability to detect varying levels of fire severity (Won, K. and J. Im, 2001). IHS can detect changes in brightness and greenness like Tasseled Cap but is unable to detect changes found on the wetness dimension. Instead of spectral values the IHS transformation uses the red-green-blue color composites of various band combinations to detect changes in multi-temporal analyses (Koustsias et al., 2000). Images are classified based on their intensity, i.e. brightness or dullness of a color, hue, i.e., the dominant wavelength (color) and saturation, i.e., the purity of the color.

2.3.1b Normalized Differenced Vegetation Index

Another type of change detection technique frequently used is the differencing vegetation index, commonly referred to as the Normalized Differenced Vegetation Index (NDVI). Initially developed as a vegetation discriminator, it has recently been used in various aspects of post-fire analysis (Viedma et al., 1997). NDVI is well correlated with crop biomass accumulation, leaf chlorophyll levels and LAI (Lillesand et al., 2004). LAI

is also widely used as an indicator of forest canopy structure and percent cover. NDVI compares the differences between visible reflectance values (TM Band 3) and near infrared (TM Band 4). When using NDVI as an indicator of a fire's severity, attention is paid to the reflectance values associated with physiological damage. In a healthy ecosystem NIR wavelength reflectance is high, whereas in an ecosystem under stress as after a fire, a lower NIR wavelength reflectance is to be expected (Rogan and Yool, 2001). Studies along the Mediterranean Coast of Spain have shown that using a multi-temporal NDVI image results in both a better fire perimeter detection and an accurate fire intensity classification (Viedma et al., 1997, Garcia-Haro, 2001). Vegetation indices are not without their problems, as NDVI classifications are known to become "saturated," meaning unable to discern areas of moderate to high levels of vegetation (Lillesand et al., 2004) and has been found to produce variable results dependent upon different cover types (Bonan, 1993), soil brightness and color (Rogan and Yool, 2001, Jensen 2000). Finally, there may be concerns with the output classifications indicating and categorizing surface burns that occur beneath a forest canopy (Major et al., 1990 and White et al., 1996) as the output pixel values are often saturated and do not indicate burned areas.

2.3.1c Normalized Burn Ratio

The Normalized Burn Ratio (NBR) was developed by the Northern Rocky Mountain Science Center, a research office within the United States Geological Survey (USGS). NBR is similar to NDVI, except that it accentuates the spectral response of TM bands 4 and 7. TM band 4 represents NIR and band 7 measures middle infrared wavelengths (MIR). NBR is currently one of the more widely adopted measures

(VanWagtendonk et al., 2004) of burn severity in the field of remote sensing. The ratio uses multi-temporal differencing to enhance the contrast from a pre- and post-fire scene, creating a differenced NBR (dNBR) classification. dNBR is based on the premise that post fire reflectance for NIR band 4 decreases when compared to a pre-fire scene, while the MIR band 7 (indicating dryness in soil and vegetation) increases in a post-fire image (Key and Benson, 2002). When processing the dNBR data transformation, pre- and post-Landsat imagery acquired approximately during the same time of the year, preferably in the spring, should be used for analysis. This ensures that the images being contrasted represent land cover in the same physiological state, as vegetation reflects more IR wavelengths in the fall than in the spring. This will reduce the variation seen between images not associated with the burn event.

In 2000, from May 9th to November 14th, the Outlet Fire burned 13,000 acres along the Northern Rim at the Grand Canyon National Park. Researchers compared pre- and post-fire NBR and NDVI classifications in the hopes of mapping the fire's severity upon the natural environment (Bertolette and Spotskey, 2001). The dNBR image was created from Landsat 7 imagery, while the NDVI image was created using Spot 4 imagery. Both images expressed wide ranges of spectral vales, but the NBR image provided the most discriminating and sensitive classification of burn severity despite a coarser resolution.

In 2001, the dNBR technique was used to classify burn intensities of the Hoover fire, a 7000 acre wildland fire occurring in Yosemite National Park. The output classification using Landsat 7 Enhanced Thematic Mapper (ETM) imagery was comparable to a dNBR classification calculated from bands 47 and 210 of the AVIRIS

hyperspectral sensor. Despite a coarser spectral resolution when compared to the AVIRIS sensor, these results validated the use of Landsat Bands 4 and 7 to quantify a fire's severity, as the Landsat imagery provided more accurate results than the AVIRIS imagery when ground-truthed (Van Wagtendonk et al., 2004).

NBR's creators (Key and Benson, 1999) consider the pre- and post-fire image differences to indicate and enable the quantification of change caused by a fire, i.e., the levels of burn severity, not burn intensity. A fire may be of low intensity (flame height, heat, etc.), but of high severity because the fire consumes what little vegetation that did exist. This distinction is stressed to clearly differentiate between fire intensity and fire (or burn) severity (Parson, 2002). In addition to clarifying the type of indicator the dNBR transformation is, the authors developed a ground truthing technique called the Composite Burn Index (CBI). The collection of CBI field data in "initial" and "extended assessments" (Key and Benson, 2004) allowed researchers to adjust their early classification system based on real fire-induced landscapes, leading to their guidelines followed today (Appendix A). The CBI will be discussed in more detail in section 2.4.2c.

2.3.2 Automated Feature Extraction

As the capability, availability and resolution of remotely sensed data has increased over the decades, image processing concepts still relied heavily on 1970's methods, dominated by the per-pixel classification methods (Blaschke, 2001). While past classification methods focused on per-pixel (spectral) methods of classifying data, current trends are towards object or contextual-based classification, as evident in the breadth of

studies in which Automated Feature Extraction (AFE) is being utilized, e.g., from detecting structurally damaged homes (Al-Khudhairy, 2005) to detecting ships (Willhauck, 2005). Specifically in the realm of natural resources the power and capability of AFE techniques are being realized in research endeavors such as stream mapping (Dillabaugh, 2002) and mapping windthrown damage to forests (Jackson, 2000, Frannon, 2001 and Schwarz, 2003).

Many forms of AFE (image segmentation, object-oriented, contextual) exist (Blaschke, 2000) from edge-based systems to region-based systems, all have the same basic idea; neighboring pixels are related to each other and can therefore be clustered together. Until 2000, most image segmentation involved singular research efforts, manipulated to fit the local area or circumstance. There were no computer software packages with the ability of image segmentation available to the general public. In 2000, Definiens of Munich, Germany, launched eCognition, packaging a robust AFE tool that was transportable to all environments. Then Visual Learning System of Missoula, Montana, introduced Feature Analyst in 2001, packaging their version of an AFE in a graphical user interface. The use and successes of both software products are described on their respected websites (http://www.definiens-imaging.com/ and http://www.featureanalyst.com/). In the following sections natural resource projects utilizing these software programs will be discussed.

2.3.2a eCognition

eCognotion approaches AFE using image segmentation, where an image is broken or segmented into units of similar spectral and spatial patterns. This process is

repeated at several scales. Beginning with a single pixel, groups of homogeneous pixels are merged together forming a series of segmented areas across an entire image. This process is repeated at a coarser scale to group the least dissimilar segments together.

eCognition was used in a study (Laliberte, 2004) to map shrub encroachment in southern New Mexico. Using 11 aerial photographs taken between 1937 and 1996 along with a Quickbird satellite image acquired in 2003, shrub encroachment resulting from years of fire suppression was mapped. Utilizing the fractal net evolution approach employed by eCognition, the images were segmented based on three attributes; shape, color, and scale. User defined parameters determined the break points that put pixels in one or another region. Beginning with a single pixel a region continues to grow, acquiring new pixels until the smallest growth does not meet the threshold defined by the user. Researchers were not only able to track the increase in shrub growth over time, but could determine in which time period shrub growth increased the most.

2.3.2b VLS Feature Analyst

Feature Analyst approaches AFE from a "machine learning" or object-oriented method of feature extraction. To map individual features, Feature Analyst utilizes the texture of a feature as well as its spectral response. To begin the process a user identifies or trains the software to look for a particular object of interest (e.g., airplanes, individual tree crowns, etc.). After creating an initial layer of "training sites" for the features of interest, Feature Analyst analyzes an image's pixels based on their proximity to other pixels. Determined by the user, a pattern recognizer is used to analyze the input image, looking for groups of pixels similar to those of the training sites. After the first iteration

incorrect and correct areas are identified and the process is run again. This hierarchal process can be repeated until desirable results are met as defined by the user.

The United States Forest Service utilized Feature Analyst in a recent mapping effort (Vanderzanden, 2002). Using Quickbird and Landsat TM remotely sensed data, 65 square kilometers of the Tongass National Forest, in Alaska, were delineated into non-forested, deciduous, mixed, and coniferous forest classes, with forest classes further segmented based on their crown closure and tree size. Three classification methodologies were explored; Feature Analyst using bands 2, 3, and 4 of a Quickbird image, a minimum variance texture filter (Woodcock and Ryherd, 1996) using Landsat TM imagery, and a supervised classification utilizing Landsat TM bands 3, 4, 5, 7, and a ratio of band 3 divided by band 4.

To start the Feature Analyst data extraction, training sites were drawn around areas representing the 11 desired classes. Initially a trial and error system allowed the researchers to determine which contextual classifier used provided the best results. After the initial acceptable run of Feature Analyst, results were modified with areas identified as incorrect and correct. This hierarchal approach allowed the classifier to learn and adjust with each iteration. The process was continued until sufficient results were obtained. An accuracy assessment of the three classifications showed that Feature Analyst out performed the other classification methodologies attempted, with 100% accuracy reported when delineating the image into the four basic classes, non-forested, deciduous, coniferous, and mixed (Vanderzanden, 2002).

2.4 Agents of Change

2.4.1a Hurricanes and Wind Damage upon Forests

The landfall of a hurricane is a relatively quick and destructive event that frequently occurs along the East and Gulf Coasts of the United States. Once inland, hurricanes begin to weaken and slow in both storm speed and strength, therefore inland areas are not only battered by strong winds but intense bands of rain for prolonged periods of time. In the past hundred years over 120 hurricanes struck between Texas and Virginia (Wade et al., 1993) and there have been numerous studies focused on the effects on vegetation after large scale wind events such as hurricanes have occurred (Brokaw, 1991, Foster and Boose, 1992, Merrens and Peart, 1992).

The wind damage suffered by deciduous and coniferous forests varies with geographic factors such as topography, soil depth and properties, and hurricane characteristics such as wind velocity, storm speed and rainfall amount. The canopy gaps created as a result of the wind damage encourage forest succession, as shade intolerant species are encouraged to grow. Forest succession or regeneration is typically driven by a single-tree death or a blow-down caused canopy gap, but large multiple-tree gaps spread over a wide geographic area do occur. These latter landscape altering events can lead to dramatic effects over a larger spatio-temporal scale (Greenberg and McNab, 1997).

Wind damage to a forest may result in the defoliation of branches, crown damage, snapping of boles, complete toppling of trees or tree-fall pits and mounds. The type of damage inflicted upon the forest has a significant impact upon forest regeneration. Depending upon the type of damage, woody debris may encourage or hinder vegetation growth, as indicated in research on forest damage created by Hurricane Opal in the Bent

Creek Experimental Forest, outside Asheville, NC, in October of 1995 (Berg and Van Lear, 2004). Bole and limb damage had little influence upon vegetation succession, except in areas directly below where they (bole and limb) came to rest; whereas tree crown debris killed young shrubs and trees by either direct impact or "smothering". Smothering refers to an area on the ground where a majority of the ground is covered by tree canopy debris. Furthermore, in areas of tree crown debris, sun thriving seedlings, tree saplings, and grasses were discouraged due to the elimination of growing space, ultimately leading to a larger canopy gap that will shape forest succession for years to come.

2.4.1b Mapping Wind Induced Forest Damage

Mapping wind induced forest damage through traditional manual air photo interpretation methods is a time consuming and expensive venture, as aerial and field reconnaissance are needed to map the extent of the damage. The use of remotely sensed data, saving both time and money, has facilitated the mapping of damaged areas. The following section gives examples of remote sensing projects that mapped windthrown forest damage.

Fransson et al., (2001) utilized CARABAS-II VHF SAR imagery to map woody debris resulting from a series of storms in Sweden in December of 1999. The CARABAS-II VHF SAR system utilizes a radar sensor to transmit pulses of electromagnetic waves. Recording backscatter from the radar, an after storm image is created to indicate areas of downed trees. With a spatial resolution of 2.5 meters,

researchers were able to rapidly map the areas of blowdown, indicated by high backscatter, from undamaged areas indicated by low backscatter.

Jackson et al., (2000) utilized an Aerial Thematic Mapper (ATM) to record windthrown gaps of the Cwm Berwyn Forest in central Wales. For this project the remotely sensed data was acquired in April of 1994, using an 11-waveband Daedalus AADS1268 ATM scanner. Spectral resolution of the 11 wavebands allowed for the collection of data from the visible to the thermal infrared portions of the electromagnetic spectrum. A feature selection of the 11 bands allowed less valuable data to be removed resulting in only 4 bands being further analyzed: band 3 (visible green), 5 (visible red), 7 (near-infrared) and 11 (thermal infrared). Using a maximum-likelihood classification algorithm, these four bands were used to create a land cover map. For an accuracy assessment of the classification, true color aerial photography at 1:10,000 scale was acquired and hand delineated for comparison. Of the 54 windthrown gaps identified manually, the ATM scanner indicated 52 of them, a 96.3 percent accuracy rate.

Schwarz et al., (2003) compared several different types of remotely sensed data to detect windthrown forest damage occurring in Switzerland in December of 1999. Different classification methods, per-pixel and object based, were compared to determine which was better suited for classifying windthrown damage. A true color aerial photograph with a spatial resolution of .15 meters was used as the reference image. The reference image was manually delineated with over 500 individual areas (0.2 hectares minimum mapping unit) indicated as windthrown areas. For the per-pixel classification comparison, a Landsat 7 ETM, Spot-4, and Ikonos image were compared. Using a parallelpiped algorithm, a supervised classification of the images resulted in an 86, 90,

and 88 percent accuracy, respectively, when compared to the manual classification. For the object-based classification method, the software package eCognition was utilized. After masking agricultural fields and urban areas, three classes were established, windthrown, other vegetation, and forest. Only Spot-4 and Ikonos imagery were compared and, despite having a coarser resolution, the Spot-4 imagery accurately classified more windthrown areas than the Ikonos imagery. The object-based classification method was slightly more accurate (92 and 90%) when compared to the per-pixel classification. Not withstanding the length of time it took to complete, the manual interpretation of the Ikonos imagery produced the best results of all the methods compared.

2.4.1c Effects of Hurricanes

Areas of extensive forest damage are subject to abnormally hot and devastating wildfires. Such was the case in the Yucatan Peninsula of Mexico, where Hurricane Gilbert made landfall in September of 1988, causing heavy forest damage to the area. Measurable increases in coarse woody debris along with fine woody debris and leaf litter were recorded. This increase in dead woody debris coupled with an increase in exposure caused by the defoliation of trees, lead to an extremely dry and volatile fuelbed. The following June – August 1989, dry season, saw numerous wildfires in the Yucatan Peninsula. These wildfires burned more intensely than usual, as almost all surface litter (fine woody debris and leaves), coarse woody debris and the duff layer of the soil were consumed (Whigham, 1991).

A similar situation occurred in the Francis Marion National Forest in South Carolina, after Hurricane Hugo came ashore and moved across the state. Approximately 75% of Francis Marion National Forest suffered damage. Overnight the potential for a destructive wildfire due to the dramatic increase in downed woody debris arose. Assessing and mapping the forest damaged areas were done using a video camera. Still images from this video were then geo-referenced using available GIS data to determine the extent and severity of damage (Jacobs, 1994). While no significant fire event occurred, millions of dollars and thousands of man hours were devoted to the removal of woody debris and the creation of firebreaks (Saveland and Wade, 1991).

2.4.2 Wildland Fire

The occurrence of wildland fire has caused many plant adaptations and is an integral part in forming many vegetation communities across the United States (Frost, 1998). From California, to Florida to Maine, wildland fires have affected, detrimentally and beneficially, the natural and human environments. Currently much research is being placed on understanding and mitigating the effects of wildland fire so it can be embraced as a safe and effective land management tool.

2.4.2a Wildland Fire Effects and the WUI

The study of fire ecology focuses on many facets of fire; from understanding the role of fire to vegetation adaptations (Pyne et al., 1996). The effects of a wildland fire can be both detrimental and beneficial with a fine line separating the difference. After decades of fire suppression, land managers are accepting fire as a necessity in order to

maintain a healthy forest ecosystem. Beneficial wildland fires; remove excess dead and alive vegetation, return nutrients to the soil, and encourage new vegetation life and growth, while detrimental wildland fires; alter soil properties leading to further environmental degradation, cause the consumption of all vegetative matter, and coupled with recent human development, lead to more costly and deadly fires.

In 1985, 1,400 homes nation-wide were destroyed in wildland fires. Furthermore, in 1991, the East Bay Hills fire in Oakland CA, destroyed over 3,000 homes and killed 25 people (Communicator's Guide Wildland Fire, FIREWISE Program, http://www.nifc.gov/preved/comm_guide/wildfire/TOC.html). While this is an extreme example, it shows that a wildland fire in the Wildland Urban Interface (WUI) can have deadly and costly consequences. WUI refers to residential areas surrounded or adjacent to wildland areas (Cohen and Saveland, 1997). Fighting fires located in the WUI is dangerous as wildland fire fighters are not accustomed to fighting structural fires and their inherent dangers.

2.4.2b Similar Studies

Beginning in 2000, a joint NPS-USGS project combined efforts of past fire science research efforts into current operational procedures for mitigating long term effects of wildland fire (National Burn Severity Mapping Website, http://burnseverity.cr.usgs.gov/fire_main.asp). By combining Landsat TM and ETM imagery, local knowledge and field sampling abilities, and the fire-effects research of the USGS, a methodology has been developed mapping a wildland fires severity upon vegetation. Because of Landsat's coarse spatial resolution, initially only large Western

US wildland fires affecting over 5000 acres were mapped. However, wildland fires occurring in both the Eastern US and those over 1000 acres are now being mapped.

To begin the documented methodology, a pre-fire and a post-fire Landsat image are acquired. Then following the NBR procedure Bands 4 and 7 of each image are contrasted with the pre-image subtracted from the post-image. The derived data is then quantified (Appendix A), indicating the fire's severity upon the vegetation. This dataset is enhanced through field measurements using the Composite Burn Index field measurement protocol. This automated/field process allows for the creation of a scalable and consistent measure of fire severity upon a landscape.

2.4.2c Use of Composite Burn Index

To validate the classifications of dNBR a field measurement called the Composite Burn Index (CBI) was developed by Key and Benson (2004). The CBI plots attempt to summarize the general fire effects upon an area recorded by the Landsat TM sensor. CBI plots are 98 feet or 30 meters in length, with field data collected subjectively by visual estimation (Appendix B). This approximation over a large area mimics the coarse spatial resolution of the Landsat TM sensor. Ground sampling is limited to areas (3x3 pixel window) showing minimal variation in dNBR value. Visual estimations are made much like Burgan and Rothermel Estimations, where a percentage of coverage for five strata (substrate, herbaceous/low shrub, tall shrub/tree saplings, intermediate trees and big trees) of the plot and other vegetation elements are estimated. Scores representing fire effects are tallied between 0.0 (little effects from a fire) to 3.0 (high effects of a fire). Areas exhibiting no burn are not tallied. The use of CBI is for calibrating the

classifications of dNBR, predicting post burn fuel loading and indicating areas of further environmental degradation from erosion.

The preceding literature review focuses on past research utilizing various remote sensing techniques in the creation of fuel load datasets. No studies were found that focus on updating existing vegetation and fire fuel load spatial datasets after a landscape altering event has occurred. Specifically no documentation was found that reports on the use of an automated feature extraction technique to map areas of forest damage with the resulting classification being directly used to update existing spatial datasets. The Normalized Burn Ratio is currently used in the National Burn Severity Mapping Program, but little research was found relating its use in updating fuel load datasets. My research focuses on the use of these techniques in mapping fuel loads. Also this research will investigate the impact of updated fuel model datasets on fire behavior as predicted by the FARSITE model.

3 Objectives

The objective of this study is to test the use of remote sensing procedures to update vegetation and fire fuel load spatial datasets. Two sub-objectives are used to perform these updates. First, using digital orthorectified photomosaics, the automated feature extraction technique Visual Learning System's Feature Analyst, is employed to delineate forest damage following a hurricane. Second, the satellite based remote sensing technique Normalized Burn Ratio, is utilized to delineate and quantify burn severity on vegetation. A third sub objective is to estimate fire behavior differences between the existing pre-event and the remotely sensed post-event fuel load datasets using the FARSITE model.

4 Study Areas

Two study sites were selected in order to test the remote sensing procedures outlined; automated feature extraction will be used on the forest damage incurred at Petersburg National Battlefield, while the NBR technique will be used to delineate the Rocky Top Fire that occurred at Shenandoah National Park.

4.1 Petersburg National Battlefield

Petersburg National Battlefield (PETE) lies partially within the Petersburg, VA city limits and is 25 miles south of Richmond, VA (Figure 1). Because of its historical significance, PETE was established as a National Military Park on July 3, 1926, and later (1962) designated a National Battlefield. PETE is not a contiguous park, but consists of four areas: Five Forks, City Point, Eastern Front and the Western Front.

Most of PETE's boundary was established nearly 80 years ago, and as a result, its vegetation makeup reflects its past land use history. Current vegetation in PETE consists of managed grasslands, deciduous forests, coniferous forests, mixed hardwood/pine forests, and abandoned pine plantations (Park website, http://www.nps.gov/pete). PETE's forest makeup consists of various hardwood species such as; American Beech (*Fagus Grandifolia*), Northern Red Oak, (*Quercus Rubra*), Yellow Poplar (*Liriodendron Tulipifera*), Red maple (*Acer Rubrum*), and Yellow Birch (*Betula Alleghaniensis*). Pine species include Loblolly (*Pinus Taeda*) and Virginia Pine (*Pinus Virginiana*). There is little under-story, shrub or grass, present, possibly because of the fire suppression that has occurred over the last 150 years. Naturally occurring fire was infrequent but Native American burning most likely occurred (Frost, 1998). Wind events (hurricanes, tornados,

and thunderstorm-caused) and ice storms account for the disturbance agents (NatureServe, 2005). Recently the Southern Pine Beetle has caused extensive damage to the park's naturally occurring pine.

Hurricane Isabel passed over PETE during the early morning hours of September 19, 2003. The Eastern Front section of PETE, suffered the most damage, but several Western Front sections also suffered damage. The Five Forks and City Point regions of PETE suffered minimal damage and are not covered in this research project.

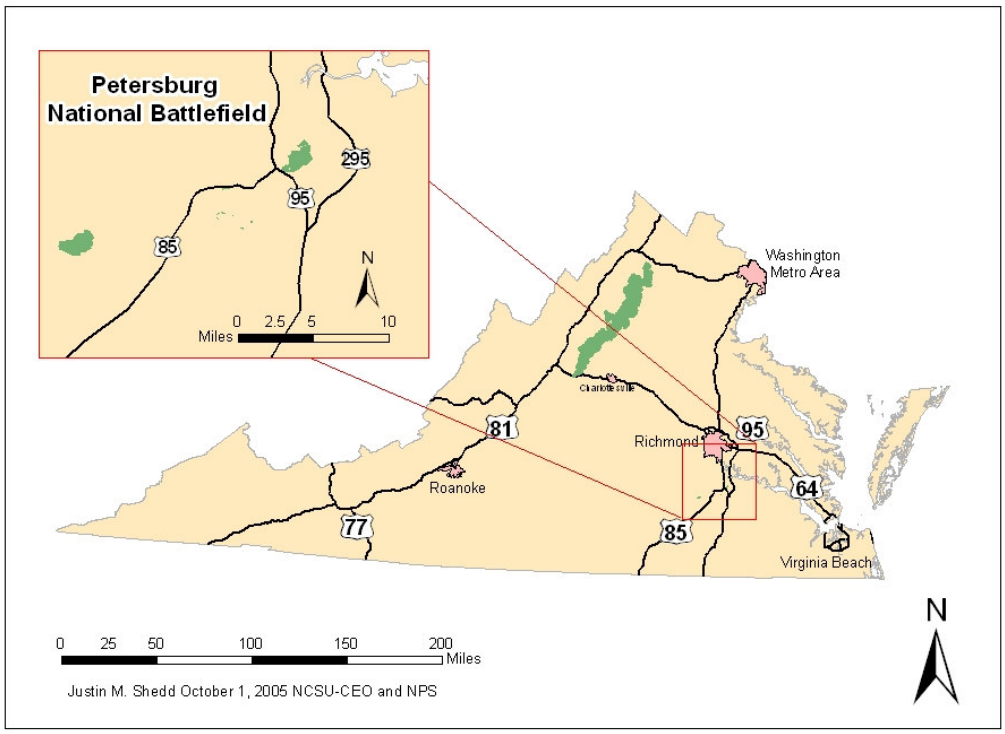

Figure 1: Petersburg National Battlefield

4.2 Shenandoah National Park

Shenandoah National Park (SHEN) lies along the crest of the Blue Ridge Mountains in the southern Appalachians of Virginia and was incorporated into the National Park Service in 1935 (Figure 2). SHEN's boundaries were carved from private land owners to create a tourism industry in the Shenandoah Valley. As a result, SHEN's land cover is influenced by past land use practices. Skyline Drive is the park's only road, following mountain ridgelines for 105 miles between the park's northern and southern boundaries. In recent years, encroachment from private development has brought the wildland urban-interface to the park's borders.

Since its inclusion into the National Park Service, SHEN's forests have undergone several transformations (Park Website, http://www.nps.gov/shen). Hemlocks (*Tsuga canadensis and Tsuga caroliniana*) have diminished as a result of an exotic forest pest, the Hemlock Woolly Adelgid, as have the Northern Red (*Quercus rubra*) and Chestnut Oaks (*Quercus prinus*) because of the gypsy moth and fire exclusion. Meanwhile, Yellow Poplar (*Liriodendron tulipifera*) stands and cove hardwood forests are increasing in area as the natural environment returns to a pre-European settlement state. While forest succession is a gradual process, there are often chaotic events, like fires and wind events that occur, directing forest succession.

SHEN has experienced several severe wildland fires, most recently the Rocky Top fire, located in the southwestern portion of SHEN, which began on July 7th 2002, from a lightning strike and burned for nearly two weeks. The resulting fire created a mosaic of burned and unburned areas across 1,500 acres of forest. The severity of the Rocky Top fire ranged from low intensity surface burns to high severity canopy burns.

The Rocky Top fire did extensive damage to the landscape and continues to have an impact on it today.

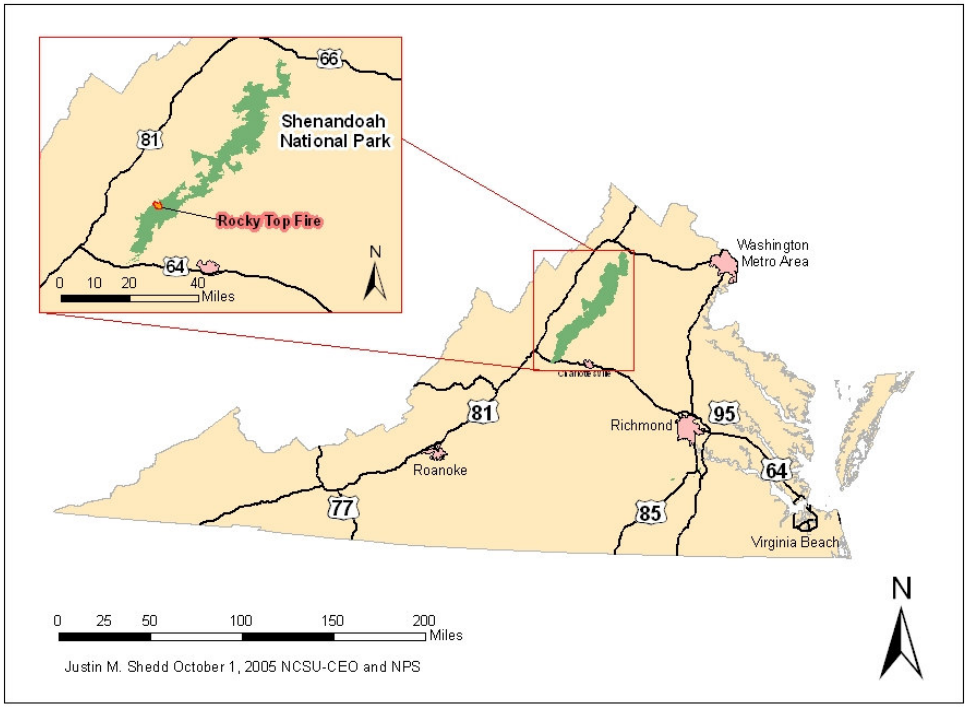

Figure 2: Shenandoah National Park

5. Methodology

Automated Feature Extraction and the Normalized Burn Ratio are the two methods used to identify and quantify areas of change. Given the different study sites and the types of change that occurred, the methods are documented in separate sections; Petersburg National Battlefield in section 5.1., Shenandoah National Park in section 5.2. Section 5.3., describes the use of the FARSITE model to evaluate the effects of vegetation/fuel load change on fire behavior.

5.1 Visual Learning System's Feature Analyst

5.1.1 Data and Initial Classification Attempts

The magnitude of Hurricane Isabel's impact upon the landscape was immediately realized after park managers surveyed the damage from the air. Digital aerial photography was chosen for this study because of its ability to capture the area of interest (PETE) at a large scale (1:6000) and at an affordable cost. True color and color infrared (CIR) photography were captured on March 13, 2004, mosaiced and orthorectified by SkyComp, Inc., of Columbia, MD, and delivered to North Carolina State University's Center for Earth Observation in the summer of 2004. Upon initial visual inspection of the aerial photography, areas of downed woody debris were easily identifiable (Figure 3 and 4). However, manual delineation of the forest damage areas presented a lengthy and costly alternative. An automated approach to classifying the areas of downed woody debris was desired.

Traditional spectral analyses using both supervised and unsupervised classifications with Leica's ERDAS Imagine 8.7 resulted in many mis-classifications.

Upon visual inspection of the resulting classifications spectral confusion existed between areas of dead herbaceous matter (mowed grassfield) and areas of downed woody debris (Figure 3). A Normalized Differenced Vegetation Index (NDVI) classification of the image was performed, but the results were poor, as there was little green vegetation upon which the index could take place (Figure 4). It became apparent that spectral values alone could not be used to identify areas of downed woody debris. Traditional methods relying entirely upon spectral responses of pixels were inadequate for updating the existing fuel load and vegetation datasets. With areas of forest damage clearly represented by downed trees, a classification technique that could map specific features is much better suited for fire potential (threat) research.

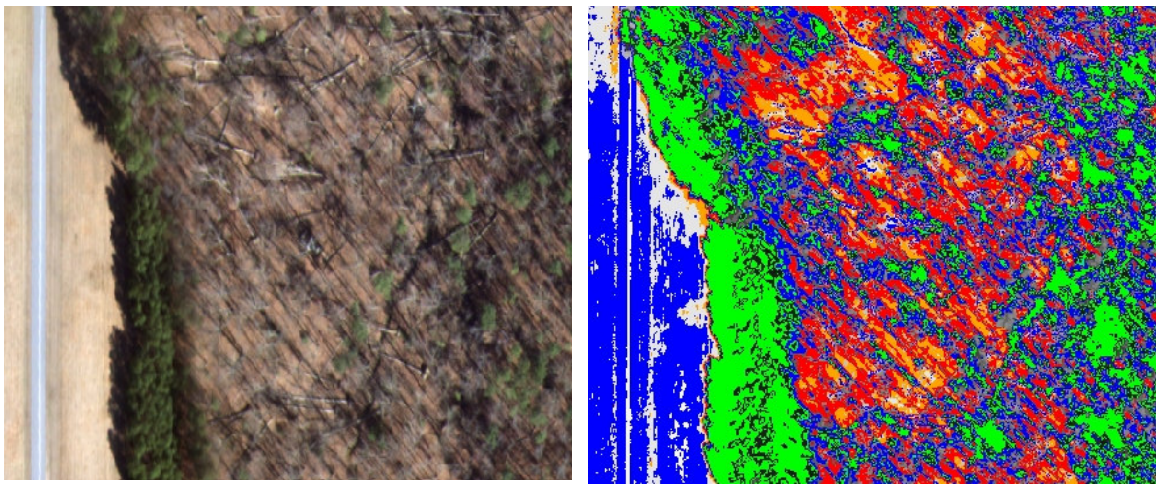

Figure 3: Unsupervised classification using 40 classes. Green indicates conifer trees.

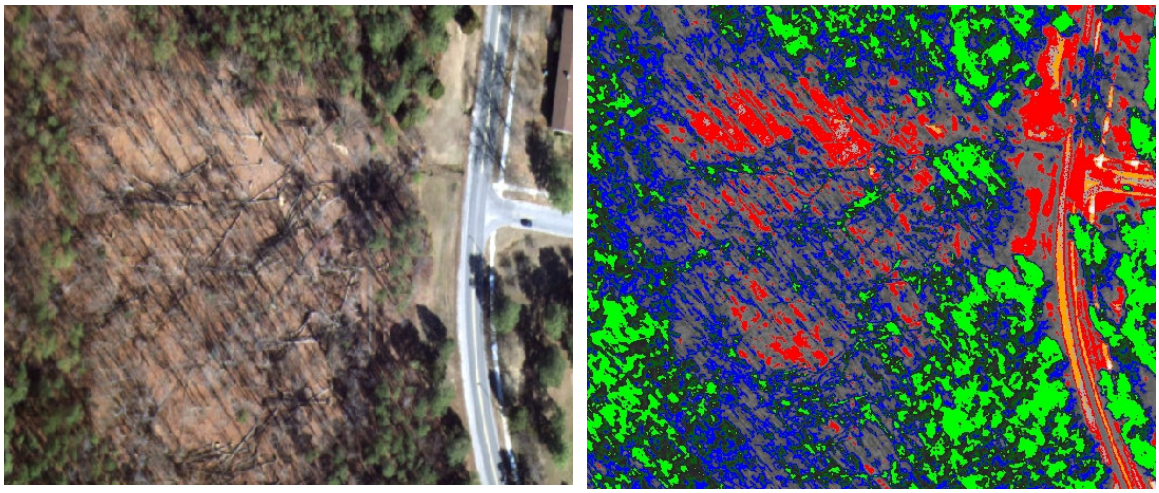

Figure 4: NDVI classification, outlines of some downed trees can be seen in blue.

5.1.2 Parameters of Feature Analyst

The following sections will outline the user defined parameters enabling Feature Analyst to classify an image based on spatial patterns. A detailed methodology of how the downed woody debris of the Fort Gregg area was classified is found in section 5.1.3. A similar procedure was followed to map other areas of PETE that had forest damage.

5.1.2a Training Sites

The ground resolution of the digital aerial photomosaics was one-half meter per pixel; making individual trees discernable in both the true color and CIR imagery. Using Visual Learning System's Feature Analyst 3.5 as an extension within ESRI's ArcMap 9.0, a polygon shapefile of downed trees was created. Using ArcMap, training sites of these downed tree areas were digitized. The training sites were selected to include the wide range of downed woody debris, from a single tree trunk and associated root-ball to the trunk and crown of a downed tree (Figure 5).

Figure 5 Example of training sites (in red) used to "train" Feature Analyst.

5.1.2b Pattern Recognizers and Initial Classification Attempts

In addition to identifying the objects of interest, Feature Analyst must also be instructed on how to look for these objects. The software includes various pattern recognizers that examine each pixel to determine if it is in the target feature you are looking for. Nine types of pattern recognizers exist: Bull's Eye 1, Bull's Eye 2, Bull's Eye 3, Bull's Eye 4, Square, Circle, Manhattan, User Defined and Foveal. Some pattern recognizers indicate linear objects better, while others are better suited to indicate different types of land cover.

Choosing an appropriate set of parameters (search window and pattern recognizers) was done by trial and error. Consistently, the Foveal pattern recognizer was found to provide better classification results for the initial identification. The Foveal classifier analyzes an image by regions, with the center of the search window very detailed with feature similarity restriction decreasing towards the outer extent of the

search window (Figure 6). This mimics a human's peripheral viewing pattern; where the object of interest is in the center of view being focused on, while the outer areas are focused on less (Feature Analyst User's Manual Version 4.0). The "best" classification was determined by visual inspection of the resulting classification.

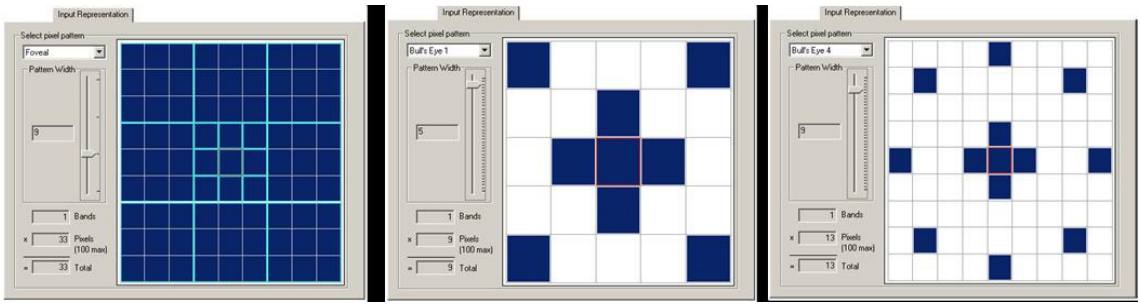

Figure 6: VLS Feature Analyst's Pattern Recognizers Foveal, Bulls Eye 1 and Bulls Eye 4 used for delineating downed woody debris.

In subsequent iterations, when a more precise classification was desired, the Bull's Eye pattern recognizer, specifically Bulls Eye 1 and Bulls Eye 4 (Figure 6), were found to provide a more accurate classification (Figure 7). After each iteration, a few areas of the "best" classification were manually identified, through visual inspection, as "correct" or "incorrect" in a process called clutter removal. This process allows Feature Analyst to adjust and learn what spatial and spectral patterns to look for in subsequent iterations (Figure 8).

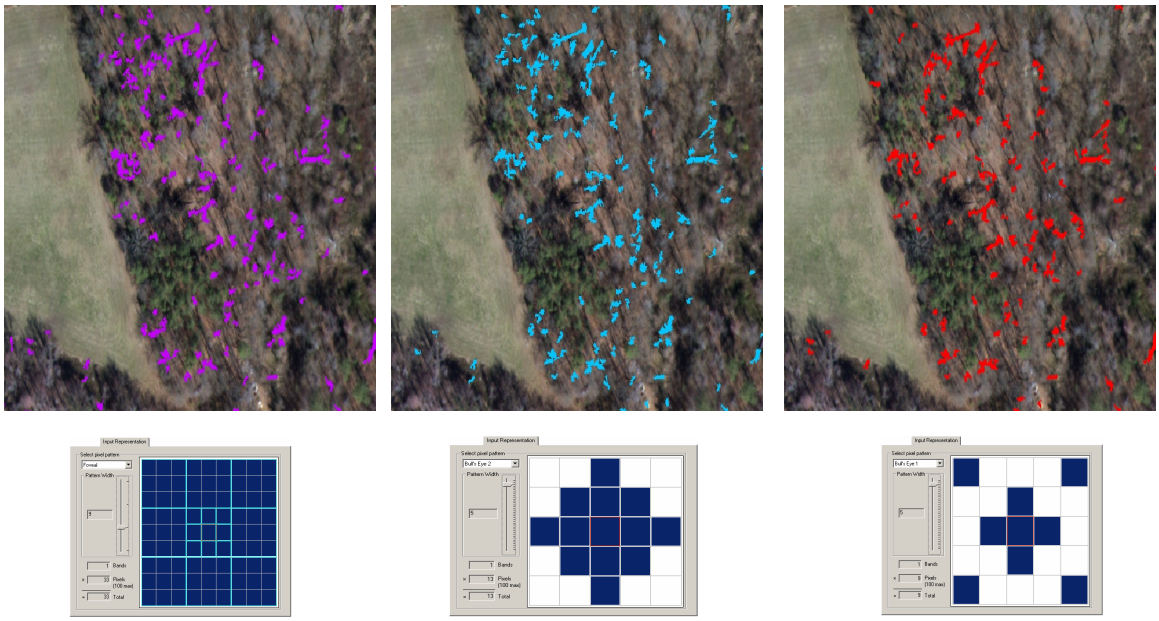

Figure 7: Classification results (left to right: Foveal, Bulls Eye 2 and Bulls Eye 1) for one iteration using different pattern recognizers.

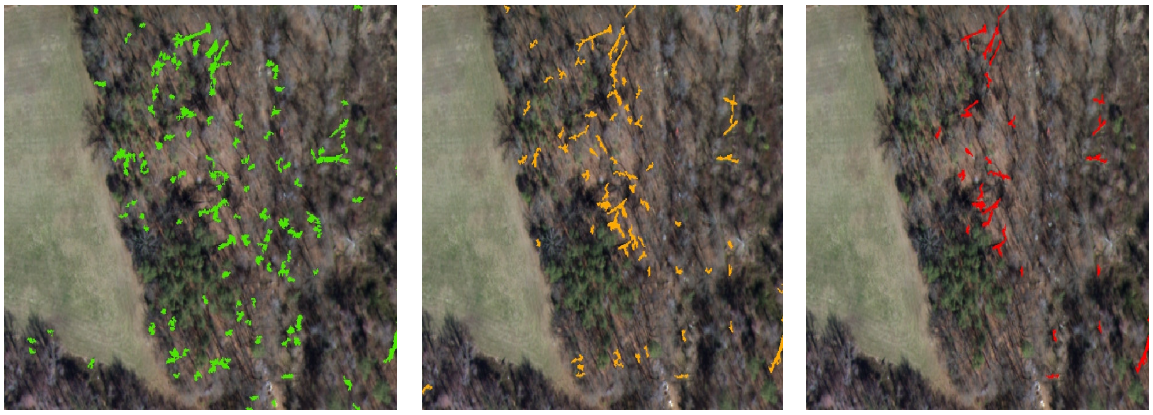

Figure 8: Classification results (left to right: Iteration 1, 2, and 3) of the three iterations needed to map downed woody debris.

5.1.2c Other User Defined Parameters

Besides choosing a pattern recognizer, the user defines other parameters as well. These include: feature selector, input bands, type of data (reflectance, texture, discrete, elevation), and learning file (learning algorithm and options such as aggregation, smoothing settings, find rotated instances.)

Feature selector allows the specification of the type of feature to be extracted from the imagery. Choices include; narrow linear feature, wide linear feature, natural feature, small manmade feature, manmade feature, landcover feature, water body feature, and building. The spatial resolution of the imagery being used is also entered.

The image's bands to be analyzed are entered next. How each band is interpreted by Feature Analyst is determined as well, as the user can choose between; reflectance, texture, discrete, and elevation. Individual bands can be entered more than once and interpreted differently. For this research, texture was chosen as the method of interpretation for all iterations.

Parameters defining the learning file were chosen next; Approach 1, or general purpose, was chosen for all iterations. In initial classification attempts, Approach 1 provided the better classification results when visually compared to the other choices (Approach 2 and Approach 3). Another choice in this section was the aggregate area. The initial iteration was set at 50 pixels and reduced to 35 in subsequent iterations to further focus the classification results. The default settings of the Bezier smoothing algorithm were used when choosing the Smooth Polygons option. Lastly, the option to look for rotated features was selected.

5.1.2d True Color versus Color Infrared

Initial efforts focused on determining which image type was better suited for mapping downed woody debris. Using the True Color image, training sites were digitized. Eight passes, four using True Color and four using CIR imagery, were done. The Foveal, Circle, Bull's Eye 4 and Square pattern recognizers were applied to both

types of imagery. The same training site polygon was used for all passes. After visual inspection of both classification results, the True Color image consistently provided a more accurate classification of downed woody debris when compared to the CIR classification, and was chosen as the type of imagery to use for mapping downed woody debris at PETE.

5.1.3 Mapping Downed Woody Debris

The following section describes the steps taken to successfully classify downed woody debris of the Fort Gregg area of PETE. This same general methodology was used on additional sections of PETE as covered in section 5.1.4.

A training site polygon consisting of six occurrences of downed woody debris representative of the forest damage was created. For example, one site represented a single tree and its rootball, with other sites consisting of multiple trees and varying amounts of crown damage. Each polygon digitized consisted of at least 20 pixels.

The first pass utilized the following parameters, feature selector set to small linear feature, followed by learning settings set to all available bands and textures. Next under the input representation tab, the pattern recognizer, Fovel was chosen with a pattern width of 100. Finally, under the Learning Settings tab, Approach 1 with a minimum area of 50 pixels set and the find rotated instances option chosen.

The second pass utilized the following parameters, feature selector set to small linear feature, followed by learning settings set to all available bands and textures. Next under the input representation tab, the pattern recognizer, Manhattan was chosen with a

pattern width of 75 chosen. Finally, under the Learning Settings tab, Approach 1 with a minimum area of 50 pixels set and the find rotated instances option chosen.

The third pass utilized the following parameters, feature selector set to small linear feature, followed by learning settings set to all available bands and textures. Next under the input representation tab, the pattern recognizer, Bull's Eye 4 was chosen with a pattern width of 35 chosen. Finally, under the Learning Settings tab, Approach 1 with a minimum area of 50 pixels set and the find rotated instances option chosen.

The fourth pass utilized the following parameters, feature selector set to small linear feature, followed by learning settings set to all available bands and textures. Next, under the input representation tab, the pattern recognizer, Circle was chosen with a pattern width of 60 chosen. Finally, under the Learning Settings tab, Approach 1 with a minimum area of 50 pixels set and the find rotated instances option chosen.

At this juncture, an extensive visual interpretation of the four classifications was done to determine the "best" classification (Figure 9). The classification that used the Foveal pattern recognizer was chosen as the "best" and selected for use in subsequent iterations. However, before this occurred, adjustments were made to the Foveal classification. Clutter Removal was done on the classification shapefile, with areas indicated as correct and incorrect. Twenty areas in total were used to identify areas as correct and incorrect.

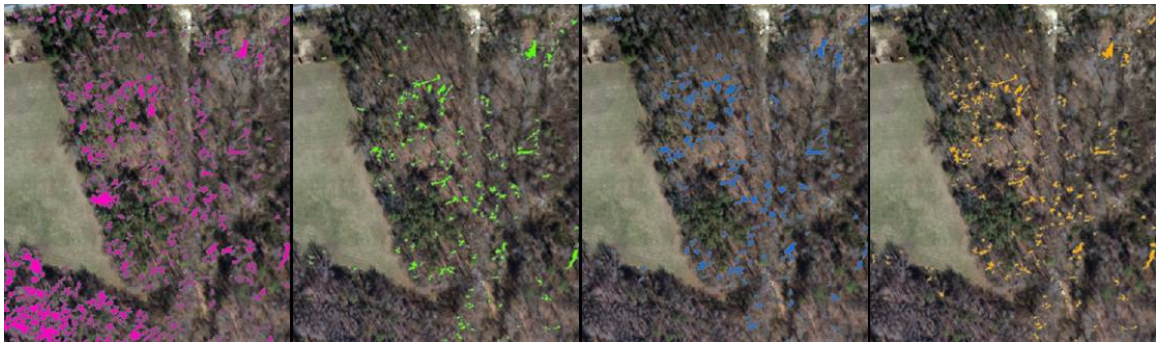

Figure 9: Example of four passes of the first iteration. After visual inspection the "best" classification is chosen for the second iteration.

With areas indicated as correct and incorrect the second iteration could begin. This time Feature Analyst analyzed only areas previously classified, and used areas identified as correct and incorrect to further focus its classification. The second iteration first pass utilized the following parameters, feature selector set to small linear feature, followed by learning settings set to all available bands and textures. Next under the input representation tab, the pattern recognizer, Foveal was chosen with a pattern width of 100. Finally, under the Learning Settings tab, Approach 1 with a minimum area of 50 pixels was set.

The second iteration second pass utilized the following parameters, feature selector set to small linear feature, followed by learning settings set to all available bands and textures. Next under the input representation tab, the pattern recognizer, Circle was chosen with a pattern width of 60. Finally, under the Learning Settings tab, Approach 1 with a minimum area of 50 pixels was set.

The second iteration third pass utilized the following parameters, feature selector set to small linear feature, followed by learning settings set to all available bands and texture. Next under the input representation tab, the pattern recognizer, Bull's Eye 1 was

chosen with a pattern width of 35 chosen. Finally, under the Learning Settings tab, Approach 1 with a minimum area of 50 pixels was set.

The second iteration fourth pass utilized the following parameters, feature selector set to small linear feature, followed by learning settings set to all available bands and textures. Next under the input representation tab, the pattern recognizer, Bull's Eye 3 was chosen with a pattern width of 35 chosen. Finally, under the Learning Settings tab, Approach 1 with a minimum area of 50 pixels was set.

Again the "best" classification of the second iteration was chosen based on visual interpretation of the image. Clutter removal was done next on the classification with areas identified as correct and incorrect. The more sites identified as correct or incorrect actually confuses the pattern recognizer in the next iteration of classifications, so it is recommended to limit areas identified to no more than 20.

The third iteration first pass utilized the following parameters, feature selector set to small linear feature, followed by learning settings set to all available bands and texture. Next under the input representation tab, the pattern recognizer, Bulls Eye 3 was chosen with a pattern width of 35 chosen. Finally, under the Learning Settings tab, Approach 1 with a minimum area of 35 pixels was set.

The third iteration second pass utilized the following parameters, feature selector set to small linear feature, followed by learning settings set to all available bands and texture. Next under the input representation tab, the pattern recognizer, Square was chosen with a pattern width of 75 chosen. Finally, under the Learning Settings tab, Approach 1 with a minimum area of 35 pixels was set.

The third iteration third pass utilized the following parameters, feature selector set to small linear feature, followed by learning settings set to all available bands and textures. Next under the input representation tab, the pattern recognizer, Manhattan was chosen with a pattern width of 27 chosen. Finally, under the Learning Settings tab, Approach 1 with a minimum area of 35 pixels was set.

The third iteration fourth pass utilized the following parameters, feature selector set to small linear feature, followed by learning settings set to all available bands and textures. Next under the input representation tab, the pattern recognizer, Bull's Eye 1 was chosen with a pattern width of 35 chosen. Finally, under the Learning Settings tab, Approach 1 with a minimum area of 35 pixels was set.

The "best" classification of the third iteration was chosen based on visual interpretation of the image and classification shapefile. Clutter removal was done again on the classification. However, on subsequent passes, the resulting classifications were actually less accurate as areas that clearly represented downed woody debris were excluded. As a result, The Bull's Eye 1 third iteration classification was chosen as the "best". Additional manual edits were done to remove polygons from the classification that were clearly not downed woody debris but closely resembled the spatial pattern of it (e.g. tree shadow on grassfield).

For all sections of PETE exhibiting downed woody debris, this trial and error process validated by visual interpretation was repeated until an acceptable classification was reached. It should be noted that there were more than four passes done per iteration; in fact, each iteration consisted of anywhere from four to eight passes, depending on the accuracy of the classifications.

5.1.4 Additional Sections of Petersburg National Battlefield

In addition to the Fort Gregg area, the Fort Wadsworth and Fort Fisher sections of the Western Front also suffered damage as a result of Hurricane Isabel. To map these areas, a polygon training site shapefile consisting of ten occurrences of both deciduous and coniferous downed woody debris was created. Using the Foveal pattern recognizer for the initial iteration, those portions of the Western Front that were definitely not downed woody debris (e.g. cars, homes, homogenous stands of trees, mowed grasslands) were eliminated from further analyses. These areas were removed from future analyses because their spatial and spectral patterns did not resemble those of the training sites. Based on visual inspection, the Bull's Eye 4 pattern recognizer was chosen as the "best" output classification for the second iteration. However, the resulting classification required the manual addition of several areas of downed woody debris as areas of coniferous species were not accurately indicated. The presence of both deciduous and coniferous trees in the training site shapefile probably led to this classification problem, as this did not occur in the Fort Gregg section.

The manual addition of an area for classification is much like creating the initial training site shapefile; classified areas are redrawn using the Polygon Reshape Deluxe Tool located on the Feature Analyst Adjustment Tool bar. Much like an ArcMap general edit session, a polygon can be redrawn to include the missed areas. In most instances the reshape option was used to include areas of downed coniferous trees. While Feature Analyst does have a "Missed Objects" option, where additional training sites are drawn around the missed target areas; this process resulted in a more erroneous classification. Therefore, this option was abandoned in favor of the Polygon Reshape Deluxe Tool. In

addition to manually adding areas of downed woody debris, several examples of "correct" and "incorrect" areas of downed woody debris were identified in the "best" classification. The downed woody debris of the Fort Wadsworth and Fort Fisher areas of the Western Front of PETE was accurately classified after six iterations.

The Eastern Front section of PETE is the largest contiguous part of the park and suffered the most damage as a result of Hurricane Isabel. With deciduous, coniferous, and mixed forests present, two sets of training sites were necessary to represent the downed woody debris present. (Coniferous trees are small in size and typically black in color while deciduous trees are larger and either white or brown in color). The deciduous downed woody debris training site consisted of ten polygons, while the coniferous training site consisted of seven polygons. Two separate training site shapefiles representing the different origin of species of the downed woody debris focused the Feature Analyst classification; ultimately reducing the number of iterations needed to achieve an acceptable classification.

For both training site shapefiles, the Foveal pattern recognizer was used for the initial iteration. Subsequent iterations used the Bull's Eye 1 pattern recognizer to reach an acceptable result. Manual addition using the Polygon Deluxe Reshape Tool was necessary in some areas, most of which were coniferous. An accurate classification of coniferous downed woody debris, was reached in four iterations, while only three iterations were needed for deciduous downed woody debris. These classifications were then merged together, using the "combine features" tool, forming the final classification of downed woody debris for the Eastern Front of PETE (Figure 10).

Once accurate automated classifications for all affected areas of PETE were reached, the results were merged into one shapefile. This shapefile was then manually edited by visual inspection to further remove those features classified as downed woody debris. Confusion still existed in areas where shadows of tree branches or the tree branches themselves overlaid homogenous areas; creating a spatial pattern similar to downed woody debris. This manual edit reduced the number of downed woody debris polygons from 14,256 to 7,726.

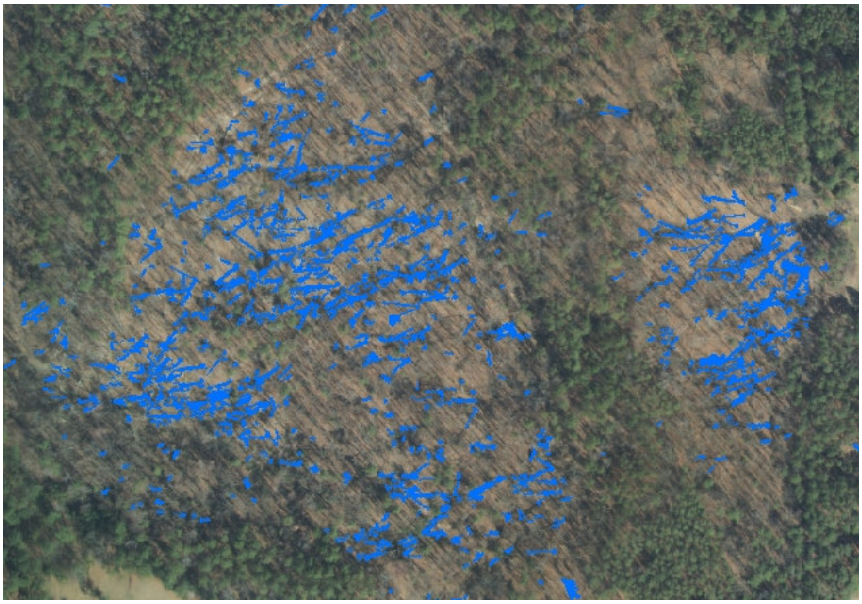

Figure 10: Example of mapped downed woody debris of the Eastern Front portion of PETE.

5.1.5 Construction of Forest Damage Polygons

Feature Analyst had identified occurrences of coarse woody debris, or fuels greater than three inches. Brown (2004) noted that this type of woody debris is extremely important for a healthy ecosystem but that it does not have a strong bearing on the start or spread of a wildland fire. Forest fuels in the 1-, 10-, and 100-hour categories are the source of wildland fire ignition and spread. However, Feature Analyst had not indicated these fuels. While a spatial resolution of ½ meter allowed for the capture of larger fuels,

smaller fuels like 1-, 10-, and 100-hour were not indicated. To capture these fuels, a generalized buffer, or forest damage polygon, was created around the mapped downed woody debris. (Examples of forest damage are uprooted tree pits and mounds and tree crowns snapped and lying on the ground, as shown in Figure 11). Applying the default settings of the Bezier smoothing algorithm (within Feature Analyst), downed woody debris represented as polygons, were converted to lines. The resulting downed woody debris line shapefile was used in ESRI's ArcToolbox's line density tool to create the generalized forest damage polygon. The output parameters, cell size and search radius, were set at one and five respectively. Cell size determined the resolution of the output grid, with each pixel measuring one meter. The search radius parameter, similar to a filter, set the size of the window that was used to calculate the cell values (0.0 to 1.0) of the resulting line density grid.

Figure 11: Examples of downed woody debris not detached from its point of origin.

The resulting grid was further refined using Spatial Analyst's raster calculator as it was divided into a presence/absence grid using the density value of .0059 as the breakpoint. Other threshold parameters were applied, but were either too restrictive, (0.003) excluding areas of previously mapped downed woody debris, or too general, (0.1) encompassing areas that were clearly not damaged. This grid was converted to a polygon

shapefile that consisted of 2,891 polygons ranging in size from .0283 to 42,127 square meters. The "eliminate" tool in ArcToolbox 9.0 was used to dissolve smaller polygons, those less than 90 square meters, into the larger surrounding polygon. The final forest damage polygon consisted of 2,368 polygons, ranging in size from 2,104 to 102,139 square meters (.002 acres to 25.2 acres) (Figure 12).

The generalization of downed woody debris captured 1-, 10-, and 100-hour fuels missed by Feature Analyst classifications and captured the horizontal spatial continuum of downed woody debris across the landscape. With a minimum mapping unit of ½ an acre, only those forest damage polygons greater than ½ acre were considered for further study (51 in total). The majority of the polygons removed from consideration represented single occurrences of downed woody debris. Single downed trees do not represent an increase in fuel loading and therefore do not warrant updating the existing fuel model spatial dataset. Of the remaining 51 forest damage polygons the acreages ranged from 0.52 to 25.2 acres.

It was important for fire behavior to quantify the density of forest damage within each of the forest damage polygons. To accomplish this, the percentage of the forest damage polygon covered by the actual mapped downed woody debris was determined. By performing a many to one relate each occurrence of downed woody debris that fell in a forest damage polygon was assigned to that polygon. The forest damage polygon's area was divided by the downed woody debris polygon's area. This resulted in a percentage of downed trees present in each forest damage polygon. The percentage of the 51 forest damage polygons covered by downed woody debris ranged from eight to 30.

5.1.6 Creating Fuel Model Maps

Anderson Fire Fuel Models 10, 11, 12, and 13 were assigned to the forest damage polygons (Table 1), based on their percentage covered as documented in the previous section. Because there was no guidance from the literature to relate percentage of downed trees for a given area to fuel models the following assignments were arbitrarily made. Fuel Model 13 represents landscapes with the greatest amount of fuel loading (tons per acre). Therefore, it was assigned to the forest damage polygons in the highest quartile of percentage covered (21-30). Fuel Model 12 represents landscapes of the second highest fuel loading levels and was assigned to the forest damage polygons of the next quartile (15-21). While Fuel Model 10 and 11 are similar in Fuel Loading totals, Fuel Model 10 was assigned to the lowest quartile of percent covered (8-13) because it is in the timber group of fuel models. Leaving Fuel Model 11 assigned to polygons with a percent cover of 13-15.

Assigned Fuel Model	10	11	12	13
Percent of "Forest damage" Covered by woody debris	8-13	13-15	15-21	21-30
Total amount (acres) of forest damage	14.2	16.9	98.2	19.8

Table 1: Initial Fuel Model Classification of PETE, Fuel Models assigned based on Percent Covered.

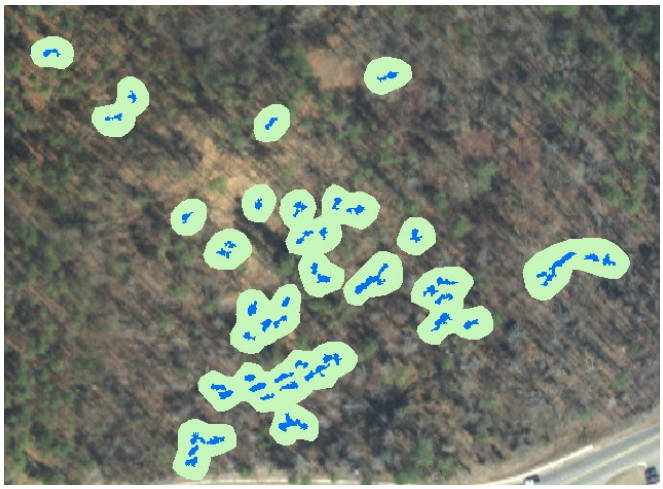

Figure 12: Example of Forest damage polygon created to capture 1-, 10-, and 100-Hour fuels.

5.1.7 Preparation for Field Work

Field work to validate Feature Analyst classifications first focused on Feature Analyst's ability to identify downed woody debris, and then on recording field measurements following Brown's Transect Guidelines (Brown 1974). Using the random point generator of Hawth's Analysis Tools (version 3.12, http://www.spatialecology.com/htools), points were placed inside mapped occurrences of downed woody debris (and in PETE boundaries), outside mapped occurrences of downed woody debris (but in PETE boundaries), and inside the 51 forest damaged polygons. A 50-foot buffer was applied to the points placed in the 51 forest damage polygons. Points with buffers extending beyond the forest damage polygon were removed from further consideration. This ensured that an entire plot (50-foot transects) would be located within an area classified as having forest damage. The random points meeting these criteria were given the following attributes: previous fuel model, NVCS vegetation formation, and percent covered.

5.1.8a Field Work – Accuracy of Feature Analyst

To assess the validity of Feature Analyst, random points representing both mapped occurrences of downed woody debris, and areas outside mapped debris occurrences were visited using a Trimble GeoXT hand-held Global Positioning System (GPS) receiver to navigate to them. Real-time differential correction was used when navigating to the pre-determined locations. After reaching the pre-determined point, any occurrence of downed woody debris within three meters and measuring two meters or more in length and 12 inches in diameter was recorded as having an occurrence of downed woody debris. A total of 40 points were visited, 20 from each category.

5.1.8b Field Work – Fuel Data Collection

Field work at PETE used Browns and Burgan-Rothermel field measurements. Twenty four predetermined points were visited, using a Trimble GeoXT hand-held GPS receiver with real-time correction. At each point, a National Park Service protocol developed by SHEN park personnel (Carmichael and Cass, 2001) was followed. Following this protocol, a combination of Brown's Transects and Burgan-Rothermel Ocular Estimations were completed. For each plot, field measurements estimating the amount of fuel loading were recorded on an HP rugged tablet PC tr30000 laptop computer and recorded into a Microsoft Office Access 2003 database. This database (Figure 13) was designed by several employees and graduate students of NCSU-CEO to streamline the data collection process and eliminate clerical errors when transposing data from paper to an excel spreadsheet. At each plot point, a three-minute positional fix was recorded to determine the exact location of each plot. Fifty-foot transects were then laid

in the North and East cardinal directions. Slope measured in degrees was taken of each transect.

Fine woody debris consisting of 1-hour (0.0 to 0.25 inch in diameter), 10-hour (0.25 to one inch), 100-hour (one to three inches), and coarse woody debris or 1000-hour (> three inches) debris along with litter and duff measurements were collected along both transects. All downed woody debris (1-, 10-, 100- and 1000-hour) was tallied for the first six feet of the transect line. From six to 12 feet, only 10-, 100-, and 1000-hour fuels were recorded. Beyond 12 feet and up to 50 feet, only 1000-hour fuels were tallied. Duff and litter measurements were made at the one-foot mark then repeated at the five-foot mark and every five feet thereafter until reaching the 45-foot mark. Duff and litter measurements were made to the nearest tenth of an inch.

Burgan-Rothermal Ocular Estimations were made for the area between the two transects. For each plot, qualitative measures of grasses, shrubs and trees were recorded. Characteristics of the litter (e.g., source and compactness) were recorded as well. Three photographs were taken at each plot along the North transect, East Transect, and middle of plot to serve as a later reference and to be linked in a Microsoft Access database. Field measurements were collected at a total of 24 plots throughout PETE (Figures 14, 15, 16).

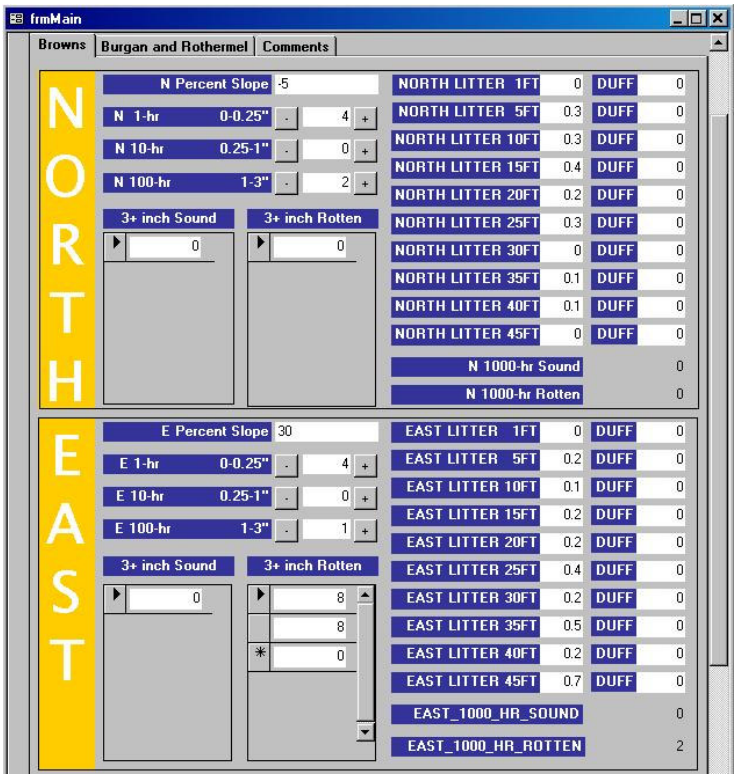

Figure 13: Microsoft Access Database designed by NCSU-CEO for collecting field data.

5.1.8c Field Work - Modification of Brown's Transect

Occurrences of partially uprooted trees were included in each plot's tally of downed woody debris. This is a modification to Brown's Transect guideline's, which calls for the counting and measuring of woody debris that is detached from its origin of growth. For example, if a tree is blown over or knocked over by another tree and the bole of the tree is not completly detached (snapped off) and a portion or the entire root ball remains in the ground, it is not considered as downed woody debris. This stipulation was not followed in this study because of the presence of numerous trees that were dead but still attached to their origin of growth. If a tree along a transect was below a height of two meters; was attached at its origin of growth and did not exhibit any semblance of growth, (e.g., change of direction in branch growth, the presence of buds), it was included

in the tally. At the time of field measurement (March 2005) the toppled trees had had one full growing season and were entering their second since the hurricane. Within one growing season, a tree can adjust to various adverse growing conditions (Whigham, 1991). If any indication of growth was noted, the tree was not included in the tally of downed woody debris.

5.1.8d Field Work – Forest Damaged Areas

In addition to plot measurements, the perimeters of several areas of forest damage were walked to validate the delineated forest damage polygons. Six perimeters were walked, three in deciduous forests, two in coniferous forests and one in a mixed forest. Using a Trimble GeoXT hand-held GPS receiver, the perimeter of an area exhibiting forest damage was walked. One field plot was located within each of the six perimeters.

5.1.9 Fuel Load Calculation

The amount of downed woody debris measured in the field was calculated using the equation provided in Brown's Transect Handbook. Using this formula, fuel loading in tons per acre was calculated for fine and coarse woody debris. This calculation is based on the number of intersects for each transect line, average squared debris diameter, specific gravity, slope correction factor, and transect line length. All data used to calculate the fuel load of a plot was initially entered into a Microsoft Office Access 2003 database via the HP rugged tablet PC and later exported into a Microsoft Office Excel 2003 spreadsheet for further data analysis.

5.1.10 Post Processing

Each night GPS measurements were post-processed to further reduce the effects of satellite location and ionospheric interference that cause inaccuracies in GPS data. This was done in addition to real-time correction, as this allowed for the visual inspection of the GPS data collected. Post-processing was done using Pathfinder Office version 3.0.

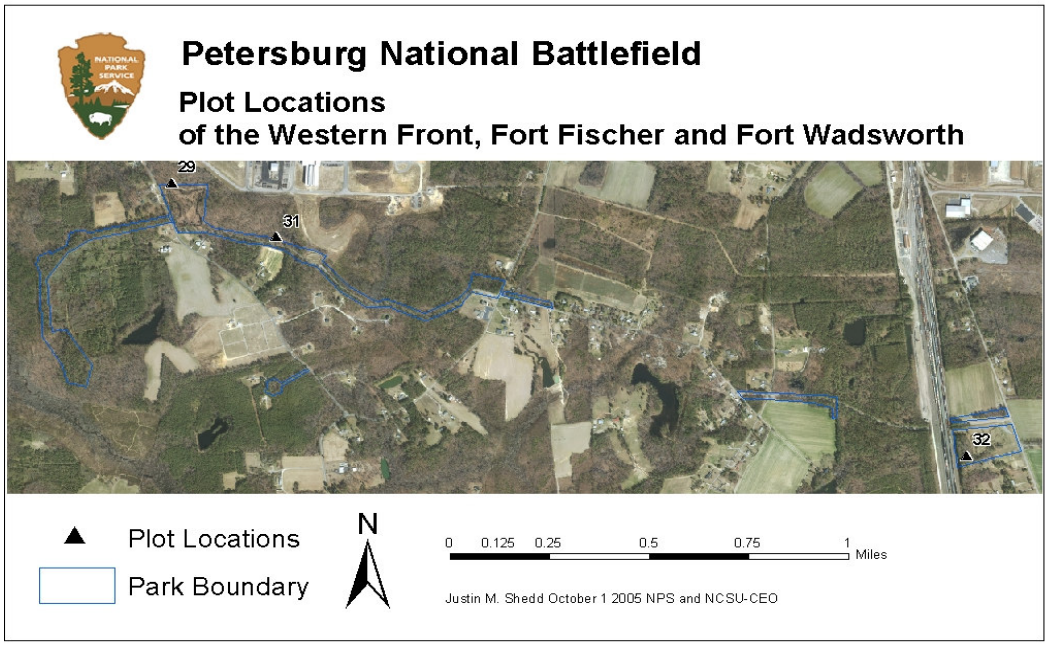

Figure 14: PETE, Western Front plot locations.

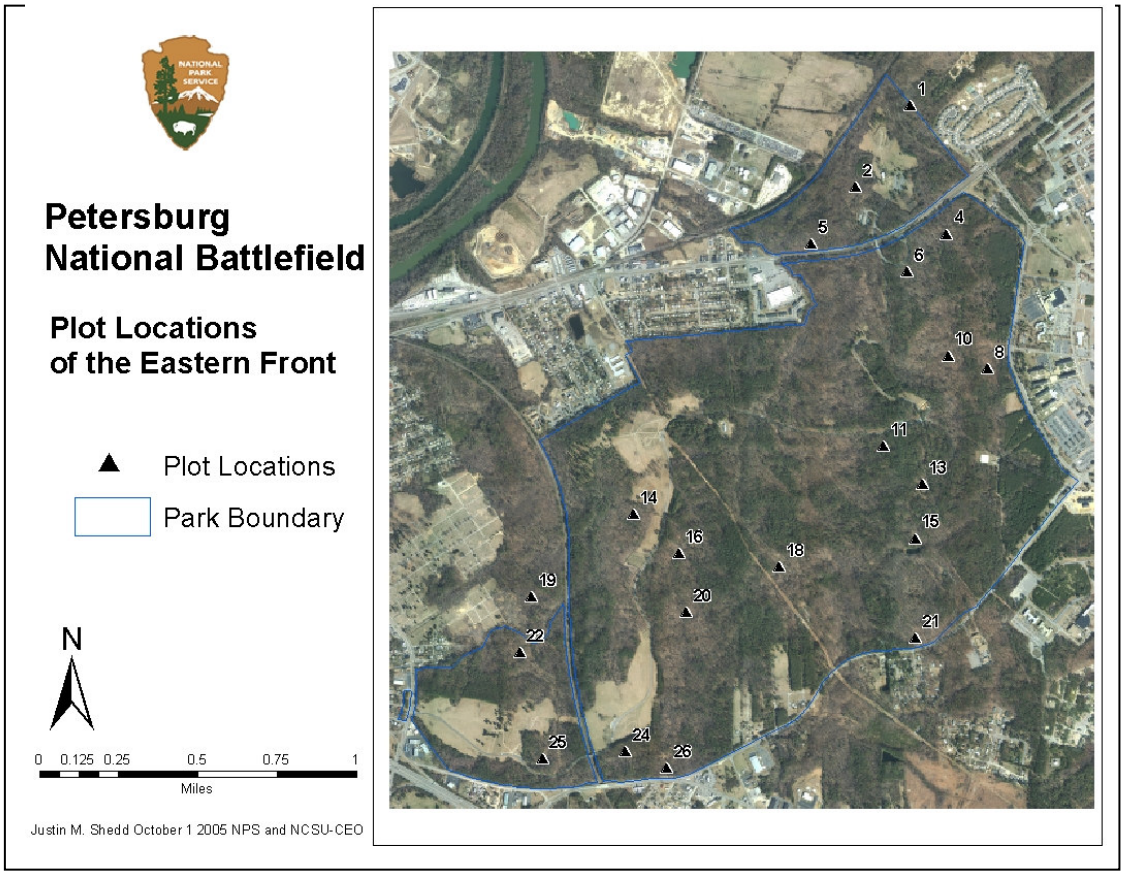

Figure 15: PETE, Eastern Front plot locations.

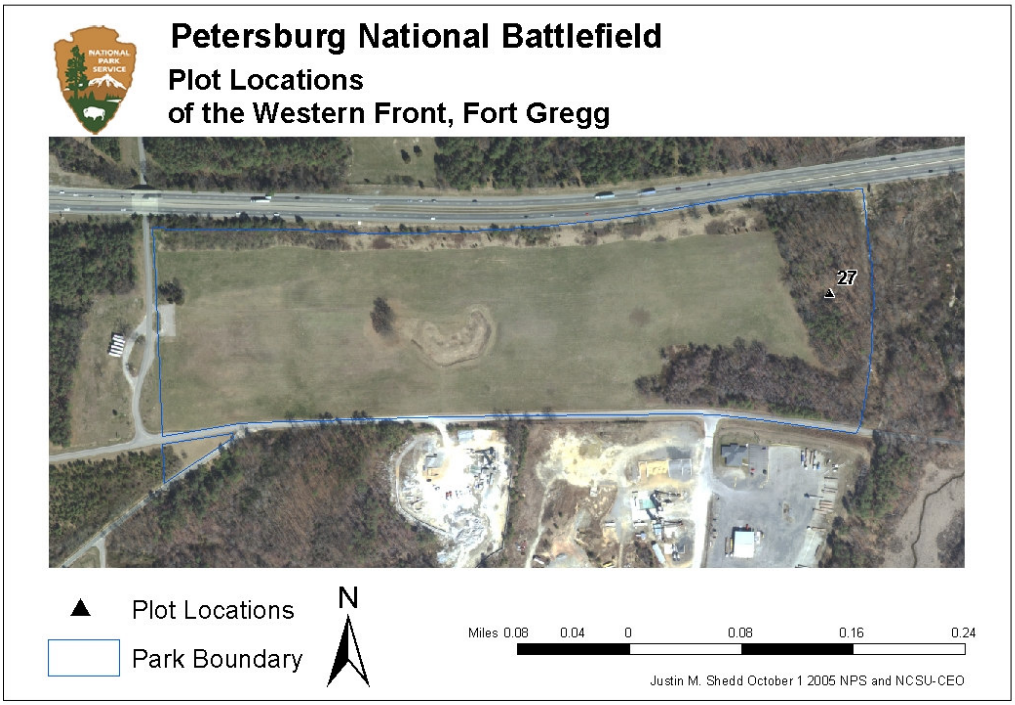

Figure 16: PETE, Fort Gregg of the Western Front plot location.

5.2 Remote Sensing Landsat

5.2.1 Data Type and Availability

Two Landsat 5 Thematic Mapper (TM) scenes, one pre-fire image dated June 30, 2001, and the other a post-fire image dated July 6, 2003 (Path: 16 Row 33 506033000318710), were acquired from the United States Geological Survey (USGS). Landsat TM data was chosen for this research project because of its temporal availability and spectral resolution.

The post-fire image, taken a year after the fire, was chosen because the objectives of this research project were to map the long-term fire impacts upon the vegetation and fuel loads and not to map the burn perimeter. In addition, an increase in green biomass is seen shortly after a burn, in some herbaceous vegetation communities. The short-term increase in herbaceous productivity caused by a release of nutrients and an abundance of sunlight would have concealed the long-term effects of the landscape, by hiding the burn impacts to the shrub and tree communities. Furthermore, related factors affecting future vegetation and fuel loading, such as seed bank availability, mass wasting, and insect infestation, are more likely to be recorded in imagery taken a year later. Since updating pre-existing geospatial datasets by indicating and classifying long term change resulting from a fire is the objective of this research, using Landsat TM imagery a year after the fire event was appropriate.

5.2.2 Pre-Processing

Geometric correction of the two Landsat images was not necessary, because both image edges matched when comparing the Shenandoah River and numerous agricultural fields. The data received from the USGS was already terrain-corrected to account for

topographic distortions and converted to at-satellite-reflectance to adjust for the effect that a change in the sun's illumination angle. The only abnormality was the appearance of diagonal stripes.

Using Leica's ERDAS Imagine 8.7 software, the radiometric enhancement tool Destripe TM Data was used on both images to reduce the visual and spectral distortion. The Destripe enhancement reduced the gaps, or areas of no data present in the images' histograms. While not fully removing the striped appearance in either image, the post-fire image, especially in the burned area, was greatly improved.

Because each image's histogram had been altered slightly due to the destripe enhancement, the radiometric enhancement, histogram match was performed. Destriped versions of the pre- and post-fire image were matched, with the post-fire image matched to the pre-fire image chosen for additional analysis, because the striped appearance was diminished the most.

Atmospheric normalization of the Landsat images used was not performed, because of an inability to locate areas large enough to collect spectral signatures representing the same object (e.g., river, field, road, etc.). However, this did not cause any discrepancies in the resulting data transformations. According to the USGS EROS Data Center for National Programs including the National Burn Severity Mapping Project, the USGS does not perform atmospheric normalization. As noted in the Normalized Burn Ratio user's guide, the improvements (if any) are not worth the time and effort (Key and Benson, 2004).

No spatial enhancements were done to the images, due to the desire to preserve the mosaic pattern of burn intensities. Because of Landsat's large spatial resolution and

the Rocky Top fire's impact on only 1,500 acres, any filter applied would likely cause the image to lose spatial information, aggregating pixels of dissimilar values together. Since the objective of this research project is to discern areas of different fire severities, the pixilated appearance of any classification was not of concern.

5.2.3 Data Transformations and Spectral Enhancements

Spectral enhancements and data transformations were applied to the images with the goal of revealing any hidden spectral patterns. The two spectral enhancements applied were the Normalized Differenced Vegetation Index (NDVI) and the Tasseled Cap, with a third data transformation, the Normalized Burn Ration (NBR), applied as well. While the NDVI and Tasseled Cap techniques were not designed specifically for burn detection, they are regularly used in post-fire analysis because they discriminate areas of change resulting from a wildland fire (Viedma 1997). NBR based on Landsat TM imagery and Western U.S. wildfire data was designed as an indicator of burn severity upon vegetation.

5.2.3a Normalized Differenced Vegetation Index

For this research study, three NDVI images were created: a pre-fire, a post-fire and a differenced NDVI (dNDVI) image. The NDVI data transformation is a standard option within Leica's ERDAS Imagine software. The following equation was applied to one image at a time, resulting in two NDVI images (pre and post) being created. An NDVI image is created by the following equation; where Landsat Band 4 is subtracted from Landsat Band 3 then divided by the sum of Landsat Bands 3 and 4.

NDVI = Band 4 – Band 3 / Band 4 + Band 3.

For further classification, a dNDVI image was created to show the varying levels of green biomass, gain and loss. In this equation the pre and post NDVI image created are contrasted, allowing for a range (positive and negative) of spectral responses to be documented. Using spatial modeler, the pre-fire NDVI classification is subtracted from the post-fire NDVI classification as seen below:

dNDVI = preNDVI – postNDVI.

The resulting dNDVI image had a wider index of values when compared to the post-fire image and therefore was used for further classification. The resulting range of spectral responses was from –163 to +68. Negative numbers represented areas where the living green vegetation decreased from a pre- to post-fire image. The closer to zero, the more likely that that area had remained the same landcover in both images. Positive numbers represented areas in which living green vegetation increased from a pre- to post-fire images; in both instances the greater the number the greater the magnitude of change.

After creating the initial dNDVI classification, the Rocky Top Fire perimeter delineated by SHEN park officials was overlaid and then pixel values within the burn perimeter were scaled. Beginning with classifying areas of high severity, five classes were used to categorize the landscape in and around the Rocky Top fire. As values were assigned to a category, they were analyzed on a thematic map to see where the corresponding pixel was in spatial relation to other pixels of similar and dissimilar values. With no established breakpoints determining the different levels of burn severity, classifying the NDVI image was a trial-and-error process.

The following break points were used to classify the dNDVI classification (Appendix C). Non-burned areas, -163.0 to +10.0, light surface burned areas, 10.01 to 15.0, moderate surface burns, 15.01 to 30.0, moderate mixed burns, 30.01 to 47.0, and high severity burns 47.01 and above.

5.2.3b Tasseled Cap

Wildland fires not only alter existing vegetation, but they modify soil properties and change moisture levels within a forested area as well. Three vegetation characteristics are mapped when utilizing the Tasseled Cap data transformation: brightness, greenness, and wetness. These measures can be used to detect a fire's severity not only upon vegetation but also across the entire landscape.

An advantage that Tasseled Cap has over other change detection techniques is that it requires only one image to determine the effects of a wildland fire. The Tasseled Cap data transformation is a standard option within Leica's ERDAS Imagine software. For this research project, all the software defaults related to the Tasseled Cap, search window and matrix, were kept. Tasseled Cap applies the same matrix to all TM bands. While possible to view all six bands at once in pseudo-color, or in various band combinations, only Band 3 was utilized in this research project; primarily because this band provided the greatest index within the burn perimeter. Higher numbers represented areas with more wetness, greenness and brightness, while lower (negative) numbers represented areas having little to no wetness, greenness, and brightness.

After creating the initial Tasseled Cap classification, the Rocky Top Fire perimeter delineated by SHEN park officials was overlaid and then the pixel values

within the burn perimeter scaled. Following the same procedure used for the NDVI classification, different levels of burn severity were established. Again with no established breakpoints to determine the different levels of burn severity, classifying the Tasseled Cap image was a trial-and-error process.

The following break points were used to classify band 3 of the Tasseled Cap data transformation: +48 to 13.01 representing non-burned areas, 13.0 to 10.01 light surface burns, +10 to –9.99 moderate surface burns, -10.0 to –23.99 mixed burns, and –24 to –128 severe burns (Appendix D).

5.2.3c Normalized Burn Ratio (NBR)

The NBR was developed after compiling large amounts of multi-spectral data on numerous Western US wildfires. Living vegetation is reflected by Landsat TM band 4, while band 7 is absorbed, as a result bands 4 and 7 generally have a profound spectral response after a wildland fire. Band 4 reflectance (near infrared: 0.76-0.90 microns) decreases after a fire, and Band 7 reflectance (mid-wave infrared: 2.08-2.35 microns) increases after a fire. The difference between band 4 and 7 exhibited the greatest variation of change when compared to other bands therefore providing a good measure of a fires effect (Key and Benson, 1999).

To start the NBR transformation, a pre-fire image and a post-fire image were created. Unlike the two previous data transformations, NBR is not found within Leica's ERDAS Imagine software. Using spatial modeler, Band 4 was subtracted from Band 7 and divided by the sum of Band 4 and Band 7 (see formula A below). This approach was

applied to both pre-fire and post-fire images. Both images were saved as continuous data with values ranging from –1 to 1.

A) $$NBR = \frac{Band\ 4 - Band\ 7}{Band\ 4 + Band\ 7}$$

B) $$dNBR = (preNBR - postNBR) * 1000$$

To create a quantitative measure of the burn, a differenced NBR (dNBR) image was created (see formula B above). Again, using spatial modeler the two NBR images were subtracted from each other, and multiplied by 1000. The resulting dNBR image expressed the fire severity, with pixel values ranging from –1,674 to + 1,791. Pixel values around zero represented unburned areas; a lower negative score represented areas of vegetation growth (lighter) caused by a low intensity surface burn while the higher the positive pixel value, the more severe the burn event (darker).

After the initial classification, the Rocky Top Fire perimeter as delineated by SHEN park officials was overlaid and pixel values within the burn perimeter scaled. Following the same procedure used for the NDVI and Tasseled Cap classifications, different levels of burn severity were established. In total five classes were used to classify the landscape in and around the Rocky Top fire. The dNBR classification used severity breakpoints recommended by the authors, Key and Benson. This allowed not only for a quicker classification but a classification based on past research, unlike the two previous techniques.

The following break points, slightly different than the previous classifications, were used to classify the dNBR classification: -1675.0 to –30.0, slight surface burns, -29.9 to +53.0 unburned areas, 53.01 to 270 moderate surface burns, 270.01 to 645 mixed burns, and 645.01 to 1,791 severe burns (Appendix E).

5.2.4 Comparison of Data Transformations

To focus field work efforts, the results of the above data transformation techniques were compared. Nineteen Composite Burn Index (CBI) plots, (Figure 17), eight initial and eleven extended assessments, were used to make a rapid evaluation of the NDVI, Tasseled Cap, and dNBR classifications. Using the Intersect Point Tool of Hawth's Analysis Tools, the CBI plots were given the gridcode value of the three classifications. These codes were then compared to the corresponding CBI plot numbers (Table 4). A CBI value of 0.0 indicates a slight burn event, while a 3.0 represents a landscape impacted greatly by a burn event. As the CBI values increase the severity level of the fire increases as well. Comparison of the 19 CBI plots suggested that the dNBR classification was better suited at classifying the Rocky Top's burn severity, when compared to the NDVI and Tasseled Cap classifications.

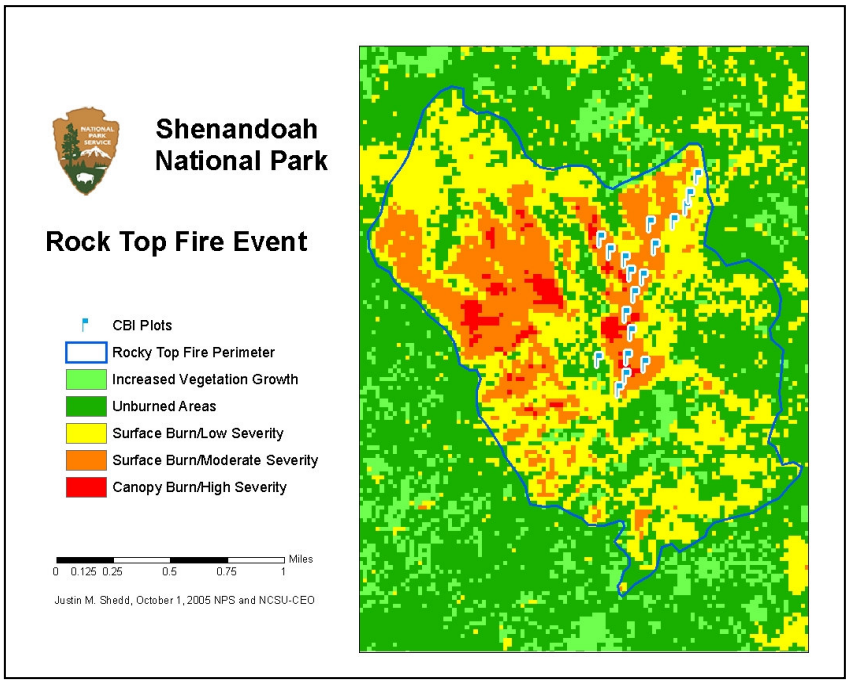

Figure 17: Locations of CBI plots used to validate remote sensing classifications.

NDVI	Tasseled Cap	dNBR	CBI values
2	1	2	0.27
2	3	3	0.72
2	3	3	0.73
2	3	3	0.99
3	4	4	0.99
3	4	3	1.04
3	4	4	1.20
4	4	4	1.36
3	5	4	1.46
4	3	4	1.61
5	3	4	1.75
3	4	4	1.84
4	4	4	2.12
3	4	4	2.14
3	4	4	2.39
3	4	4	2.60
3	4	4	2.60
4	4	4	2.60
4	4	4	2.78

Table 2: Comparison of CBI values with NDVI, Tasseled Cap and dNBR classifications.

5.2.5 Preparation for Field Work

Validation of dNBR classification with field work was based on the sampling protocol developed by SHEN park officials (Carmichael and Cass, 2001) that followed a modified Brown's Transect and Burgan-Rothermel Ocular Estimation Protocol. Using Hawth's Analysis Tools, random point generator, and following an unstratified random sampling design, 60 points were distributed throughout the burn perimeter. A 50-foot buffer was placed around the points. Any buffer that crossed two severity classes was removed from further consideration, ensuring that the entire plot would fall within one dNBR classification code. The points meeting this criterion (57 in total) were assigned the corresponding burn severity code. While random in their placement, accessible points were chosen after consultation with SHEN park officials to ensure data collection was

representative of the landscape. Using DNR Garmin version 4.4.2 extension within ArcView 3.3, 57 points were loaded into a Trimble GeoXT and a Garmin 4 hand held GPS receiver.

5.2.6 SHEN Field Work

Field work to validate the remote sensing classifications of SHEN was completed in June of 2005. Due to the mountainous terrain, reliable real-time navigation using the Trimble GeoXT hand held GPS receiver was not always available. As a result, a Garmin etrex hand held GPS receiver was used for general navigation, with the GeoXT used for locating the exact point. At the predetermined point, a three minute fixed positional point was taken to determine the exact location of the plot. At the plot, a National Park Service protocol (Carmichael and Cass, 2001), developed by SHEN including Brown's Transects and Burgan-Rothermel Ocular Estimations was followed.

For each plot, field measurements were recorded on an HP rugged tablet PC tr3000 laptop computer into a Microsoft Office Access 2003 database. Fifty foot transects were laid in the North and East cardinal directions. Slope measured in degrees was taken along each transect. Fine woody debris consisting of 1-hour (0.0 to 0.25 inch in diameter), 10-hour (0.25 to one inch), 100-hour (one to three inches), and 1000-hour (> three inches) or coarse woody debris, along with litter and duff measurements were made along transects. All downed woody debris (1-, 10-, 100- and 1000-hour) was tallied for the first six feet of the transect line. From six to 12 feet, only 10-, 100-, and 1000-hour fuels were recorded. Beyond 12 feet to up to 50 feet, only 1000-hour fuels were tallied. Duff and litter measurements were made at the one-foot mark then repeated at the five-

foot mark and every five feet thereafter until reaching the 45-foot mark. Duff and litter measurements were made to the nearest tenth of an inch.

Burgan-Rothermal Ocular Estimations were collected for the area between the two transects. For each plot qualitative (type) and quantitative (bulk density) measures of grasses, shrubs and trees were recorded. Characteristics of the litter (e.g., source and compactness), were recorded. Four photographs were taken at each plot along the North transect, East Transect, middle of plot and canopy of plot, to serve as a later reference and to be linked to the Microsoft Access database. Field measurements were collected at a total of 17 plots throughout the Rocky Top Fire's perimeter (Figure 18).

5.2.7 Fuel Load Calculation

The amount of downed woody debris measured in the field was calculated using the equation provided in Brown's Handbook. Using this formula, fuel loading in tons per acre was calculated for fine and coarse woody debris. This calculation is based on the number of intersects for each transect line, average squared debris diameters, specific gravity, slope correction factor, and transect line length. All data used to calculate the fuel load of a plot was initially entered into a Microsoft Office Access 2003 database via the HP rugged tablet PC and later exported into a Microsoft Office Excel 2003 spreadsheet for further data analysis.

5.2.8 Post Processing

Each night the GPS measurements were post-processed to reduce the effects of satellite location and ionospheric interference that cause inaccuracies in GPS data, especially since real-time differential correction was not always available. Post-processing was done using the Pathfinder Office version 3.0.

5.3 Field Work Recap

At PETE, field measurements were collected at 24 plots, (Figure 14, 15, and 16) throughout the battlefield, with most located in the Eastern Front. The first day of field work consisted of validating Feature Analyst's ability to indicate downed woody debris. The remainder of the field work followed protocols for Brown's Transects and Burgan Rothermel Ocular Estimations. At SHEN, field measurements were collected at 17 plots (Figure 18). Field measurements adhering to Brown's Transects and Burgan Rothermel Ocular Estimation Protocols were collected at each plot. Field measurements and ocular estimates from both study sites were used to validate the remote sensing techniques used in this study to confirm their ability for use in updating pre-existing geospatial datasets.

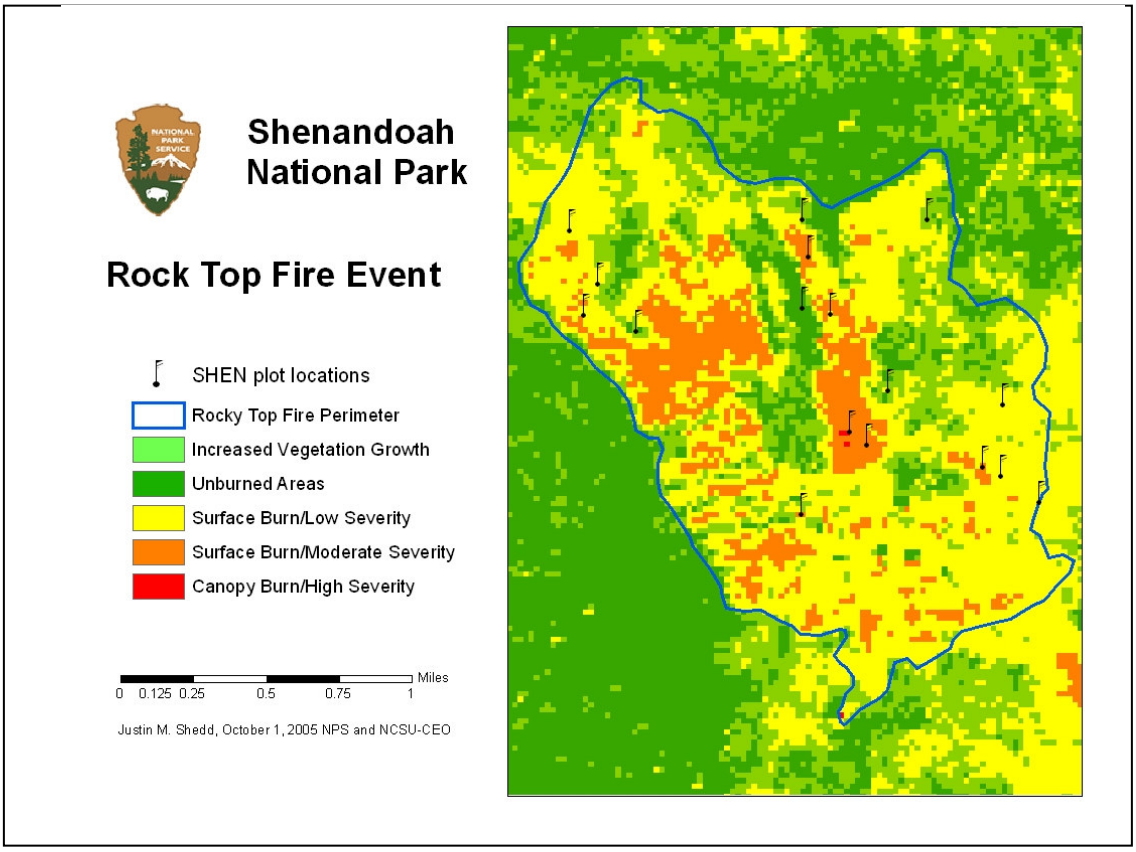

Figure 18: Locations of plots where Brown's Transects and Burgan Rothermel data were collected.

5.4 Creation of FARSITE Layers

To determine the effects of the changed fuel loads the fire behavior model, FARSITE version 4.1.0 was used. The National Park Service requires that each park provide a fire management plan that describes resources available, outlines a potential plan of action in the event of a wildland fire and highlights hazardous areas that may have the potential to cause damage to park resources and neighboring areas. The use of the fire behavior model FARSITE, allows park managers to make informed decisions on issues related to prescribed and wildland fire management.

To operate FARSITE, five spatial data layers are required: aspect, canopy closure, elevation, fuel model, and slope. Other spatial data layers such as; stand height, crown

bulk density and crown base height can be used but are not required. All input data layers must represent the same spatial extent and have the same cell size for FARSITE to operate. Using ArcGIS's Spatial Analyst Toolbar, Surface Analysis option, aspect and slope data layers were derived from the digital elevation model (DEM). Each data layer was set to match the extent and cell size of the DEM. For PETE the output cell size was set to 10 meters. While at SHEN the output cell size was set to 17 meters, matching that of the Fuel Model and Canopy Closure datasets.

The canopy closure data layer for PETE was created using the NVCS formation code attribute of the existing vegetation data layer. FARSITE allows canopy closure to be entered in one of three ways: as an exact number, categorically (1-4), or as a constant number. When the original PETE vegetation dataset was created (Millinor 2001), canopy closure was not one of the attributes collected. Using the same methodology employed by Smith (2003), each vegetation formation polygon was assigned a canopy closure percent based on the average canopy closure percent of the polygons visited of the same formation, except in areas mapped as forest damage. Forest damage areas were assigned the average percent canopy closure of the 24 plots visited, 10 percent. With the majority of PETE's canopy closure derived from outside park data sources, it was concluded that in lieu of using an actual number, the categorical approach would be used. Canopy closure Category 1 represents 1 to 25 percent coverage, Category 2 represents 26 to 50, Category 3 represents 51 to 75 and Category 4 represents 76 to 100. For areas with no canopy, zero was entered. The canopy closure layer was created by adding a field to the vegetation attribute table, assigning a value from 0-4, based on the formation code. Evergreen forests (I.A.), deciduous forests (I.B.), and mixed evergreen-deciduous forests

(I.C.) were assigned 4, except areas of forest damage, which were assigned 1. Areas classified as: evergreen shrubland (I.I.I.A.), Perennia graminoid vegetation (V.), transportation, commercial, residential, agriculture, or reservoir were assigned 0 (Grossman, 1998).

The SHEN canopy closure data layer was created by following the guidelines of the Fire Behavior Prediction Fuel Models Crosswalk currently in development by SHEN and USGS officials. Again, canopy closure was assigned categorically. Two canopy closure data layers were created, pre-and post-fire. To create the pre-fire data set, categories (1-4) were assigned to the vegetation polygons based on the appropriate crosswalk values. To create the post-fire canopy closure data layer the average canopy closure value of the plots, per dNBR category, were used to assign new categories. For areas classified as dNBR classes 1, 2, and 3, the same pre-fire canopy closure values were assigned, while for areas classified as dNBR class 4 and 5 a canopy closure values of 1 was assigned. For both PETE and SHEN the canopy closure data layers were then converted to a grid based on the canopy closure attribute. Cell size and extent were set to the specifications mentioned earlier, as required by FARSITE. Each grid was then converted to an ASCII text format, using ESRI's ArcToolbox.

To validate the need for updating the fire fuel load spatial datasets after the respective landscape altering event had occurred several fuel model grids were created; a pre-event, a post event and an alternative post-event. An alternative post-event grid was created to further document the differences in similar fire fuel models. The differences of the fire fuel models were expressed by using the fire behavior model FARSITE. For PETE, a pre-hurricane (Fuel Model 8 and 9), original post-hurricane (Fuel Model 10 and

13), and alternate post-hurricane grid (Fuel Model 12 and 13) were created. For SHEN, the pre-fire fuel model dataset, (that was near and within the Rocky Top Fire's perimeter) was assigned to fuel model 6, with a few areas of 8 and 9. The post-fire fuel model dataset was assigned the values based on the dNBR classification. Areas classified as dNBR 1, 2, or 3 were not changed from the original dataset; while areas classified as dNBR 4 and 5 were assigned fuel model 5. The alternative post-fire fuel model dataset used the same fuel models as the pre-fire dataset; with only areas previously called fuel model 9 changed to fuel model 8. Each fuel model grid, six in total, was converted to an ASCII text format as required by FARSITE.

Wildland fire spread is highly dependent upon local weather and wind patterns. To run a simulation in FARSITE, weather (.wtr) and wind (.wnd) files must be created. The .wtr file represents, the high and low temperatures, time of day at which the high and low temperatures were reached, high and low relative humidity, cloud cover, and daily precipitation for the area. The .wnd file represents the hourly wind speed and direction for the area. These files can be created using actual daily weather data or from a historic daily or monthly average. For this research, instead of using average historical weather and wind data, actual daily weather and hourly wind data were used. For PETE the weather and wind files used were created from the James City remote automated weather station (RAWS) approximately 30 miles east of PETE. Data from this site is available online at http://www.wrcc.dri.edu/cgi-bin/rawMAIN.pl?ncVJAM. Data were entered into a space delimited text file representing the weather and wind for the dates of August 2nd – August 9th 2005.

For SHEN the weather and wind files used were from the Umholt RAWS weather station. Data from this site is available online at http://www.wrcc.dri.edu/cgi-bin/rawMAIN.pl?ncVUMH. Data were entered into a space delimited text file representing the weather and wind for the dates of July 6th - July 11th 2003, the time frame in which the Rocky Top Fire started.

Two more files are required in order to run the FARSITE simulation: an adjustment (.adj) and an initial fuel moisture (.fms) file. The .adj file represents data to adjust or fine tune the observed or actual fire spread patterns for the area. For this research project the .adj file used in FARSITE simulations was the default file provided by FARSITE. The .fms file represents the moisture contents of 1-, 10-, and 100-Hour woody debris in addition to live herbaceous and woody material. Determined by size, weather conditions and exposure to wind and sun, the presence or absence of fuel moisture affects the conductivity of a fuel and thus the rate of a fire's spread by the flame front (Finney, 2004). The fuel moisture contents of the 1-, 10-, and 100-Hour fuels were provided as part of the average daily weather data collected from the RAWS sites, while the live herbaceous and woody material moisture content was assigned based on professional opinion (KellyAnn Gorman, SHEN Fire Ecologist and Gregg Kneipp, Fire Management Officer, FRSP). With all required data files, spatial and numeric created, the FARSITE simulations were ready to begin.

The five required spatial data layers in ASCII format were uploaded into FARSITE, creating a landscape (.lcp) file. The landscape file was then added to a project file (.fpj) where the .wtr, .wnd, .adj, and .fms files are input. A burn period file (.bpd) was then created. This file set the daily burning constraint, the time that an active fire

can occur (8am to midnight), and matched the duration of the weather and wind files. Before finalizing the .fpj file, an ESRI shapefile representing park roads and rivers (firebreaks) was added. This file restricted the FARSITE simulation, preventing a fire from spreading in certain directions.

In order to start the simulation, an ignition point must be chosen. For PETE, using Hawth's random point generator, a point was placed inside a polygon that represented areas of high visitor impact and areas of forest damage. This point was saved as a separate shapefile and opened in FARSITE as the ignition file. For SHEN, a randomly chosen point within the Rocky Top Fire perimeter was used for the simulations. This point was saved as a shapefile and opened in FARSITE as the ignition file. For both study locations the same ignition point was used for all FARSITE simulations.

6. RESULTS

To quickly recap both study sites: at PETE, hurricane damage was mapped using Feature Analyst. Field work was performed to validate the Feature Analyst's results and to collect field measurements following Brown's Transects and Burgan-Rothermel Ocular Estimations. At SHEN, the Rocky Top Fire had affected nearly 1,500 acres of mountainous terrain. Using the NBR data transformation, vegetation change as a result of the fire was classified. Field work following Brown's Transects and Burgan-Rothermel Ocular Estimations was done. To validate the classification methodologies and test the variability of FARSITE simulations; the data input, fuel model was adjusted.

Given the different situations, results of the field work will be discussed in separate sections: PETE in section 6.1, SHEN in section 6.2, and the FARSITE simulation results in section 6.3.

6.1 Petersburg National Battlefield

6.1.1 PETE Results

Validation addressed two objectives: 1) the ability of Feature Analyst to identify downed woody debris and 2) to collect field measurements in areas indicated by Feature Analyst.

6.1.2 Feature Analyst Results

Feature Analyst excelled in its ability to identify areas of downed woody debris. Forty points, 20 representing damaged and 20 representing non-damaged areas, were used to validate Feature Analyst's mapping results. All of the points labeled damaged had downed woody debris within three meters of the predetermined point. Of the points

labeled non-damaged, 16 of the 20 points did not have any downed woody debris within three meters for an overall accuracy of 90% (Table 3). These values were tabulated to provide the errors of omission and commission. An omission error occurred if Feature Analyst failed to indicate downed woody debris that was observed on the ground as actually having downed woody debris within three meters. A commission error occurred if Feature Analyst identified downed woody debris, but downed woody debris was not observed at the point on the ground. Points misidentified, called non-damaged but actually were damaged, were found in areas where coniferous species dominated.

		Reference				
		Damage	No Damage	Total	Commission Error	% Commission Accuracy
Classification	Damage	20	0	20	0	100
	No Damage	4	16	20	4	80
	Total	24	16	**40**		
	Omission Error	4	0			
	% Omission Accuracy	83	100			***Overall 90***

Table 3: Error Matrix of Feature Analyst Classification at PETE.

6.1.3 Fuel Loading Calculation

The fuel loading values for PETE were calculated by entering the downed woody debris information collected in the field following the formula developed by Brown (1974).

0 to 3 inch downed woody material $\frac{11.64 * n * s * a * c}{Nl}$

3 + inch downed woody material $\frac{11.64 * \sum d^2 * s * a * c}{Nl}$

Where n is the number of downed woody intercepts along the transect line, d^2 is the squared average diameter for each class, s is the measure of specific gravity, a is the non-horizontal angle correction factor, c is the slope correction factor, and *Nl* is the total length of the transect plane. Information collected in the field was entered into the formula above with results tabulated in an Excel spreadsheet (Appendix C).

Fuel loading for the 1-Hour (Figure 19) or 0 to 0.25 inch class showed the least variation among the 24 plots measured at PETE. The smallest fuel load was 0 tons per acre while the greatest was 0.36 tons per acre. The plot recording zero 1-Hour intercepts was located in the flood plain of a stream, which may account for the lack of fine woody debris. The average tons per acre for 1-Hour fuels were 0.135.

Fuel loading for the 10-Hour (Figure 20) or 0.25 to 1.00 inch class varied greatly among the 24 plots. The smallest fuel load measured was 0.304 tons per acre, while the greatest measured was 7.298 tons per acre, which was measured at two different plots. The average tons per acre for 10-Hour fuels were 3.115.

Fuel loading for the 100-Hour (Figure 21) or 1 – 3 inch class varied as well. The smallest fuel load measured, occurring in three plots was 0, while the greatest measured was 10.891 tons per acre. The average tons per acre for the 100-Hour fuels were 3.03.

The number of 1000-Hour (sound and rotten), or fuels greater than three inches increased dramatically as a result of Hurricane Isabel (Figure 22). The least number of intercepts measured was 1 while the greatest was 21. The occurrence of 1000-Hour fuels greatly increased the total tons per acre of the 24 plots at PETE. The average total tons per acre calculated was 47.83, with the highest calculated at 163.69.

These numbers express a drastic increase in the amount of downed woody material, both in the fine and coarse woody debris classes. Smith's work completed in 2003, recorded the following measurements; average 1-Hour fuel load, 0.084, average 10-Hour fuel load 0.23, average 100-Hour fuel load 0.61, and the average 1000-Hour fuel load 3.11. This validates the need for an updated fire fuel dataset; as large portions of PETE saw an increase in forest fuel loads.

6.1.4 Forest Damage Polygons

The accuracy of the forest damage polygon created to capture 1- , 10-, and 100-hour fuels and help in the quantification of downed woody debris appears to be directly related to the forest canopy cover. As a result, the ability of the forest damage polygons to capture the horizontal continuum of fuels was site dependent; as the three perimeters representing forest damage well were in deciduous forests, the forest damage area not completely representing the full extent was in a mixed forest, and the two forest damage areas that were too general in their classifications were located in coniferous forests.

The ability and inability of the forest damage polygon to accurately represent the horizontal continuum of fuels was determined by Feature Analyst's ability to indicate downed woody debris. Feature Analyst was unable to map downed woody debris in coniferous areas because it could not analyze features under the canopy cover; whereas in deciduous areas downed woody debris was indicated and the forest damage polygon created, adequately predicted the horizontal continuum of fuels.

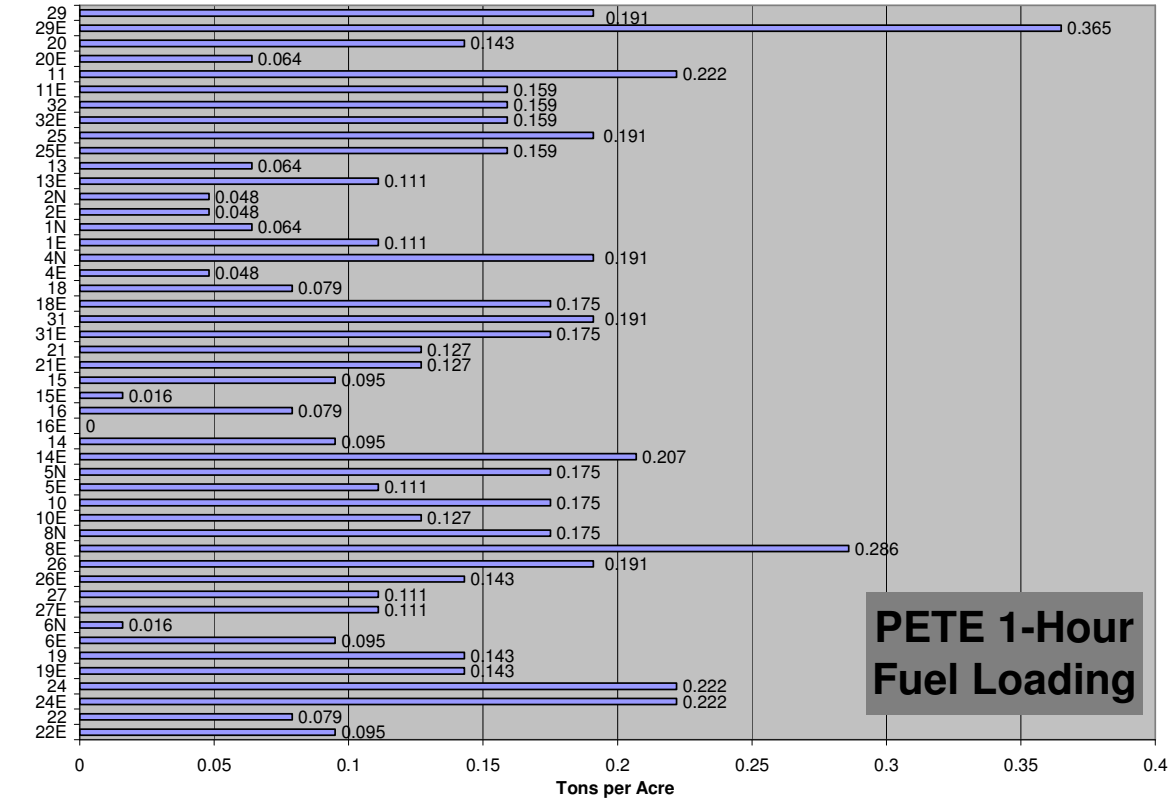

Figure 19: 1-Hour Fuel Loading for plots at PETE.

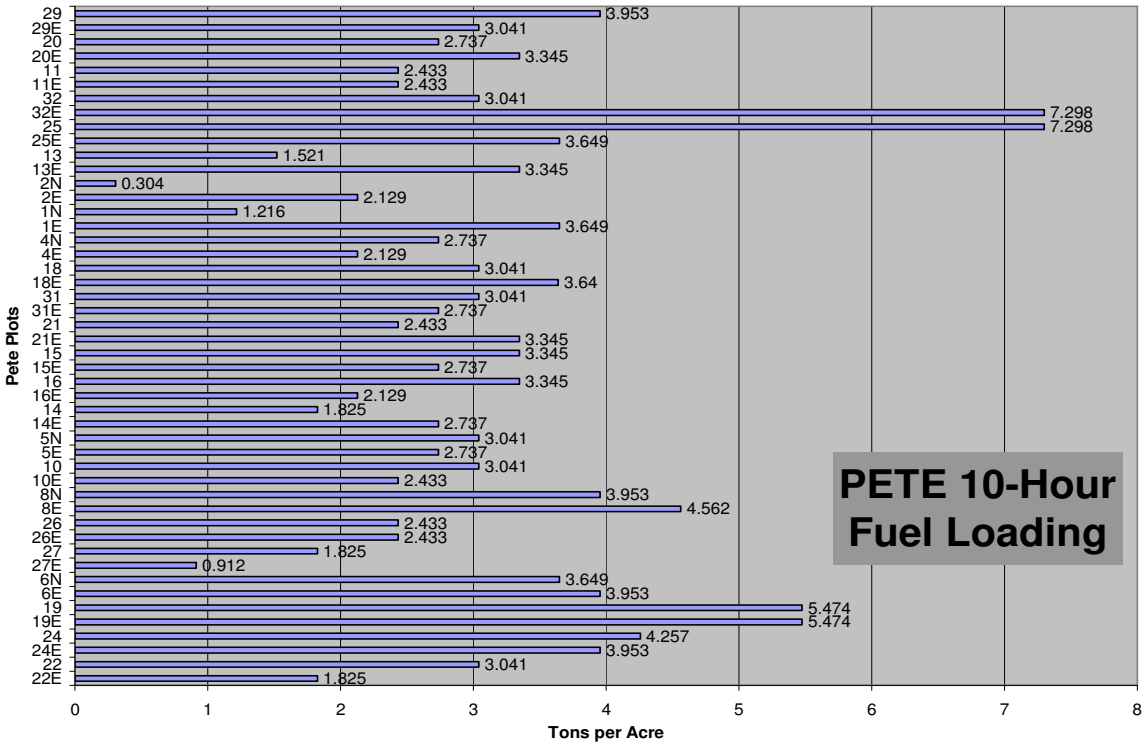

Figure 20: 10-Hour Fuel Loading for plots at PETE.

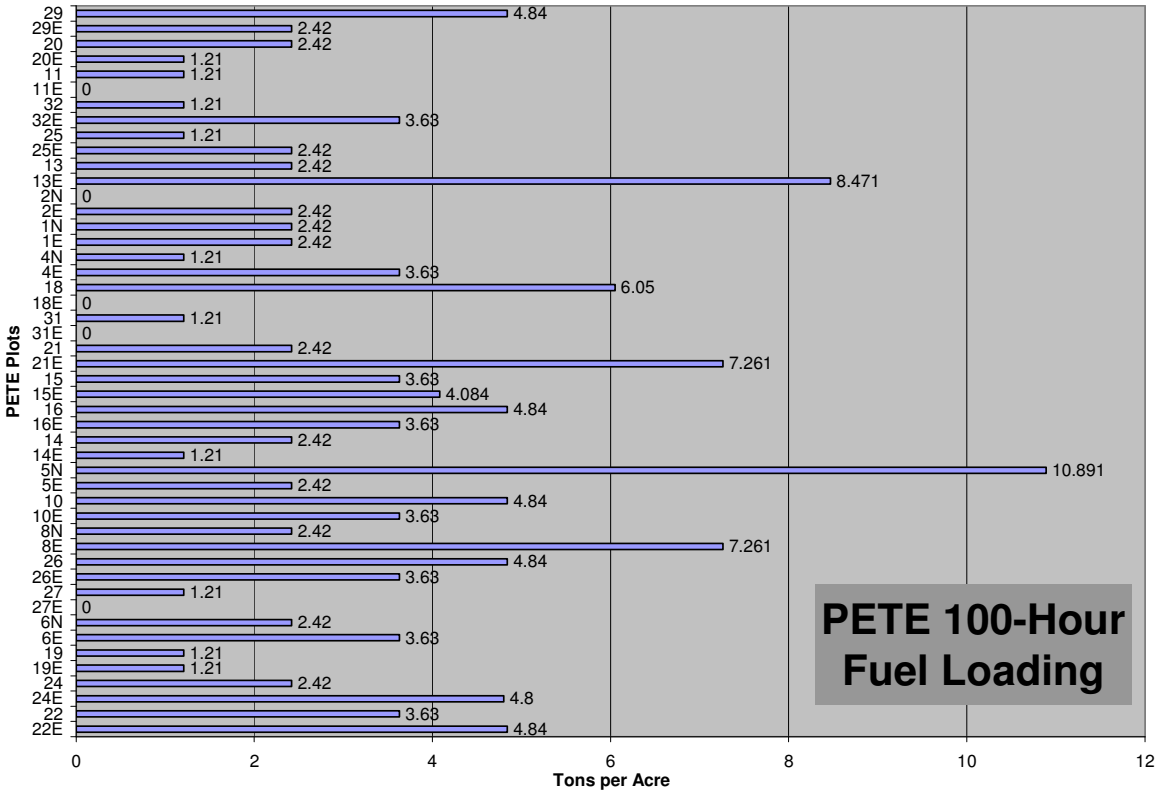

Figure 21: 100-Hour Fuel Loading for plots at PETE.

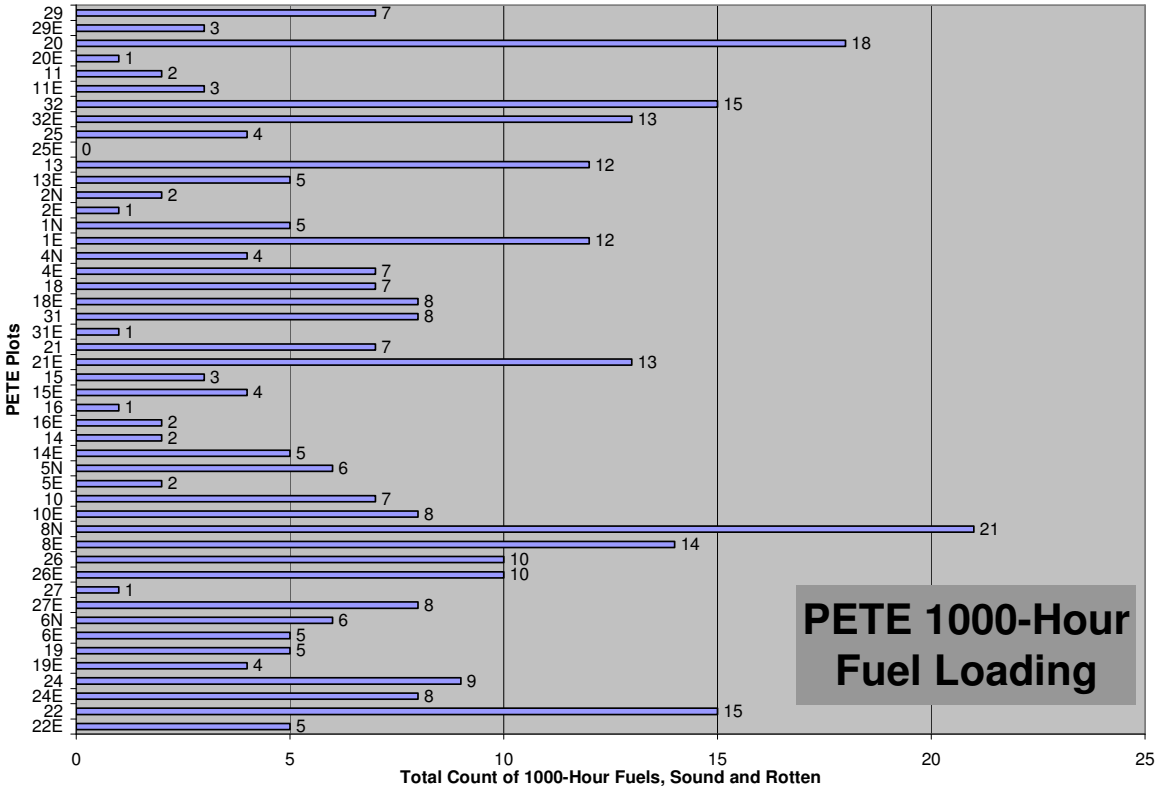

Figure 22: Sound and Rotten 1000-Hour Fuel Counts for plots at PETE

6.1.5a New Fire Fuel Model

The forest damage shapefile was used to map the horizontal continuum of fuels in addition to quantifying the forest damage areas. By calculating the percentage of an area covered by downed woody debris, forest damage polygons were assigned a fuel model.

After completing field measurements it was determined that the percentage of a forest damaged area covered by downed woody debris had no correlation with the appropriate fuel model that was to be assigned. Fuel loading measurements ranged from 27 to 173 tons per acre, with only five plots recording fuel loading measurements matching the guidelines of Fuel Model 12 with the remaining 19 plots recording fuel loadings greater than or equal to that of Fuel Model 13's guidelines. However, after completing initial FARSITE simulations and discussing the outputs with fire-behavior professionals, it was decided that assigning fuel models based on the anticipated fire behavior of the landscapes, instead of following the fuel loading guidelines, was a more appropriate approach. Therefore, for the fire fuel model dataset (Appendix D) Fuel Model 10 was assigned to most polygons because of the abundance of smaller fuels and suggestions of KellyAnn Gorman, SHEN's Fire Ecologist. Fuel model 13 was chosen for all other forest damaged areas, because of the appearance of flash fuels (red slash). This was consistent with previous work completed by Doug Raeburn, former NPS fire ecologist (KellyAnn Gorman personal communication, 2005).

6.1.5b New Vegetation Spatial Dataset

While fuel models were assigned to the forest damage areas, updating the vegetation dataset and assigning the appropriate Nature Conservancy, National Vegetation Classification System (NVCS) formation code was not as straight forward. Field work done at PETE included Burgan-Rothermel Estimations which provided a qualitative measure of the vegetation in a plot.

According to the NVCS classification guideline all forests must exhibit a minimum of 60 percent canopy cover. If less than 60 percent then they are considered woodland. All 24 plot points at PETE had a canopy closure less than 60 percent; overall the average was 26 percent. Strictly speaking these areas were now woodlands, which are characterized as having 25-60 percent canopy cover. Woodlands, however, are not caused by meteorological events, but by environmental gradients like soil depth, soil properties, and rainfall amount. After consulting with NatureServe Ecologists Milo Payne and Don Faber-Langendoen, and University of North Carolina - Chapel Hill Professor Dr. Robert Peet, (personal communication, 2005) the 60 percent artificial breakpoint was disregarded in favor of a classification based on the floristic's of the plot, which in this case resulted in keeping the forest formation codes for the damaged areas.

Since the completion of PETE's original vegetation spatial dataset, by Millinor in 2001, the park has seen an infestation of the Southern Pine Beetle, which has killed the majority of coniferous trees in the park. Some of these areas, particularly in the Eastern Front portion of PETE, suffered windthrown damage and were mapped as areas of forest damage. These are the only areas where the existing NVCS vegetation code was changed. A 2.4 acre area, near the park's visitor center was changed from I.A.8.N.b.,

temperate needle leaved forest to I.C.3.N.d., saturated mixed evergreen cold deciduous forest. Another 1.3 acre area, near the visitor center with the previous formation code of I.C.3.N.a., mixed evergreen cold deciduous forest, was changed to I.B.2.N.a., cold deciduous forest. There were other areas in which the vegetation codes were changed; but these two locations represent the only qualitative type of change made (Appendix E).

6.2 Shenandoah National Park

6.2.1 SHEN Results

To determine the post fire vegetation and fuel loading of the area affected by the Rocky Top Fire, three data transformations were carried out, with the fire's effect or severity upon existing vegetation indicated and quantified. Each data transformation carried out, NDVI, Tasseled Cap, and NBR, resulted in an image with different fire severity classifications.

6.2.2 Classification Comparison

The dNBR classification was chosen as the best available and was to be validated with field work. It was briefly discussed in the previous section, but few specifics were given as to the actual results of the three classification techniques performed. The following paragraphs illustrate their results.

The NDVI transformation (Appendix F) delineated the burn perimeter adequately, except for the southeastern portion, because of spectral irregularities in the image created by the shadow of a cloud. The NDVI transformation was of little assistance when determining the severity of the fire. Few high severity areas were indicated, as the

majority of the burn was classified as moderate severity. Large sections of the NDVI classified image were the same value, resulting in a washed out appearance, especially in areas occurring in the center of the burned areas. The NDVI image appeared to be greatly affected by the shadow of the cloud, expressing these areas (which the cloud's shadow darkened), as areas of moderate severity.

The Tasseled Cap transformation's ability to discern spectral differences in the moisture levels in soils and vegetation allowed for a more precise delineation of the burn perimeter, including areas underlying the cloud's shadow (Appendix G). Areas of different spectral responses within the known burn area were noticed, areas that the NDVI transformation had not been able to detect. The Tasseled Cap transformation was successful at highlighting not only the burn perimeter more effectively, but areas of differing fire severity, when compared to the NDVI transformation. However, there were still large numbers of pixels within the known burned area recorded as the same value.

The dNBR classification (Appendix H) delineated the burn perimeter with more accuracy than the other techniques. The mosaic pattern of the burned area was indicated, as the range of pixel values varied within the burn perimeter, allowing for the delineation of areas experiencing high severity burns. The dNBR classification indicated areas experiencing light surface burns that resulted in an increase of growth in the herbaceous community. Following the recommendations for severity breakpoints outlined in the Landscape Assessment, NBR publication (Key and Benson, 2004), a classification based on past research was quickly reached and unlike the previous classifications which required lengthy trial and error.

Overall, the dNBR classification was accurate, indicating and quantifying the different burn severities that occurred at the Rocky Top fire as indicated by the error matrix (Table 4). Misclassification of burn severity occurred more in the lower severity classes, particularly 1, 2 and 3; than the higher severity classifications. Areas classified as Class 2, non-burned areas, had signs of a burn as indicated by charred pieces of wood and tree trunks recorded and furthermore areas classified as a Class 3, low severity area, were areas experiencing increased vegetation growth.

		Reference							
		Class 1	Class 2	Class 3	Class 4	Class 5	Total	Commission Error	% Commission Accuracy
Classification	Class 1	0	0	0	0	0	0	0	100
	Class 2	2	3	0	0	0	5	2	60
	Class 3	2	0	4	0	0	6	2	67
	Class 4	0	0	1	4	0	5	1	80
	Class 5	0	0	0	0	1	1	0	100
	Total	4	3	5	4	1	17		
	Omission Error	4	0	1	0	0		5	
	% Omission Accuracy	0	100	80	100	100			***Overall 71***

Table 4: Error Matrix of dNBR classification at SHEN.

6.2.3 Fuel Loading Calculation of dNBR Results

The dNBR classification was validated in June of 2005, by field measurements taken at 17 plots located within the Rocky Top Fire's burn perimeter. Brown's Transects were followed in order to calculate the amount of fuel loading present, while Burgan Rothermel Ocular Estimations were followed to record a qualitative measure of the vegetation present. The fuel loading values for SHEN were calculated by following the same method as PETE, which is by entering the downed woody debris values collected in

the field into the formula developed by Brown. Then that data was further analyzed in an excel spreadsheet (Appendix I).

Due to time constraints and inaccessibility because of mountainous terrain, no field measurements were collected at plots located in areas classified as light surface burns or Class 1 (Figure 23). This dNBR class accounted for only 41 out of a total of 1463 acres; which was the lowest of all classes.

Field measurements were made at six plot points (Figure 24) that were located in dNBR class 2, (i.e. not burned). Fuel loading for the 1-Hour or 0-0.25 inch class averaged 0.15 tons per acre. Fuel loading in the 10-Hour or 0.25 – 1.00 inch class averaged 1.63 tons per acre. Fuel loading in the 100-Hour or 1-3 inch class averaged 2.07 tons per acre. The average fuel bed depth was 1.50 inches, the highest of the four dNBR classes in which field measurements were made. The average total tons per acre were 3.98. Three of the plots, exhibited burn scars on the 100- and 1000-Hour fuels present indicating a burn had actually occurred. Each plot had at least 1 inch of accumulated litter, mostly from hardwood leaf litter.

Field measurements were made at five plot points (Figure 25) that were located in dNBR class 3, (i.e. low severity). Fuel loading for the 1-Hour class averaged 0.114 tons per acre. Fuel loading in the 10-Hour class averaged 2.18 tons per acre. Fuel loading in the 100-Hour class averaged 1.31 tons per acre. The average fuel bed depth was 1.21 inches. The average total tons per acre were 3.82. Plot point 33 experienced extensive surface and mid-story burns, but is located at a lower elevation than other points in the same dNBR class. Because of the lower elevation, (and more favorable growing conditions), understory vegetation growth was accelerated. As a result an increase in fine

woody debris was recorded. This plot elevated all of the fuel loading classifications calculations for dNBR class 3.

Field measurements were made at five plot points (Figure 26) that were located in dNBR class 4, (i.e. moderate burns). Fuel loading for the 1-hour class averaged 0.07 tons per acre. Fuel loading in the 10-hour class averaged 1.18 tons per acre. Fuel loading in the 100-hour class averaged 1.51 tons per acre. The average fuel bed depth was 0.18 inches. The average total tons per acre were 3.03. This class had the most recordings of fuels in the 1000-hour class, which may have been caused by the falling of snags after the fire. All 1000-hour fuels were recorded as rotten.

While more plot points representing dNBR class 5 were desired, their remote location led to the collection of data at only one point (Figure 27). Fuel loading for the 1-Hour class was 0.06 tons per acre. Fuel loading in the 10-Hour class was 0 tons per acre. Fuel loading in the 100-Hour class was 1.81 tons per acre. The depth of the fuel bed was 0.22 inches. The total tons per acre for this class was 2.01, the lowest of the four dNBR classes in which field measurements were made.

Appendix J shows each fuel loading class (Fuel Bed Depth, 1-, 10-, 100-Hour) categorized by the dNBR classification.

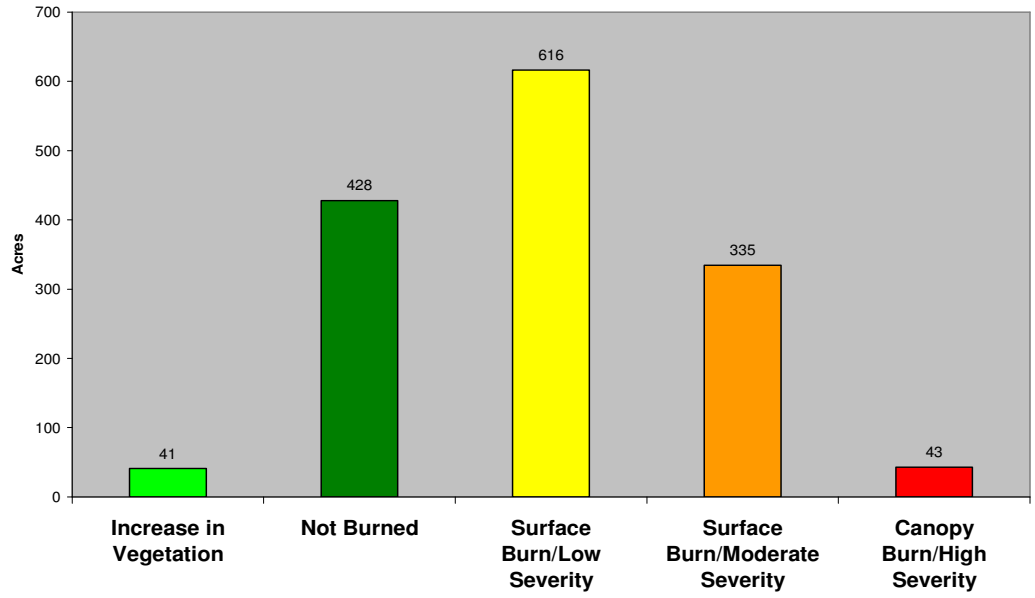

Figure 23: Acreage per dNBR Classification of the Rocky Top Fire

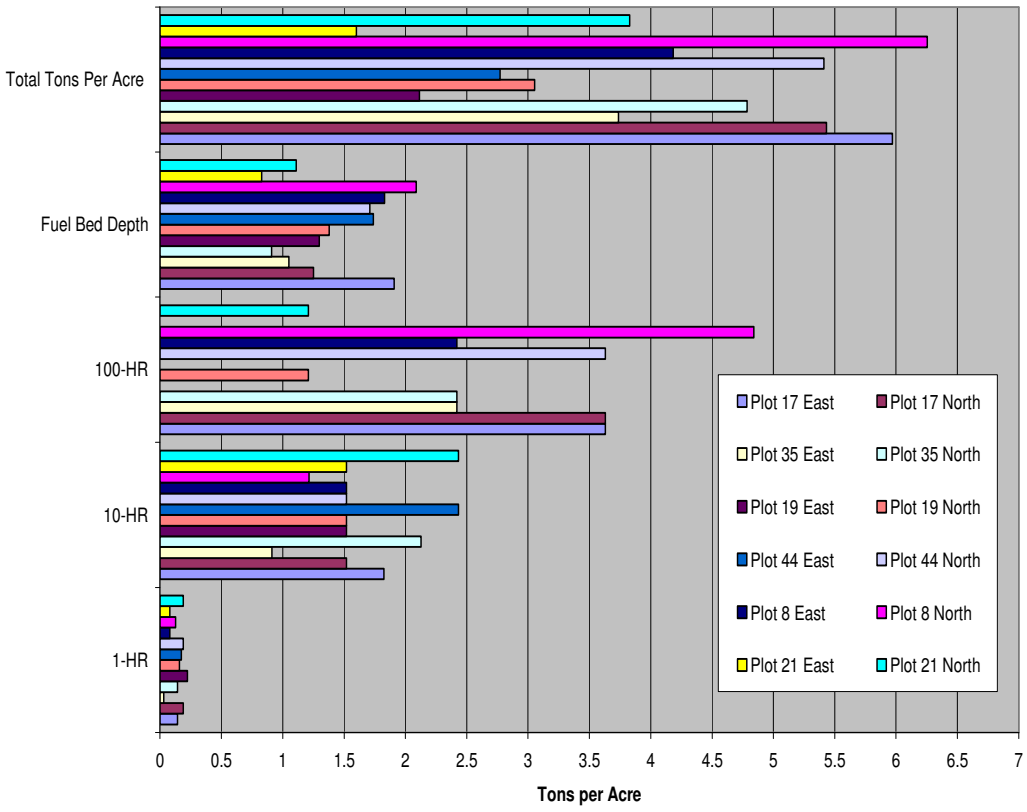

Figure 24: SHEN dNBR Class 2 Fuel Loading.

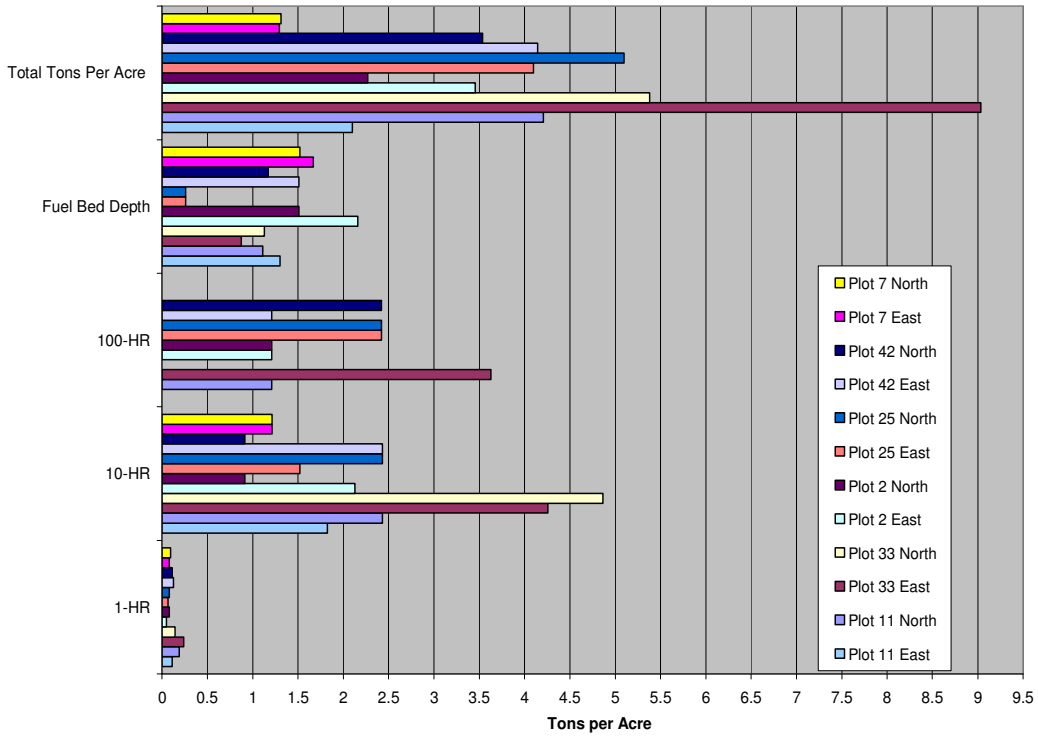

Figure 25: SHEN dNBR Class 3 Fuel Loading

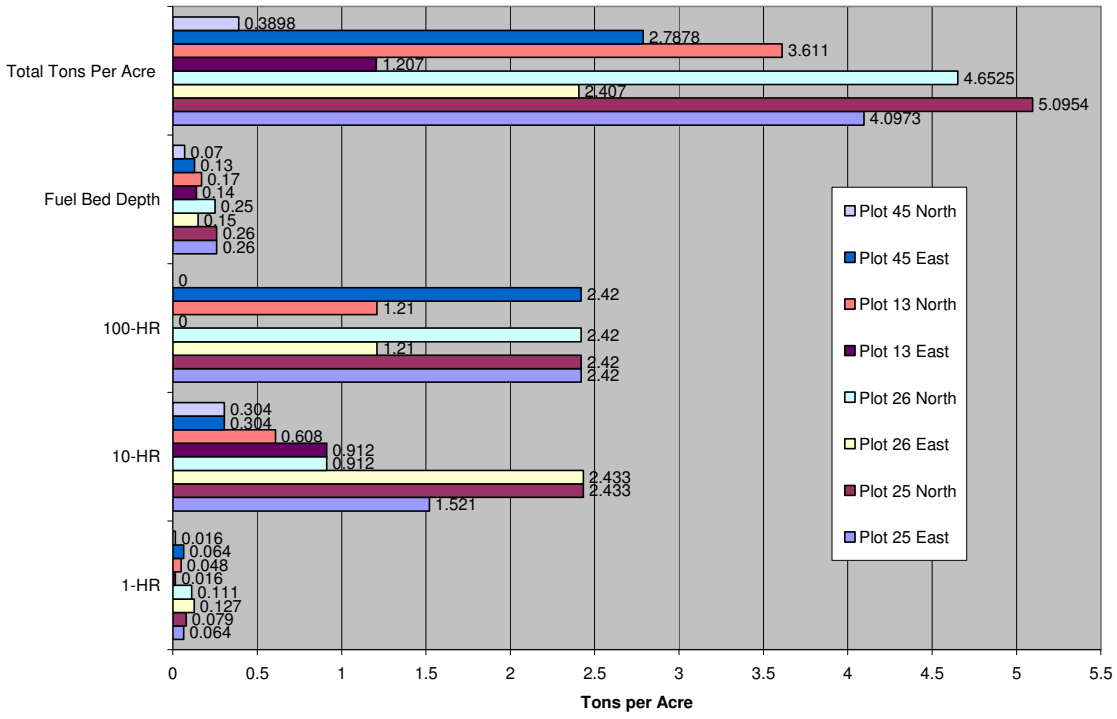

Figure 26: SHEN dNBR Class 4 Fuel Loading

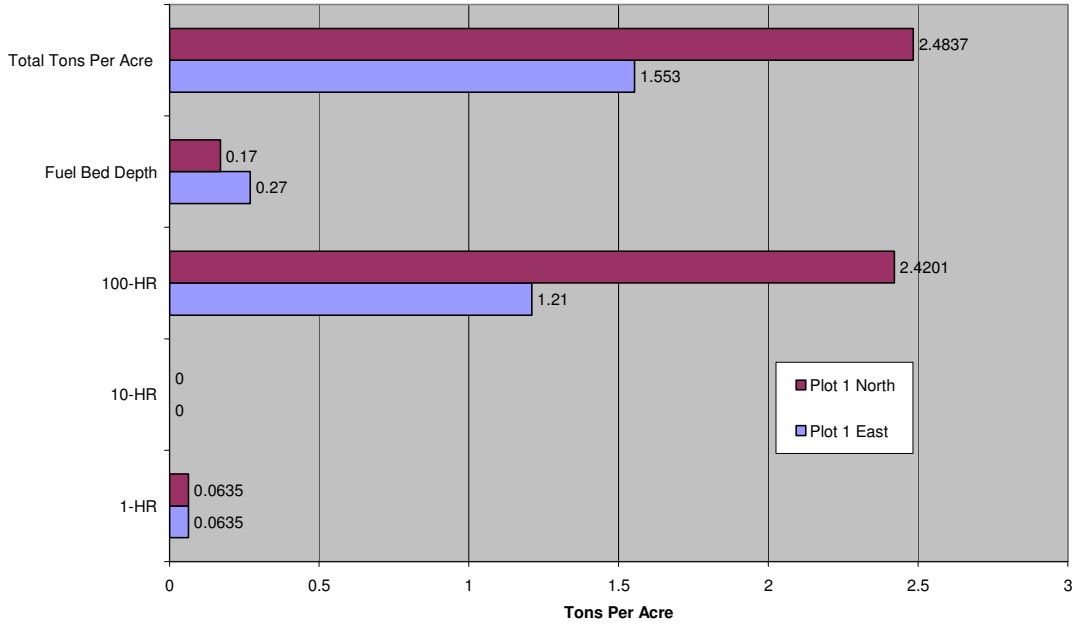

Figure 27: SHEN dNBR Class 5 Fuel Loading

6.2.4 Qualitative Measure of Vegetation

By itself a dNBR classification can not completely update a vegetation dataset. The amount, type and rate of vegetation growth is determined by a combination of environmental factors, such as slope, aspect, elevation, exposure, and rainfall, as well as pre-fire vegetation.

In all plots measured in dNBR class 3 severity, the post-fire vegetation documented was the same as the vegetation that existed before the fire. The forest canopy structure remained the same, as the fire consumed only surface fuels. Plots located within these dNBR classifications had little grass present, on average covering less than three percent of the plot. With an average of 56 percent coverage at a height of three feet, the understories of these plots were dominated by shrub growth. The combination of these factors led to measurable litter and duff in these plots, thus encouraging further vegetation growth.

In plots measured in dNBR classes 4 and 5 severity, post-fire vegetation documented was dominated by pre-existing shrubs (mainly Mountain Laurel) and early successional grasses. On average these plots were covered by 12 percent grass, most commonly Eastern Turkeybeard. Shrub depth, consisting mainly of Mountain Laurel measured 2.5 feet in height and covered 50 percent of the plot. Only one of the six plots had a tree canopy. The high site exposure resulted in increased wind and water erosion that further discouraged plant growth. These plots had no measurable duff and a litter depth of 0.34 inches.

6.2.5a Formation of New Spatial Datasets – Fuel Model

The fire behavior spatial dataset of SHEN is currently being developed from the vegetation dataset. The Fire Behavior Fuel Model Crosswalk, developed by SHEN and USGS officials includes values for the Fuel Model, canopy base height, canopy bulk density, percent canopy closure, maximum stand height, and crown fire potential of the different vegetation types found in SHEN.

Not all of the forest canopy attributes mentioned above were collected, but they can be inferred from the Burgan Rothermel Ocular Estimation data that was collected. After tabulating field measurements and the visual interpretation, the areas classified as dNBR class 1, 2, and 3 did not need to be updated. While a reduction in woody material was seen in dNBR class 3 plots, those areas will soon recover to their original pre-fire state. Therefore, the updated fire behavior dataset for these areas will be the same as the original pre-fire dataset. For the areas classified as dNBR class 4 and 5, the average of the measurements recorded for plots in these areas was used to assign new values to the

canopy base height (in meters), maximum stand height (in meters), and percent canopy closure (categorical). The following values were used to create the updated fire behavior dataset: a canopy base height of 1, a maximum stand height of 5, and a percent canopy closure of 1. The pre-existing fire behavior dataset classified the majority of the burned area as fuel model 6, with some areas classified as fuel models 8 and 9. Fuel model 5 was used for the updated dataset (Appendix K), as the associated fire behavior of Fuel Model 5 is less volatile than that of Fuel Model 6. The current landscape is better represented by Fuel Model 5 because the wildland fire event removed almost all dead woody debris and the landscape is dominated by re-sprouting grasses and shrubs. These landscapes are better represented by Fuel Model 5 as documented by Anderson (1983). In addition, areas that had been classified as Fuel Model 9 were now classified as Fuel Model 8. Fuel Model 8 represents a landscape with less fine fuels when compared to Fuel Model 9, as these fuels were consumed by the Rocky Top Fire.

6.2.5b Formation of New Spatial Dataset - Vegetation

The vegetation map of SHEN was completed by the University of Maryland's Environmental Center using May 2000 and July 2001, AVHRR hyperspectral imagery. A total of 35 alliance level classifications were derived for SHEN. Only 15 classifications were found within the Rocky Top burn perimeter, the majority of which were six classifications, all derivations of an oak forest. The plot points used for this research fell in four different vegetation types, again all oak forests. This does not include one plot that was located outside SHEN's boundary where the vegetation type was not delineated.

For the areas classified as dNBR class 1, 2, and 3, it was determined that the minor floristic changes that did occur did not warrant an update of the vegetation dataset (Appendix L). The areas classified as dNBR class 4 and 5, were updated to the NVCS formation code I.I.I.A.2.N.b., a temperate evergreen shrubland. Because of the dominance of various shrub species, in particular Mountain Laurel and the absence of tree species, the Alliance classification; A.744 Rhododendron – Kalmia Latifolia Shrubland was chosen for the new vegetation dataset (Milo Pyne Personal communication, 2005).

6.3 FARSITE Simulation Results

For PETE three grids were created to test the simulations of FARSITE: the pre-hurricane grid (Fuel Models 8 and 9), the original post-hurricane grid (Fuel Models 10 and 13), and an alternative post-hurricane grid (Fuel Models 12 and 13). For SHEN three different grids were created as well: a pre-fire fuel model (Fuel Model 6), a post-fire fuel model (Fuel Model 5), and an alternate post-fire fuel model (Fuel Model 6).

A total of ten simulations per fuel model dataset, or 60 in total, were run. This was done to not only express the differences seen in simulation outputs when using different data inputs, but to see variation among FARSITE simulations when using the same data inputs. With each FARSITE simulation a polygon shapefile was created that represented the fire's perimeter. In addition, three raster datasets were created representing various characteristics of the fire, specifically the flame length (in feet), the fire line intensity (in British Thermal Units, BTU, per feet per second), and the fire's rate of spread (in feet per minute).

For the PETE FARSITE simulations (Table 5), the fire perimeters using the post-hurricane fire fuel model dataset were the largest, averaging 117.75 acres, but had the greatest variation of total acreage among the simulations at 1.03 acres. FARSITE simulations using the pre-hurricane fuel model were second largest averaging 46.0 acres with a variation of 0.148 acres. Measuring the least in acreage was the FARSITE simulations using the alternative post-hurricane fuel models, averaging 15.86 acres, as well as the least variation, 0.134 acres (Figure 28). Attention must be paid to the scale of each simulation, as it may be misleading.

	Pre-Hurricane Fuel Models 8 and 9	**Post-Hurricane Fuel Models 10 and 13**	**Alt-Post-Hurricane Fuel Models 12 and 13**
Simulation #1	45.8845	117.9496	15.8658
Simulation #2	46.0248	118.3586	15.8658
Simulation #3	46.0248	117.3627	15.9174
Simulation #4	46.0248	117.3627	15.8682
Simulation #5	46.0248	118.3586	15.7897
Simulation #6	46.0248	117.3627	15.8945
Simulation #7	46.0248	117.3627	15.7897
Simulation #8	46.0248	118.3586	15.8658
Simulation #9	46.0248	117.6367	15.9174
Simulation #10	46.032	117.3627	15.8682
Average Acreage	**46.0115**	**117.7476**	**15.8643**
Range	0.1475	0.9959	0.1277

Table 5: FARSITE simulation's for PETE using various fuel models as input data.

For the SHEN FARSITE simulations (Table 6), the fire perimeter using the alternative post-fire fuel model dataset was the largest averaging 1,508 acres per simulation, with a variation of 1.34 acres. The pre-fire fuel model simulations averaged

1,467 acres, with a variation of 0.40, while the post-fire fuel model averaged 1129 acres, with a variation of 0.66 acres (Figure 32).

	Pre-Fire Fuel Model 6	**Alt-Post-Fire Fuel Model 6**	**Post-Fire Fuel Model 5**
Simulation #1	1467.69	1509.04	1130.42
Simulation #2	1467.35	1508.40	1129.81
Simulation #3	1467.35	1508.40	1129.82
Simulation #4	1467.35	1508.40	1129.82
Simulation #5	1467.35	1508.40	1129.86
Simulation #6	1467.35	1508.40	1129.85
Simulation #7	1467.35	1509.04	1129.82
Simulation #8	1467.35	1507.70	1129.76
Simulation #9	1467.29	1508.40	1129.82
Simulation #10	1467.35	1508.40	1129.82
Average Acreage	**1467.37**	**1508.46**	**1129.88**
Range	0.40	1.34	0.66

Table 6: FARSITE simulation's for SHEN using various fuel models as input data.

Flame lengths for PETE simulations (Figure 29) were relatively constant during the entire burning period. The maximum flame length seen in the pre-hurricane and in the alternative post-hurricane fuel model was one foot, which occurred in areas of downed trees. The post-hurricane fuel model simulations expressed the most variation, with two-foot flame lengths recorded in areas of downed woody debris, with other areas mapped as forest damage recording one-foot flame lengths. For SHEN, the pre-fire simulations (Figure 33) recorded flame lengths varying from zero to five feet, most areas experiencing one or two foot flame lengths, with very few areas recording four or five foot flame lengths. The alternative post-fire simulation recorded flame lengths of zero to five feet as well. Again most areas recorded one or two-foot flame lengths, as the canopy closure spatial data layer was the only substantial change among simulations. In the post-fire simulations, flame lengths varied from zero to four feet, with most areas experiencing

one and two foot flame lengths. The majority of the previously burned areas had flame lengths of zero or one foot, with three and four foot flame lengths recorded in areas that had not previously burned.

For PETE, a slower spreading fire (Figure 30) was recorded in the pre-hurricane and alternate post-hurricane fuel model simulations, with the majority of the burn area recording a rate of spread of less than one foot per minute. The greatest fire spread recorded, equaling one foot per minute, was located in areas of downed woody debris. The rate of spread slightly increased in simulations using the post-hurricane fuel model. In small pockets of downed trees, a spread rate of two feet per minute was reached. Again, most areas recorded a rate of spread equal to or less than one foot per minute. For SHEN, the fire's rate of spread (Figure 34) was much faster. The rate of spread for the alternative post-fire simulations, varied from 0 to 34 feet per minute. The pre-fire simulations had similar rates of spread, recording 0-33 feet per minute. The post-fire simulation showed the least variability ranging from 0-24 feet per minute. Faster spread rates, for all fuel model datasets were recorded in areas of high slope, while the slower spread rates (for the post-fire simulations) were recorded in previously burned areas.

Little variation was seen in the fire line intensities of PETE simulations (Figure 31). When the alternative post-hurricane fuel model was used for simulations, BTUs (per second per foot) of zero to six were recorded. Higher BTUs were recorded in areas classified as Fuel Model 9, but not in the areas of downed woody debris which were classified as Fuel Model 11. For the pre-hurricane fuel model simulations, BTUs rose slightly, ranging from zero to eight. The highest BTU occurred in areas classified as Fuel Model 9 and in areas of downed woody debris, which were found in both Fuel Model 8

and 9. For the post-hurricane simulation, BTUs were recorded from 0 to 55, with the highest recorded in areas of downed woody debris (Fuel Model 10). For SHEN simulations (Figure 35) the pre-fire fuel model dataset varied the most, recording values from 0 to 255 BTUs. The alternative post-fire fuel model simulation, recorded values from 0-252 BTUs, while the post-fire fuel model simulation, recorded values from 0-167 BTUs. The areas of the highest BTUs were located in non-burned areas with high slope. The lowest intensities were recorded in the previously burned areas.

For PETE simulations using the pre- and post-hurricane fuel model dataset, it appears that the rate of spread, the flame length, and the fire line intensity are related. While topographic characteristics such as slope had little to do with the fire behavior seen at PETE, "jackpots" or areas of intense fuel loading in an otherwise low fuel loading area (NIFC, http:www.nifc.gov) were the driving force behind the fire simulations. The FARSITE simulations exhibited greater spread rates, flame lengths and fire line intensities in areas classified as Fuel Model 10. Furthermore, the parameters associated with the different fuel models (Fuel Model 10 and 12) were evident, as illustrated by the differences in the burn perimeters of the FARSITE simulations. For the SHEN simulations topographic characteristics like slope were the driving force of the fire line intensity and flame lengths of the output simulations. The different fuel model (Fuel Model 5 and 6) parameters were evident in the post- and alternative post-fire datasets, as the output simulations expressed differences in burn perimeters, spread rates and fire line intensities. The SHEN simulations also demonstrated that the canopy closure dataset (Figure 36) can affect simulation results as well. Higher rates of spread were seen in

areas classified as canopy closure 1 in the alternative post-fire simulation, than in the pre-fire simulations classified as a 3 or 4, despite the same fuel model being used.

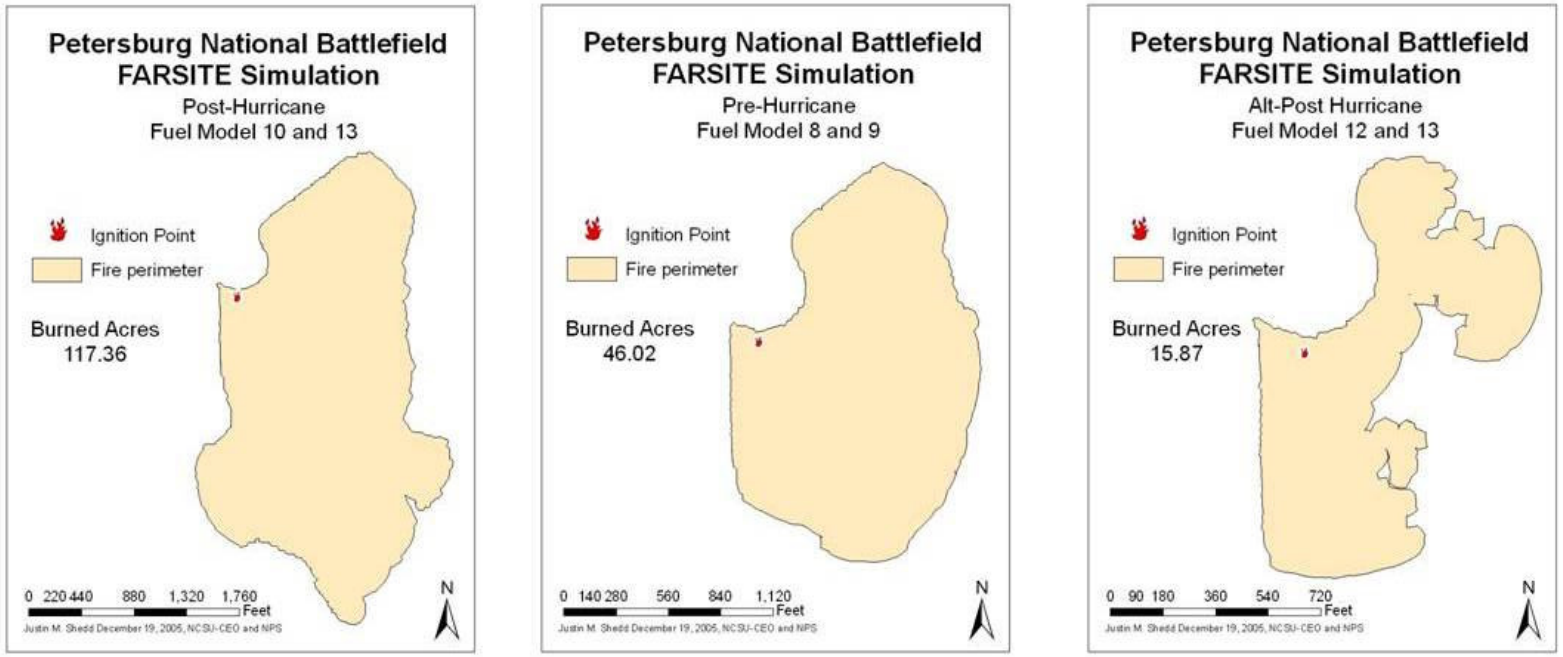

Figure 28. FARSITE, PETE All Perimeters

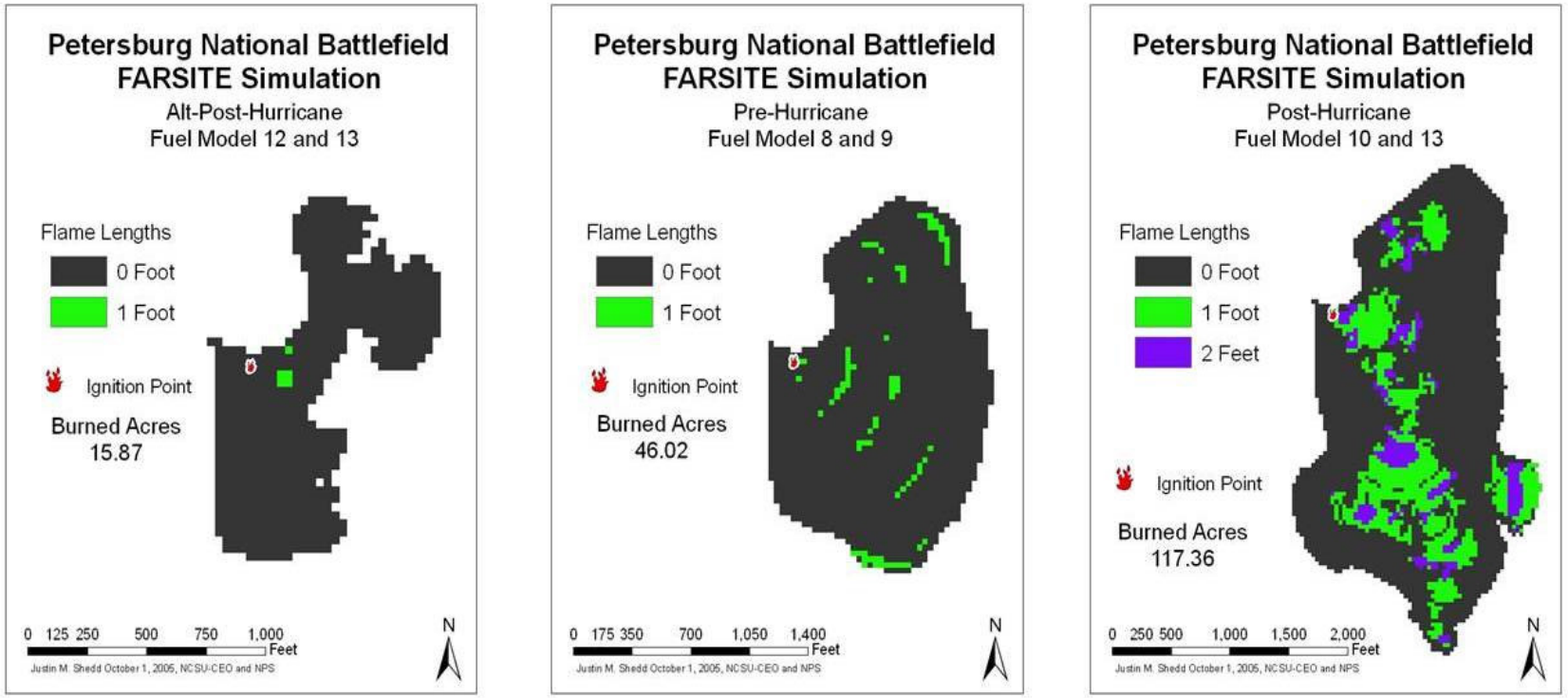

Figure 29. FARSITE, PETE All Flame Length Simulation Results

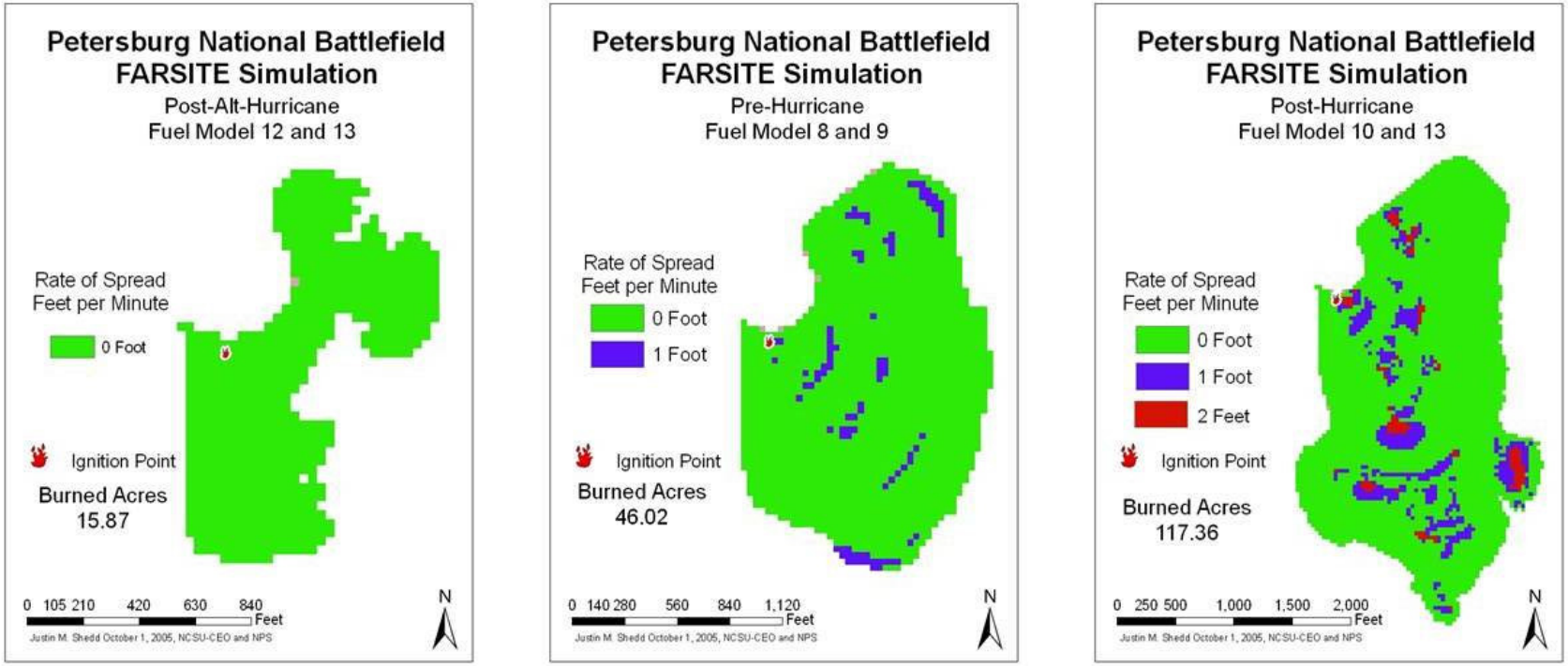

Figure 30. FARSITE, PETE All Rate of Spread Simulation Results

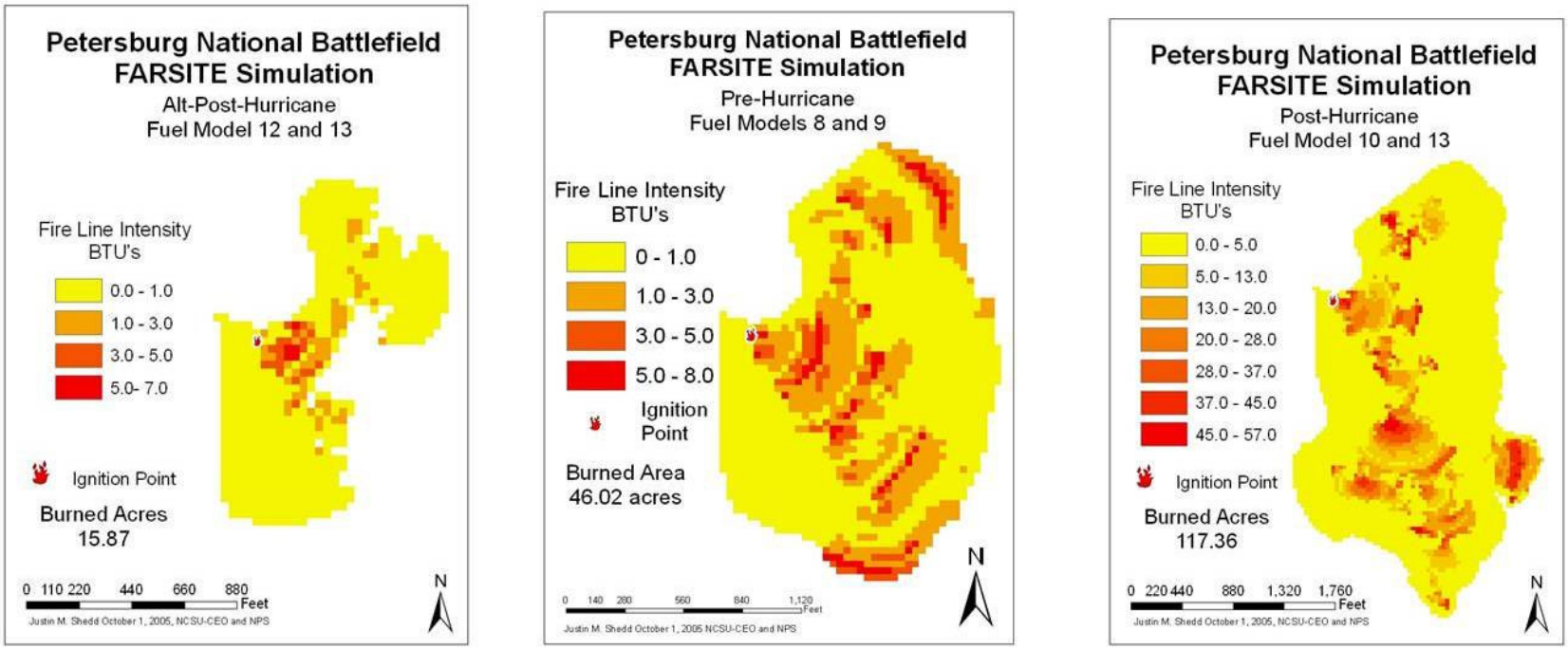

Figure 31. FARSITE, PETE All Fire Line Intensity Simulation Results

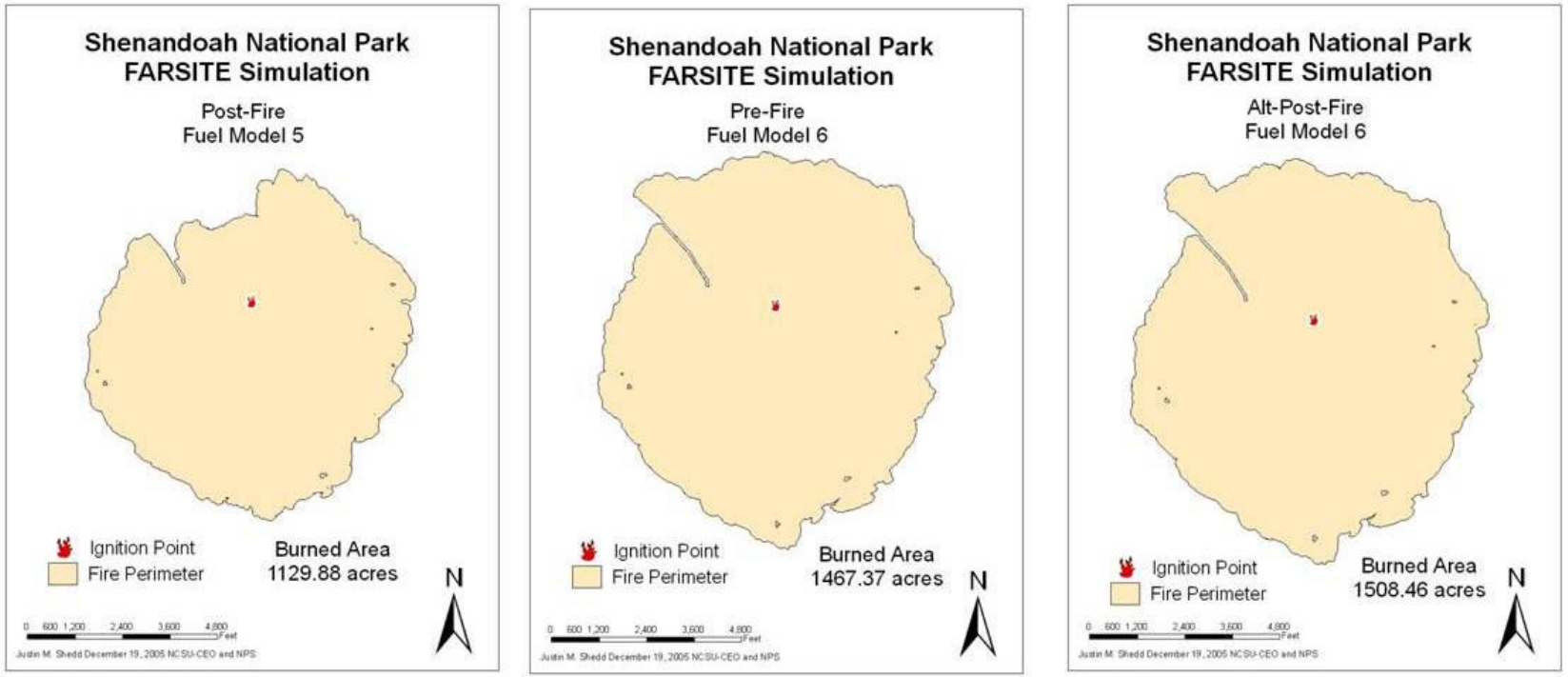

Figure 32. FARSITE, SHEN All Perimeters

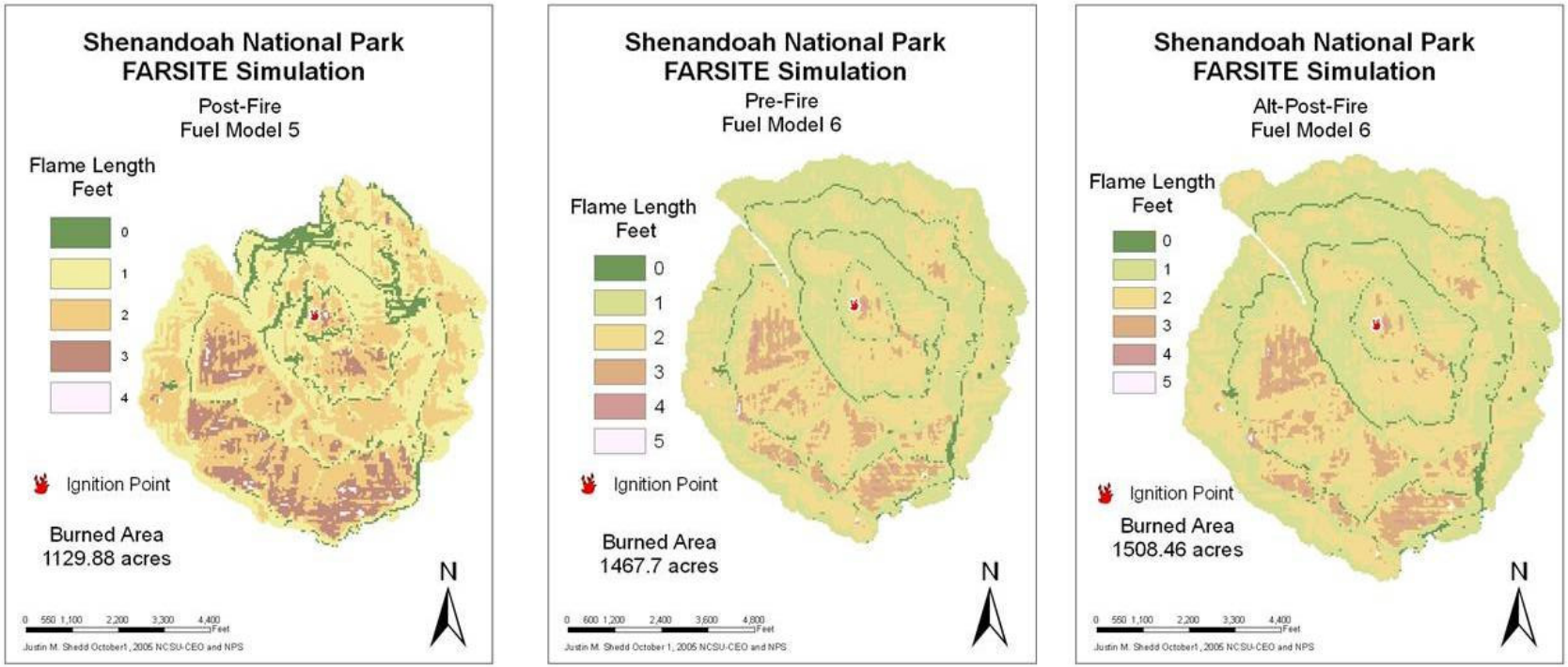

Figure 33. FARSITE, SHEN All Flame Length Simulation Results

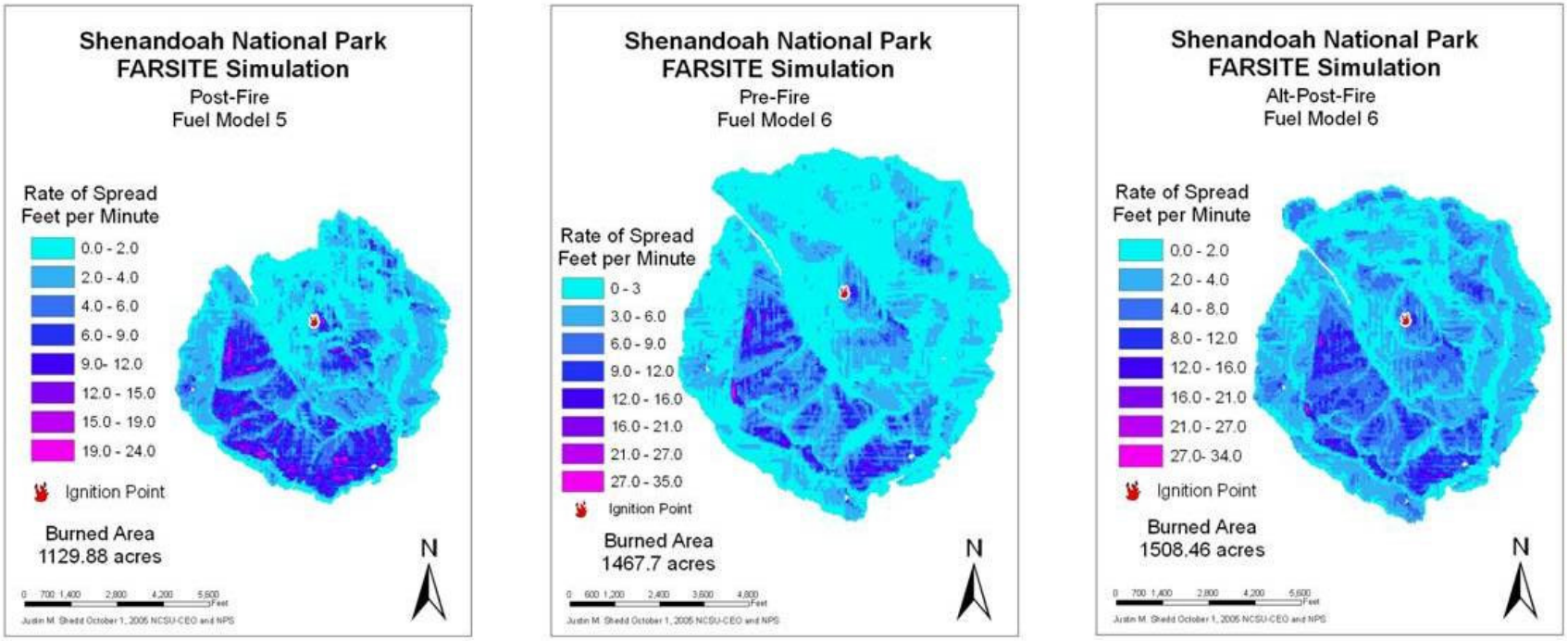

Figure 34. FARSITE, SHEN All Rate of Spread Simulation Results

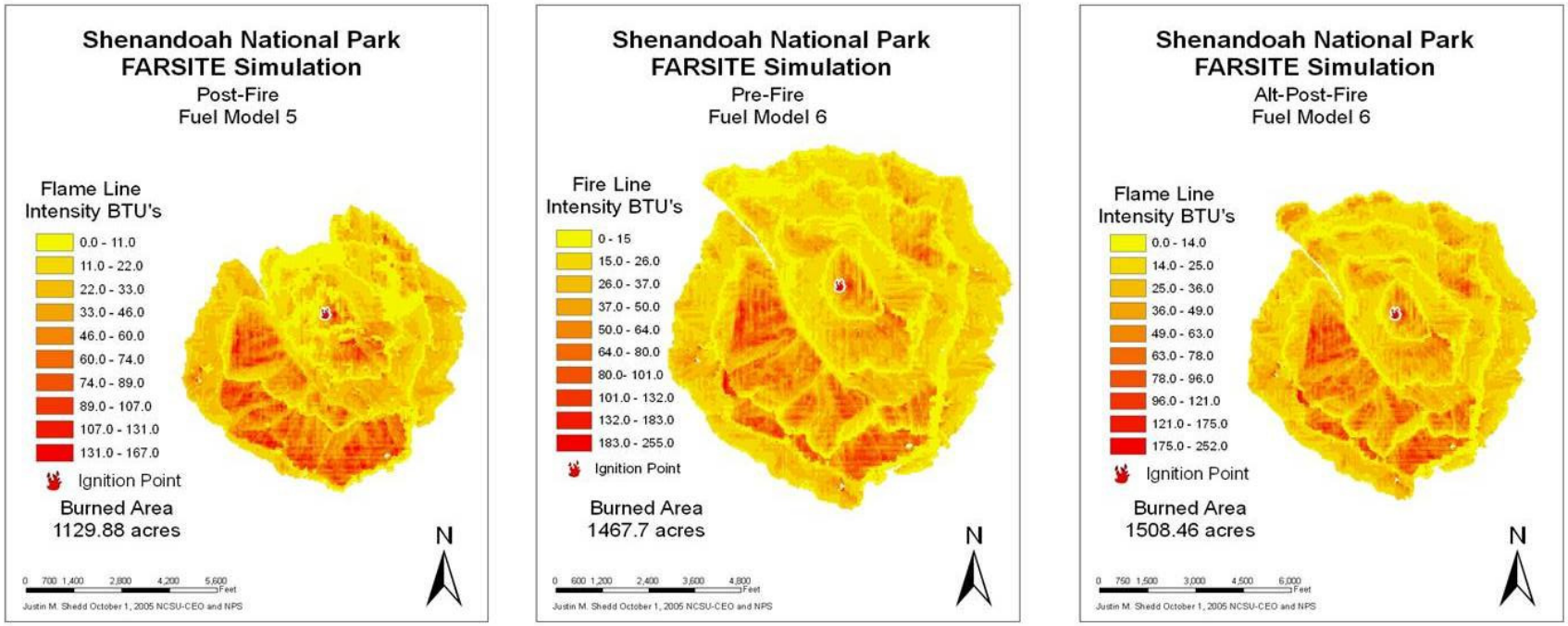

Figure 35. FARSITE, SHEN All Fire Line Intensity Simulation Results

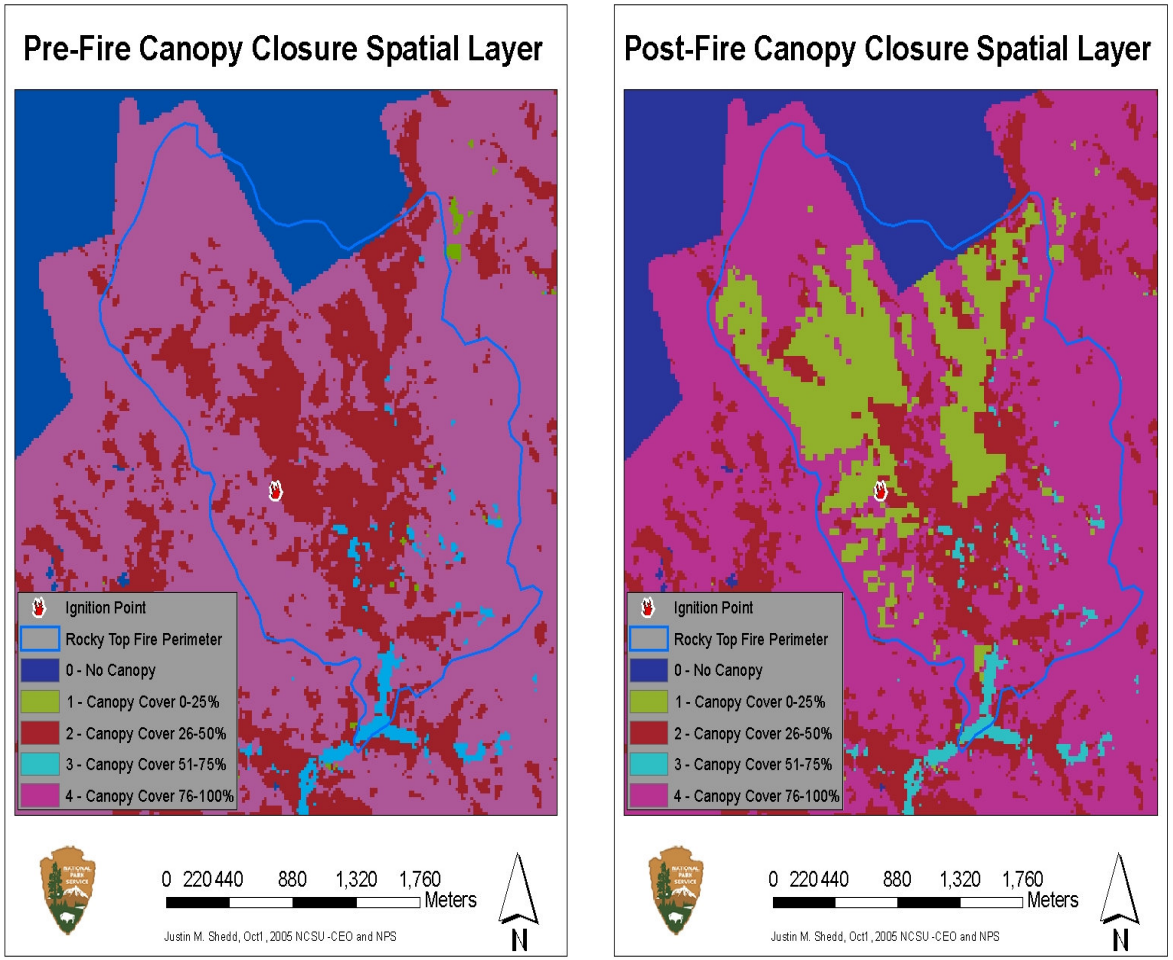

Figure 36. SHEN FARSITE Canopy Cover input spatial data layer

7. Discussion

7.1.1 The use of Digital Aerial Photography

Earlier research (Millinor 2000, Koch 2001, and Smith 2003) utilized hardcopy aerial transparencies which were scanned into the digital environment using a high resolution scanner. Research at PETE utilized digital aerial photography and with the images already in digital form, a reduction in cost and turn-around time was evident. In past research projects, upwards to a month was spent just scanning and color balancing the aerial photographs. Only a few years ago digital imagery's spatial resolution was a concern. For this research project, at a cost of $4000 dollars, digital aerial photography at a resolution of ½ meter per pixel at a scale of 1:6000, was obtained, easily allowing for the delineation of real world features. Digitally acquired aerial photomosaics, that meet Class 1 National Map Accuracy Standards, provide the land managers with an excellent decision making resource; as demonstrated by this research.

7.1.2 Feature Analyst

As the spatial resolution of remotely sensed data continues to increase, classifying an image based on the ability to use groups of pixels will prove more valuable than reliance on a single pixel. Downed woody debris could not be classified based on spectral values alone, only by utilizing the spatial patterns of downed woody debris were areas of forest damage successfully mapped. In addition, combining the spectral values with the spatial patterns of downed trees (light and dark linear patterns) enabled additional downed woody debris to be classified. Training the software to classify an image based on spatial relationships was time consuming, taking anywhere from two

days to two weeks, depending on the size of the image. The ease in which Feature Analyst operated, negated the need for technical expertise and statistical knowledge, reducing the overall time and cost of the project.

Using leaf-off photography, Feature Analyst was successful at mapping downed woody debris as indicated by the 90% overall accuracy rate. While identifying downed woody debris occurring in deciduous forests was successful, Feature Analyst was not as successful in coniferous forests. This is attributed to Feature Analyst's inability to see beneath the forest canopy. If multi-temporal imagery is available, a surrogate to mapping downed woody debris could be to map canopy gaps. A change analysis could indicate gaps created as a result from downed trees. While not being able to indicate individual downed trees, inferences could be made about the number of downed trees, from the size of the canopy gap. Furthermore, if LIDAR is available, a terrain map of the tree canopy could be created, with holes in the canopy indicating canopy gaps. These methods could prove useful to land managers of areas dominated by evergreen species.

7.1.3 PETE - Updating Vegetation and Fuel Load Datasets

PETE's existing vegetation dataset was developed by Millinor in 2000, while the fuel load spatial dataset was created in 2003 based on the crosswalk developed from Smith's work, (Smith, 2003) which resulted in most vegetation polygons of PETE being assigned to either Fuel Models 8 or 9. In this research project, expected fire behavior and written descriptions not pictorial descriptions and total fuel loading measurements, were used to assign the appropriate Fuel Model to a forest damaged area.

This research demonstrated the importance of the different types of fuel loading that are found in a hurricane damaged landscape. Elevated fuel loading levels can be heavily influenced by the occurrence of coarse woody debris; in this case the boles of trees. As evidenced by FARSITE, attention should be paid to not only the amount of fuel loading (tons per acre) but the type of fuel loading, as well. Finer fuels (1-, 10-, and 100-hour) are responsible for the spread of wildland fire, while 1000-hour fuels increase the amount of fuel loading but have little affect of the spread of wildfires.

The anticipated fire behavior for the forest damaged areas of PETE was slow spreading but intense with high flame lengths as "jackpots" existed across the landscape. The horizontal continuum and vertical arrangement of the forest damaged areas was conducive for a more intense fire with higher flame lengths. The existing fuel models (8 and 9) did not account for this, therefore Fuel Model 10 was assigned to forest damaged areas of PETE, despite the fuel measurements meeting the guidelines of Fuel Model 12. The written description of Fuel Model 10 specifically mentioning "resulting from…natural event that creates a large load of dead material on the forest floor," (Anderson, 1983) led to it being assigned to the areas of forest damage. Likewise other forest damaged areas met the Fuel Model 12 fuel load guideline but the presence of flash fuels (red slash) led to those areas being assigned to Fuel Model 13. Fuel Model 13, per its written description is associated with more intense and rapidly spreading fires. (There was not enough "red slash" in these areas to warrant classifying them as Fuel Model 4, as recommended in Anderson's Guide). Furthermore, FARSITE's simulations using the different post-hurricane fuel models, validated the choice of Fuel Model 10, as the

anticipated results (rate of spread, burn perimeter) were seen using Fuel Model 10, not Fuel Model 12.

Updating the vegetation dataset of PETE was necessary in only a few areas, as not many polygons met the minimum mapping unit established for this project. These changes exemplify the gradual successional changes of a forest as a result of the southern pine beetle, not Hurricane Isabel; areas that had been I.A. (evergreen) were now I.C. (mixed evergreen and deciduous) and areas that were I.C. were now classified as I.B. (deciduous).

7.1.4 Determining Forest Damaged Areas

In this research, the creation of the forest damage polygon used to represent the extent of the downed woody debris, was done based on the frequency of downed woody debris. While this method allowed for the creation of a generalized polygon other methods should be explored that may capture the horizontal continuum of forest damage. One such method would involve determining the nearest neighbor of each mapped occurrence of downed woody debris, after establishing a threshold distance these occurrences could be grouped together. The threshold distance would represent the distance in which the flaming front of a fire could affect nearby forest fuels. In addition, this would map the "jackpots" as well as the larger areas of increased fuel loading. A buffer around the clustered groups could be set to create the generalized forest damage polygon. This method may account for any patches of downed woody debris lost when converting it from polygons to lines.

7.2.1 Normalized Burn Ratio

The Normalized Burn Ratio accurately delineated and quantified the Rocky Top Fire's effect upon the vegetation across the landscape, as evident in the field measurements recorded. While use of other remote sensing techniques (NDVI, Tasseled Cap) to delineate a fire's perimeter has been documented, these techniques were unable to quantify the severity of the fire. NBR's ability to quantify the severity of a fire allows land managers to properly allocate needed resources and, as demonstrated in this research, use these classifications to facilitate the update of pre-existing vegetation and fuel load spatial datasets. Furthermore, the suggested dNBR classification parameters aid in the classification of a dNBR image, allowing researchers to confidently classify a burn's severity in less time.

However, the dNBR is not without its concerns. Designed using Landsat imagery of the Western U.S. and historical wildland fire data from the Western U.S., the NBR may not be an appropriate measure of burn severity in the Eastern U.S. When compared to Western U.S. forests, not only do Eastern U.S. forests have more types of vegetation but an additional vertical level of vegetation as well. In addition to the forest canopy and surface vegetation, many older Eastern U.S. forests have a mid-story canopy, occurring anywhere from 6 to 20 feet off the ground. At SHEN, areas classified as high burn severity had extensive re-growth less than three years after the fire had occurred. Does the existence (and removal) of the mid-story vegetation layer cause the NBR classification to exaggerate the effect of a wildland fire? The removal of one type of vegetation by the fire, specifically Mountain Laurel, may cause the dNBR classification to exaggerate the fire's severity level because of Mountain Laurel's spectral reflectance

values. While the NBR classification has the field measurements of the CBI to validate its classification, a study comparing Western and Eastern U.S. forest vegetation growth rates of areas experiencing a high severity burn should be considered, allowing for the calibration of the dNBR for future use in the Eastern U.S.

7.2.2 SHEN – Updating Vegetation and Fuel Load Datasets

When determining the appropriate fuel model for the burned areas the issue of potential vegetation versus actual vegetation arose. As time and growing seasons pass the severely burned areas will return to their pre-burn vegetative (I.B.) and fuel model (Fuel Model 6) classifications. However, today these areas should be represented as shrublands (I.I.I.a.) and Fuel Model 5.

Barring an insect infestation or human development, these areas will return to their pre-fire state. However, the purpose of this research project was to update the actual vegetation and fuel loads, not their potential. This leads to the question, when constructing or updating spatial datasets, especially vegetation, how much influence should future or potential vegetation growth have on its creation?

The dNBR technique shows promising results for use when updating fire fuel model spatial datasets. However, updating vegetation spatial datasets, using the dNBR technique is less reliable because other environmental influences affect the rate of vegetation re-growth after a fire. Direct and in-direct environmental gradients such as; rainfall, elevation and site exposure have more influence on the establishment and growth rate of vegetation than the occurrence of a fire of high severity. While the fuel loading measurements were similar, the plots classified as a dNBR 4 or 5 at lower elevations had

more vegetation growth than did plots at higher elevations. Future research should incorporate elevation and aspect into the creation of an updated vegetation spatial dataset, as these factors may capture the rates of vegetation re-growth more accurately, especially in areas classified as dNBR 4 or 5.

7.2.3 FARSITE and Canopy Cover

The ignition and spread of wildland fires are determined by a number of meteorological and environmental factors. All of these factors are represented in FARSITE as either a spatial data layer or a numerical input file and canopy cover is one such factor. As demonstrated in the SHEN FARSITE simulations, canopy cover does have an effect upon the rate of spread of a wildland fire.

In post-fire simulations, the majority of the burn (831 acres) recorded spread rates of three feet or less, there were however more areas (40 acres) experiencing 4-8 foot spread rates, when compared to the pre-fire simulations. These results indicate the effect a canopy has on wildland fire. With a forest's canopy removed, there is less overhead shading, which affects fuel moisture contents and increases surface winds, thus drying forest fuels faster and increasing a fire's rate of spread. As a result, winds can quickly spread the flaming front of a fire, which is unlike the slower surface fire commonly associated with forests having high canopy cover, especially in the Eastern U.S. With the majority of forests in the Eastern U.S. having greater than 50% canopy cover, areas of reduced canopy cover may slow the spread rates of a wildland fire, especially if a large volume of downed woody debris or standing dead trees are located in these areas.

While FARSITE allows for the use of custom fuel models, this research project employed the 13 fire fuel models developed by Rothermel and Albini and further described by Anderson (1982). FARSITE version 4.1.3 allows for the use of the new fire fuel models developed by Joe Scott and Robert Burgan (2005). The increase in available fuel models from 13 to 49 will not only allow for more fuel variability (fuel moisture content) but fuel types as well, particularly in the Timber litter/understory and Slash-blowdown fuel types. FARSITE simulations using the new fuel models may cause a decrease in the over-prediction of fire spread that was commonly seen (Finney, 2004 and Scott and Burgan, 2005). Future fire-related research projects should utilize these new fuel models as they may provide a better representation of a wildland fire.

8. Conclusions

With a decreasing budget and increased scrutiny over the spending of federal money on large multi-year projects, the Department of the Interior, National Park Service, needs to find a balance between, costly and precise, and cheap but less precise geospatial datasets. This research project presents two examples in which geospatial datasets, once accurate but now outdated, were successfully updated by employing remote sensing techniques designed to not only identify areas of change, but to quantify them as well. Visual Learning Systems Feature Analyst successfully mapped downed woody debris caused by Hurricane Isabel at Petersburg National Battlefield. The Normalized Burn Ratio, developed by Carl Key and Nate Benson (2002), not only indicated the perimeter of the Rocky Top Wildland Fire that occurred at Shenandoah National Park, it quantified the fire's effect upon the vegetation and the fuel load as well. As a result of these remote sensing techniques and their associated classifications, the creation of updated accurate geospatial datasets was achieved in a timely and cost-effective manner.

Automated-Feature Extraction offers a valid method of mapping features on a remotely sensed image. The use of Feature Analyst led to a time efficient and accurate classification of downed woody debris. The Feature Analyst mapping results focused the efforts of field work to areas that definitely had an increase in downed woody debris, reducing the time and cost of field operations.

The NBR data transformation is better suited for indicating differing fire severity levels when compared to the NDVI and Tasseled Cap transformations. The NBR utilizing Landsat TM Bands 4 and 7 is an excellent indicator of not only burned areas, but

at quantifying the burned areas as well. While the Near Infrared band (Band 4) was generally accepted as the more appropriate discriminator of detecting burn severity, it was not until more recent studies (White et al., 1996; Key & Benson, 2002; Miller and Yool, 2002) were completed that the Mid-Infrared band (Band 7) was found to be more indicative of burn severity across an entire landscape. The Mid-Infrared band record changes to canopy moisture and the underlying soils, allowing for a more accurate quantification of the change. These findings expand wildland fire impacts analysis beyond just vegetation to encompass the entire landscape, i.e. soils, erosion, and even wildlife. The NBR approach allows for a better characterization of a fire's true impact upon the landscape, which is the ultimate goal of change detection and why it was utilized in this research project. Furthermore, fire fuel model spatial datasets can be created based on the quantified NBR results. Utilizing a pre-existing fuel model dataset and the NBR classification, fuel loading values can be inferred, as areas classified as NBR 1, 2, or 3 (unburned to low intensity) should not be changed and areas classified as NBR 4 and 5 (moderate and severe intensity) need to be adjusted to reflect the current fuel load situation. The assigned fuel models, standard or custom, can be validated using FARSITE with attention given to the differences seen in the assigned post-fire and alternative post-fire fuel models.

The fire modeler FARSITE is used by various federal and state level land management agencies. Since simulation models are simplifications of reality and are based on numerous assumptions, their results are often in question (Van Wagtendonk, 1996). Fuel models used by FARSITE aide in the decision making process by generalizing the complex nature of wildland fire spread. Fuel models, especially those in

the Logging Slash group, produce very different simulation results as presented by this research. When assigning fuel models, consultation with an individual knowledgeable in fire behavior is essential, because field data may lead to one conclusion, but the expected or anticipated fire behavior of the fuel complex may lead to another conclusion. Such was the case with Petersburg National Battlefield, as the field data collected led to Fuel Model 12, but the anticipated fire behavior led to Fuel Model 10.

Future work involving Automated Feature Extraction should explore the possibility of indicating a surrogate as well as the feature of interest as an alternative approach. In many cases a natural or manmade feature may be located underneath the forest canopy. For example in my research, Feature Analyst had difficulty indicating downed woody debris under the canopy of coniferous forests.

Future research involving the mapping of wildland fire perimeters and severity levels should continue to use the NBR classification technique with attention paid to quantification of the impacts of the pre-processing steps, i.e. TM de-striper, histogram match.

References

Albini, Frank A. 1976. Estimating wildfire behavior and effects. USDA Forest Service Intermountain Forest and Range Experiment Station, GTR-INT-30.

Al-Khudhairy, D.H.A and S. Giada, 2005. Structural Damage Assessments from Ikonos Data Using Change Detection, Object-Oriented Segmentation, and Classification Techniques. Photogrammetric Engineering & Remote Sensing Vol. 71, No. 7, pp. 825-837.

Anderson, Hal. 1982. Aids to determining fuel models for estimating fire behavior. USDA Forest Service, Intermountain Forest and Range Experiment Station GTR-INT-122.

Andrews, Patricia. 1986. BEHAVE: Fire behavior prediction and fuel modeling system-BURN subsystem, part 1, USDA Forest Service Intermountain Research Station GTR-INT-194.

Baatz, M., & Schaepe, A. 2000. Multiresolution segmentation: an optimization approach for high quality multi-scale image segmentation. In J. Strobl, & T. Blaschke (Eds.), Angewandte geographische informationsverarbeitung, vol. XII. (pp. 12– 23). Heidelberg, Germany7 Wichmann.

Bertolette, Don and Dan Spotskey, 2001. Remotely sensed burn severity mapping. From: Crossing Boundaries in Park Management: Proceedings of the 11th Conference on Research and Resource Management in Parks and on Public Lands. The 2001 biennial Conference.

Beyer, H. L. 2004. Hawth's Analysis Tools for ArcGIS. Web Site, (accessed 3 October, 2004). Accessible at http://www.spatialecology.com/htools.

Blaschke, T., & Strobl, J. 2001. What's wrong with pixels? Some recent developments interfacing remote sensing and GIS. GeoBIT/GIS, 6, 12– 17.

Blaschke, T., Lang, S., Lorup, E., Strobl, J., Zeil, P. 2000. Object-oriented image processing in an integrated GIS/remote sensing environment and perspectives for environmental applications. In: Cremers, A. und Greve, K. (Hrsg.): Umweltinformation für Planung, Politik und Öffentlichkeit / Environmental Information for Planning, Politics and the Public. Metropolis Verlag, Marburg, vol 2; 555–570.

Brokaw, Nicholas V.L. and Lawernce R. Walker, 1991. Summary of Effects of Caribbean Hurricanes on Vegetation, Biotropica 23(4a): 442-447.

Brown A.A. and Davis K.P., 1973. Forest fire: Control and use. McGraw-Hill: New York pp. 686.

Brown, James K., 1974. Handbook for inventorying downed woody material. USDA Forest Service Intermountain Forest and Range Experiment Station, GTR-INT-16.

Brown, James K., Elizabeth Reinhardt, and Kylie Kramer, 2003. Coarse Woody Debris: Managing Benefits and Fire Hazard in the Recovering Forest. USDA Forest Service, Rocky Mountain Research Station, GTR RMRS-GTR-105, Fort Collins Co., 2003.

Berg, Erik C and David H.Van Lear. 2004. Survivorship and Growth of Oak Regeneration in Wind-Created Gaps. USDA Forest Service, Southern Research Station, GTR-SRS-73.

Burgan, Robert and Richard Rothermel. 1984. BEHAVE: fire behavior prediction and fuel modeling system-FUEL subsystem. USDA Forest Service Intermountain Research Station, GTR-INT-167.

Cohen, Jack and Jim Saveland. 1997. Structure Ignition Assessment Can Help Reduce Fire Damages in the W-UI. Fire Management Notes 57(4): 19-23.

Carmichael, Becky J. and W. Cass. 2001. Vegetation Fuel Mapping Protocol. SHEN-N-021.001. Assessment of Vegetation Communities.

Communicator's Guide, Wildland Fire. "The I-Zone: A Human Dimension of Wildland Fire," FIREWISE Program. Available online at http://www.nifc.gov/preved/comm_guide/wildfire/TOC.html.

Crist, Eric P. and Richard C. Cicone, 1984. "Application of the Tasseled Cap Concept to Simulated Thematic Mapper Data," in Photogrammetric Engineering and Remote Sensing, pp. 343-352.

Definiens 2004. Definiens Imaging, eCognition. Web Site, (accessed 21 July, 2004). Accessible at http://www.definiens-imaging.com.

Dillabaugh, C., K. Niemann, D. Richardson. 2002. Semi-Automated Extraction of Rivers from Digital Imagery, GeoInformatica, 6:3, 263-284.

Finney, Mark. 1998. FARSITE Fire Area Simulator – Model Development and Evaluation. USDA Forest Service, Rocky Mountain Research Station Research Paper, RMRS-RP-4.

Finney, Mark. 2004. FARSITE Fire Area Simulator – Model Development and Evaluation. USDA Forest Service, Rocky Mountain Research Station Research Paper, RMRS-RP-4 (revised).

Firestone, L., S. Rupert, J. Olson, and W. Mueller. 1996. Automated Feature Extraction: The Key to Future Productivity, Photogrammetric Engineering and Remote Sensing, vol. 62, no 6, pp. 671-674.

Foder, Melissa. “Rocky Top Fire.” E-mail to Justin Shedd. 11 Nov 2004.

Foster, David R., and Emery R. Boose. 1992. Patterns of forest damage resulting from catastrophic wind in central New England, USA., Journal of Ecology, 80: 79-98.

Fransson, J. E. S., Walter, F., Blennow, K., Gustavsson, A. & Ulander, L. M. H. 2002. Detection of storm-damaged forested areas using airborne CARABAS-II VHF SAR image data. IEEE Trans. Geosci. Remote Sens. 40: 2170-2175.

Geman, D., and B. Jedynak. 1996. "An active testing model for tracking roads in satellite images," IEEE Transactions on Pattern Analysis and Machine Intelligence, Vol 18(1):1-14.

Garcia-Haro, F.J., M.A. Gilabert and J. Melia. 2001. Monitoring fire effected areas using Thematic Mapper data. International Journal of Remote Sensing, Vol 22., No. 4, 533-549.

Gorman, KellyAnn. "SHEN fire." E-mail to Justin Shedd. 1 Jan 2005.

Greenberg, Cathryn H. and W. Henry McNab. 1997. Forest Disturbance in hurricane-related downbursts in the Appalachian mountains of North Carolina. Forest Ecology and Management 199X: 179-191.

Grossman, D.H., et al. 1998. International classification of ecological communities: Terrestrial vegetation of the United States. Volume I: The national vegetation classification standard. Arlington, VA. The Nature Conservancy. Available online at http://www.natureserve.org/library/vol1.pdf.

Harrington, Steve. 2005. Measuring Forest Fuels: An Overview of Methodologies, Implications for Fuels Management. Forest Guild Research Center Working Paper 19.

Jackson, R. G., Foody, G. M. & Quine, C. P. 2000. Characterising windthrown gaps from fine spatial resolution remotely sensed data. Forest Ecology Management. 135: 253-260

Jacobs, Dennis M. 2000. February 1994 ice storm: forest resource damage assessment in northern Mississippi. USDA Forest Service Southern Research Station, RB-SRS-54.

John R. Jensen. 2000. Remote Sensing of the Environment An Earth Resource Perspective, New York, Prentice Hall.

Jordan, C.F. 1969. Derivation of leaf area index from quality measurements of light on the forest floor. Ecology, vol. 50, pp. 663-666.

Kauth, R. J. and G. S. Thomas. 1976. The Tasseled Cap - A Graphic Description of the Spectral-Temporal Development of Agricultural Crops as Seen by Landsat. Proceedings

of the Symposium on Machine Processing of Remotely Sensed Data. West Lafayette, IN: Purdue University, pp. 4B-41 to 4B-51.

Kessell SR. 1976. Gradient modeling: A new approach to fire modeling and wilderness resource management. Environmental Management 1(1), 39–48.

Keane, Robert E., Robert Burgan and Jan van Wagtendonk. 2001. Mapping wildland fuels for fire management across multiple scales: Integrating remote sensing, GIS, and biophysical modeling. International Journal of Wildland Fire, 10, 301-319.

Key, C., and Benson, N.C. 2002. Fire Effects Monitoring and Inventory Protocol; Landscape Assessment. U.S. Geological Survey, Northern Rocky Mountain Science Center, Glacier Field Station, WestGlacier, Montana.

Key, C., and Benson, N.C. 2004. Ground Measure of Severity, The Composite Burn Index. FIREMON: Fire Effects Monitoring and Inventory System. USDA Forest Service GTR-RMRS-XXX.

Kneipp, Greg. "FARSITE layer." E-mail to Justin Shedd. 4 July 2005.

Koch, Frank Henry, Jr. 2001. A comparison of digital vegetation mapping and image orthorectification methods using aerial photography of Valley Forge National Historical Park. Master's Thesis, North Carolina State University.

Koutsias, Nikos, Michael Karteris, and Emilio Chuvieco. 2000. The Use of Intensity-Hue-Saturation Transformation of Landsat-5 Thematic Mapper Data for Burned Land Mapping. Photogrammetic Engineering and Remotre Sensing. Vol 66, No. 7 pp 829-838.

Kulakowski, Dominik and Thomas T. Veblen. 2002. Influences of fire history and topography on the pattern of a severe wind blowdown in a Colorado subalpine forest. Journal of Ecology 90, 806-819.

Kushla J. D., and W.J. Ripple. 1998. Assessing Wildfire Effects with Landsat Thematic Mapper data. International Journal of Remote Sensing Vol 19., No 13., 2493-2507.

Gruber M., F. Leberl, R. Perko. 2003. "The Ultracam Large Format Aerial Digital Camera System," Proceedings Of The American Society For Photogrammetry & Remote Sensing Anchorage, Alaska, 5-9 May, 2003.

Lillesand, Thomas M., Kiefer, Ralph W., Chipman Jonathan W. 2004. Remote Sensing and Image Interpretation fifth ed. New York, John Wiley and Sons INC.

Lu, D., P.Mausel, E. Brondizio and E. Moran. 2004. Change Detection Techniques. International Journal of Remote Sensing. Vol. 25 No.12, 2365-2407.

McGarigle, B. 1997. Mar. Digital aerial photography flies. Government Technology, Accessible at http://govtech.net.

Merrens, Edwards J. and David R. Peart. 1992. Effects of hurricane damage on individual growth and stand structure in a hardwood forest in New Hampshire, USA, Journal of Ecology 80: 787-795.

Millinor, William A. 2000. Digital vegetation delineation on scanned orthorectified aerial photography of Petersburg National Battlefield. Master's Thesis, North Carolina State University.

National Park Service (NPS) 2005 Fire Management Program – Wildland Fire. Web site (accessed 20, June, 2004). Accessible at http://www.nps.gov/fire/fire/fir_wildland.html.

National Park Service (NPS). 2003. Petersburg National Battlefield visitor guide. Web Site (accessed 1 June, 2004). Accessible at http://www.nps.gov/pete/index.htm.

National Park Service (NPS). 2004. Shenandoah National Park visitor guide. Web Site (accessed 1 September, 2004). Accessible at http://www.nps.gov/shen/index.htm.

NatureServe, 2005. International Ecological Classification Standard: Terrestrial Ecological Classifications, DRAFT Terrestrial Ecological Systems of the Southern Appalachian Region, US, Legend for Landfire Project.

National Interagency Fire Center, Web Site (accessed 1 May, 2004). Accessible at http://www.nifc.gov/.

Parson, Annette, and Andrew Orlemann. Mapping Post-Wildfire Burn Severity Using Remote Sensing and GIS, ESRI Conference 2002, USDA Forest Service, Remote Sensing Applications Center, Salt Lake City, UT.

Patterson, M.W. & Yool, S.R. 1998. Mapping fire induced vegetation mortality using LANDSAT TM data: A comparison of Linear transformation techniques. Remote Sensing of Environment. 65. 132-142.

Pyne, S. 1982. *Fire in America*. Princeton, NJ: Princeton University Press.

Pyne, S., Andrews, P., & Laven, R. 1996. Introduction to wildland fire. 2nd ed. New York: John Wiley & Sons.

Rogan, J. & Yool, S.R. 2001. Mapping fire induced vegetation depletion in the Peloncillo Mountains, Arizona and New Mexico. International Journal of Remote Sensing. 22, (16). 3101-3121.

Rothermel, R.C. 1972. A mathematical model for predicting fire spread in wildland fuels.

USDA Forest Service, Intermountain Forest and Range Experiment Station GTR-INT–115.

Rouse, J. W., R. H. Haas, J. A. Schell, and D. W. Deering. 1973. Monitoring Vegetation Systems in the Great Plains with ERTS, Proceedings, Third ERTS Symposium, Vol. 1, pp. 48-62.

Sandberg, David V., Roger D.Ottmar, and Geoffrey H. Cushon. 2001. Characterizing fuels in the 21st Century. International Journal of Wildland Fire, 10, 381-387.

Saveland, J.M. and D. Wade, Fire Management Ramifications of Hurricane Hugo, Presented at the 11th Conference on Fire and Forest Meterology, April 16-19, 1991.

Schwarz, M., C. Steinmeier, F. Holecz, O. Stebler, and H. Wagner. 2003. Detection of Windthrow in Mountainous Regions with Different Remote Sensing Data and Classification Methods. Scandanavian Journal of Forest Research 18: 525-536.

Smith, Mark P. 2003. Predicting Fuel Models and Subsequent Fire Behavior from Vegetation Classification Maps. Master's Thesis, North Carolina State University.

Thomas M. Lillesand, Kiefer, Ralph W., Chipman Jonathan W.; Remote Sensing and Image Interpretation fifth ed. John Wiley and Sons Inc., 2004.

Van Wagtendonk, J. W. and Ralph Root. 1999. Use of thematic mapper imagery to map fuel models. Proceedings 13th Conference on Fire and Forest Meteorology. International. Association of Wildland Fire, Fairfield, WA.

Van Wagtendonk, J. W., Root, R. R., & Key C. H. 2003. Comparison of aviris and landsat etm+ detection capabilitites for burn severity. Remote Sensing of Environment, *92*, 397-408.

Vanderzanden, Dave and Mike Morrison, 2002. High Resolution Image Classification: A Forest Service Test of Visual Learning System's Feature Analyst. USDA-Forest Service Remote Sensing Applications Center, Salt Lake City UT 84119. Available online at http://www.featureanalyst.com/feature_analyst/publications/reviews/forest_service.pdf.

Viedma, O., Melia, J., Segarra, D., & Garcia-Haro, J., 1997. Modeling Rates of Ecosystem Recovery after fires by using Landsat TM data. Remote Sensing of Environment 61; pp. 383-398.

Visual Learning System, Feature analyst. Wed Site (Accessed 15 June, 2004). Accessible at http://www.featureanalyst.com.

Visual Learning System Feature Analyst 2004. Visual Learning Systems Feature Analyst 4.0 Reference Manual. Available at http://www.featureanalyst.com.

Wade, Dale D., James K. Forbus, James M. Saveland. 1993. Photo Series for Estimating Post-Hurricane Residues and Fire Behavior in Southern Pine. USDA Forest Service, Southeastern Forest Experiment Station, GTR-SE-82.

Whigham, Dennis F., Ingrid Olmsted, Edgar Cabrera Cano, and Mark Harmon. 1991. The Impact of Hurricane Gilbert on Trees, Litterfall, and Woody Debris in a Dry Tropical Forest in the Northeastern Yucutan Peninsula, Biotropica 23(4a): 434-441.

White, J. D., Ryan, K. C., Key, C. C., and Running, S. W. 1996. Remote Sensing of forest fire severity and vegetation recovery. International Journal of Remote Sensing, 6, 125–136.

White, K., and Hesham M. El Asmar. 1999. Monitoring changing position of coastlines using Thematic Mapper imagery, an example from the Nile Delta. Geomorphology 29, 93-105.

Willhauck, G., J.J. Caliz, C. Hoffmann, I. Lingenfelder, M. Heynen, 2005. Object-oriented ship detection from VHR satellite images. In: Proceedings of Semana Geomática, 8 - 11 February, Barcelona, Spain.

Won, K. and J. Im, 2001. Fire severity mapping using a single post-fire Landsat 7 ETM+ Imagery, Journal of the Korean Society of Remote Sensing, 17(1): 85-97.

Xian, G., and Mike Crane. 2005. Assessments of urban growth in the Tampa Bay watershed using remote sensing data. Remote Sensing of Environment 97, 203-215.

Zhang, Y., 2000. A method for continuous extraction of multispectrally classified urban rivers. Photogrammetric Engineering and Remote Sensing, Vol. 66(8): 991-999.

Appendices

Appendix A: dNBR Classification Guideline

Ordinal severity levels and *example* range of dNBR (scaled by 10^3) are shown:
SEVERITY LEVEL ΔNBR RANGE

Enhanced Regrowth High	-500 to -251
Enhanced Regrowth Low	-250 to -101
Unburned	**-100 to +99**
Low Severity	+100 to +269
Moderate-low Severity	+270 to +439
Moderate-high Severity	+440 to +659
High Severity	+660 to +1300

(These value ranges are flexible; scene-pair dependent; shifts in thresholds ±100 points are possible. **dNBR** less than about -550, or greater than about +1350 may occur, but usually are *not* considered burned. Rather, they likely are anomalies caused by mis-registration, clouds, or other factors not related to real land cover differences).

Appendix B. Composite Burn Index.

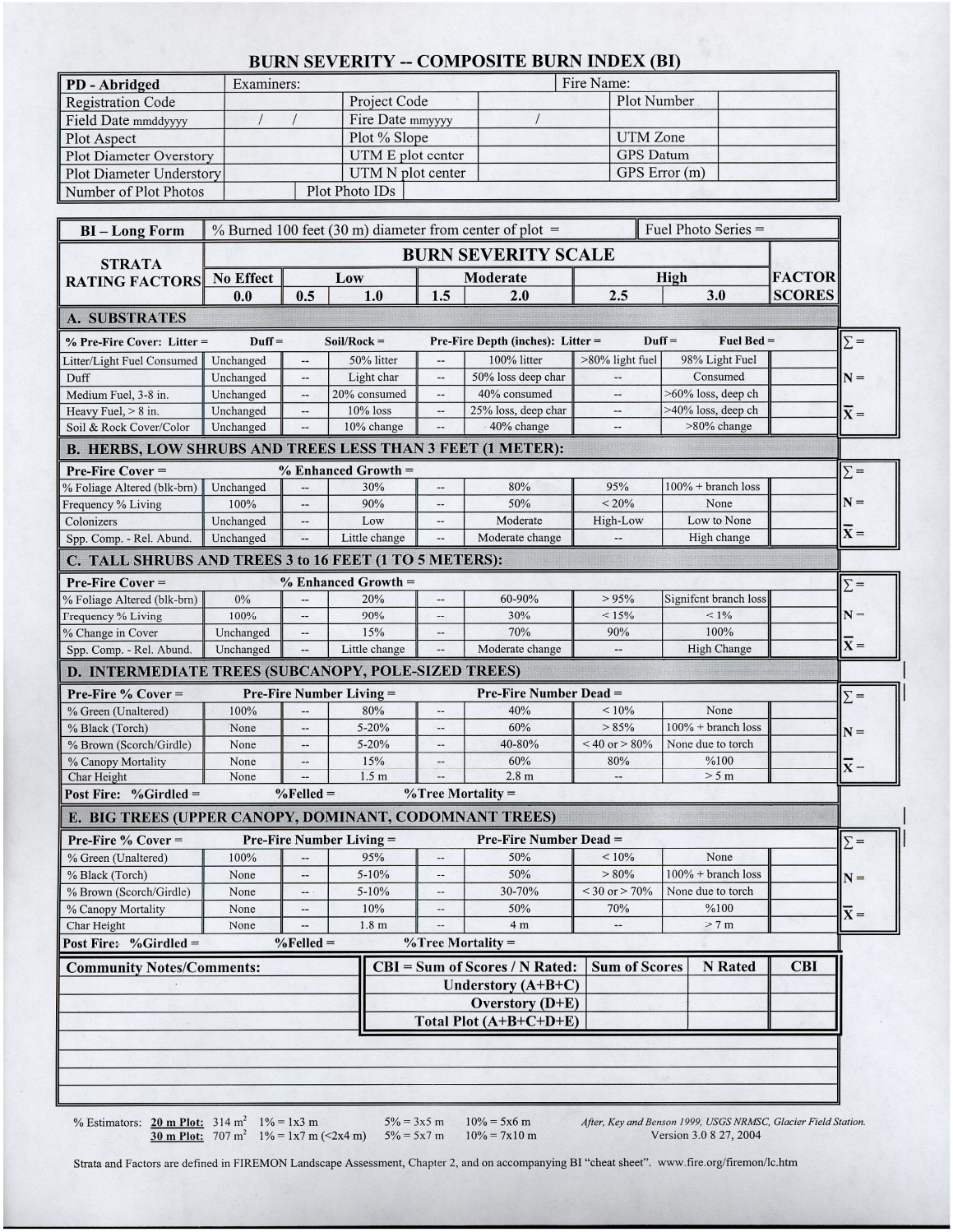

BURN SEVERITY -- COMPOSITE BURN INDEX (BI)

PD - Abridged	Examiners:		Fire Name:			
Registration Code		Project Code		Plot Number		
Field Date mmddyyyy	/ /	Fire Date mmyyyy	/			
Plot Aspect		Plot % Slope		UTM Zone		
Plot Diameter Overstory		UTM E plot center		GPS Datum		
Plot Diameter Understory		UTM N plot center		GPS Error (m)		
Number of Plot Photos		Plot Photo IDs				

BI – Long Form	% Burned 100 feet (30 m) diameter from center of plot =	Fuel Photo Series =

STRATA RATING FACTORS	BURN SEVERITY SCALE							FACTOR SCORES
	No Effect	Low		Moderate		High		
	0.0	0.5	1.0	1.5	2.0	2.5	3.0	
A. SUBSTRATES								
% Pre-Fire Cover: Litter =	**Duff =**		**Soil/Rock =**		**Pre-Fire Depth (inches): Litter =**	**Duff =**	**Fuel Bed =**	∑ =
Litter/Light Fuel Consumed	Unchanged	--	50% litter	--	100% litter	>80% light fuel	98% Light Fuel	
Duff	Unchanged	--	Light char	--	50% loss deep char	--	Consumed	N =
Medium Fuel, 3-8 in.	Unchanged	--	20% consumed	--	40% consumed	--	>60% loss, deep ch	
Heavy Fuel, > 8 in.	Unchanged	--	10% loss	--	25% loss, deep char	--	>40% loss, deep ch	$\bar{X}$ =
Soil & Rock Cover/Color	Unchanged	--	10% change	--	40% change	--	>80% change	
B. HERBS, LOW SHRUBS AND TREES LESS THAN 3 FEET (1 METER):								
Pre-Fire Cover =			**% Enhanced Growth =**					∑ =
% Foliage Altered (blk-brn)	Unchanged	--	30%	--	80%	95%	100% + branch loss	
Frequency % Living	100%	--	90%	--	50%	< 20%	None	N =
Colonizers	Unchanged	--	Low	--	Moderate	High-Low	Low to None	
Spp. Comp. - Rel. Abund.	Unchanged	--	Little change	--	Moderate change	--	High change	$\bar{X}$ =
C. TALL SHRUBS AND TREES 3 to 16 FEET (1 TO 5 METERS):								
Pre-Fire Cover =			**% Enhanced Growth =**					∑ =
% Foliage Altered (blk-brn)	0%	--	20%	--	60-90%	> 95%	Signifcnt branch loss	
Frequency % Living	100%	--	90%	--	30%	< 15%	< 1%	N =
% Change in Cover	Unchanged	--	15%	--	70%	90%	100%	
Spp. Comp. - Rel. Abund.	Unchanged	--	Little change	--	Moderate change	--	High Change	$\bar{X}$ =
D. INTERMEDIATE TREES (SUBCANOPY, POLE-SIZED TREES)								
Pre-Fire % Cover =			**Pre-Fire Number Living =**		**Pre-Fire Number Dead =**			∑ =
% Green (Unaltered)	100%	--	80%	--	40%	< 10%	None	
% Black (Torch)	None	--	5-20%	--	60%	> 85%	100% + branch loss	N =
% Brown (Scorch/Girdle)	None	--	5-20%	--	40-80%	< 40 or > 80%	None due to torch	
% Canopy Mortality	None	--	15%	--	60%	80%	%100	$\bar{X}$ =
Char Height	None	--	1.5 m	--	2.8 m	--	> 5 m	
Post Fire: %Girdled =			**%Felled =**		**%Tree Mortality =**			
E. BIG TREES (UPPER CANOPY, DOMINANT, CODOMNANT TREES)								
Pre-Fire % Cover =			**Pre-Fire Number Living =**		**Pre-Fire Number Dead =**			∑ =
% Green (Unaltered)	100%	--	95%	--	50%	< 10%	None	
% Black (Torch)	None	--	5-10%	--	50%	> 80%	100% + branch loss	N =
% Brown (Scorch/Girdle)	None	--	5-10%	--	30-70%	< 30 or > 70%	None due to torch	
% Canopy Mortality	None	--	10%	--	50%	70%	%100	$\bar{X}$ =
Char Height	None	--	1.8 m	--	4 m	--	> 7 m	
Post Fire: %Girdled =			**%Felled =**		**%Tree Mortality =**			

Community Notes/Comments:	CBI = Sum of Scores / N Rated:	Sum of Scores	N Rated	CBI
	Understory (A+B+C)			
	Overstory (D+E)			
	Total Plot (A+B+C+D+E)			

% Estimators: **20 m Plot:** 314 m^2 1% = 1x3 m 5% = 3x5 m 10% = 5x6 m
30 m Plot: 707 m^2 1% = 1x7 m (<2x4 m) 5% = 5x7 m 10% = 7x10 m

After, Key and Benson 1999, USGS NRMSC, Glacier Field Station.
Version 3.0 8 27, 2004

Strata and Factors are defined in FIREMON Landscape Assessment, Chapter 2, and on accompanying BI "cheat sheet". www.fire.org/firemon/lc.htm

Appendix C. Calculation of Fuel Loading at PETE Plot Locations.

Formation Type:	I.B.2.N.g								
Plot Number	4								
Transect	Size Class	Constant	N	D^2	S	A	C	NL	Tons/Acre
East	0 - .25	11.64	3	0.0151	0.48	1.13	1	6	0.0476672
	.25 - 1.00	11.64	7	0.289	0.48	1.13	1	6	2.12871389
	1.00 - 3.00	11.64	3	2.76	0.40	1.13	1	12	3.6302832
	3.00 + S	11.64		129	0.40	1.00	1	50	12.01248
	3.00 + R	11.64		554	0.30	1.00	1	50	38.69136
								Total	56.5105043
	Size Class	Constant	N	D^2	S	A	C	NL	Tons/Acre
North	0 - .25	11.64	12	0.0151	0.48	1.13	1	6	0.19066879
	.25 - 1.00	11.64	9	0.289	0.48	1.13	1	6	2.73691786
	1.00 - 3.00	11.64	1	2.76	0.40	1.13	1	12	1.2100944
	3.00 + S	11.64		65	0.40	1.00	1	50	6.0528
	3.00 + R	11.64		181	0.30	1.00	1	50	12.64104
								Total	22.831521
Formation Type:	I.B.2.N.a								
Plot Number	6								
Transect	Size Class	Constant	N	D^3	S	A	C	NL	Tons/Acre
East	1 - .25	11.64	6	0.0151	0.48	1.13	1	6	0.09533439
	.25 - 1.00	11.64	13	0.289	0.48	1.13	1	6	3.95332579
	1.00 - 3.00	11.64	3	2.76	0.40	1.13	1	12	3.6302832
	3.00 + S	11.64		742	0.40	1.00	1	50	69.09504
	3.00 + R	11.64		0	0.30	1.00	1	50	0
								Total	76.7739834
	Size Class	Constant	N	D^3	S	A	C	NL	Tons/Acre
North	1 - .25	11.64	1	0.0151	0.48	1.13	1	6	0.01588907
	.25 - 1.00	11.64	12	0.289	0.48	1.13	1	6	3.64922381
	1.00 - 3.00	11.64	2	2.76	0.40	1.13	1	12	2.4201888
	3.00 + S	11.64		500.5	0.40	1.00	1	50	46.60656
	3.00 + R	11.64		16	0.30	1.00	1	50	1.11744
								Total	53.8093017

Formation Type: I.B.2.N.a
Plot Number 27

Transect	Size Class	Constant	N	D^3	S	A	C	NL	Tons/Acre
East	1 - .25	11.64	7	0.0151	0.48	1.13	1	6	0.11122346
	.25 - 1.00	11.64	3	0.289	0.48	1.13	1	6	0.91230595
	1.00 - 3.00	11.64	0	2.76	0.4	1.13	1	12	0
	3.00 + S	11.64		412.25	0.4	1.00	1	50	38.38872
	3.00 + R	11.64		29.25	0.3	1.00	1	50	2.04282
								Total	41.4550694

	Size Class	Constant	N	D^3	S	A	C	NL	Tons/Acre
North	1 - .25	11.64	7	0.0151	0.48	1.13	1	6	0.11122346
	.25 - 1.00	11.64	6	0.289	0.48	1.13	1	6	1.8246119
	1.00 - 3.00	11.64	1	2.76	0.4	1.13	1	12	1.2100944
	3.00 + S	11.64		9	0.4	1.00	1	50	0.83808
	3.00 + R	11.64		0	0.3	1.00	1	50	0
								Total	3.98400976

Formation Type: I.C.3.N.a
Plot Number 32

Transect	Size Class	Constant	N	D^4	S	A	C	NL	Tons/Acre
East	2 - .25	11.64	10	0.0151	0.48	1.13	1	6	0.15889066
	.25 - 1.00	11.64	24	0.289	0.48	1.13	1	6	7.29844762
	1.00 - 3.00	11.64	3	2.76	0.4	1.13	1	12	3.6302832
	3.00 + S	11.64		432	0.4	1.00	1	50	40.22784
	3.00 + R	11.64		0	0.3	1.00	1	50	0
								Total	51.3154615

	Size Class	Constant	N	D^4	S	A	C	NL	Tons/Acre
North	2 - .25	11.64	10	0.0151	0.48	1.13	1	6	0.15889066
	.25 - 1.00	11.64	10	0.289	0.48	1.13	1	6	3.04101984
	1.00 - 3.00	11.64	1	2.76	0.4	1.13	1	12	1.2100944
	3.00 + S	11.64		1084	0.4	1.00	1	50	100.94208
	3.00 + R	11.64		130	0.3	1.00	1	50	9.0792
								Total	114.431285

Formation Type: I.B.2.N.e
Plot Number 31

Transect	Size Class	Constant	N	D^4	S	A	C	NL	Tons/Acre
East	2 - .25	11.64	11	0.0151	0.48	1.13	1	6	0.17477972
	.25 - 1.00	11.64	9	0.289	0.48	1.13	1	6	2.73691786
	1.00 - 3.00	11.64	0	2.76	0.4	1.13	1	12	0
	3.00 + S	11.64		0	0.4	1.00	1	50	0
	3.00 + R	11.64		25	0.3	1.00	1	50	1.746
								Total	4.65769758

	Size Class	Constant	N	D^4	S	A	C	NL	Tons/Acre
North	2 - .25	11.64	12	0.0151	0.48	1.13	1	6	0.19066879
	.25 - 1.00	11.64	10	0.289	0.48	1.13	1	6	3.04101984
	1.00 - 3.00	11.64	1	2.76	0.4	1.13	1	12	1.2100944
	3.00 + S	11.64		457	0.4	1.00	1	50	42.55584
	3.00 + R	11.64		16	0.3	1.00	1	50	1.11744
								Total	48.115063

Formation Type: I.B.2.N.d
Plot Number 15

Transect	Size Class	Constant	N	D^5	S	A	C	NL	Tons/Acre
East	3 - .25	11.64	1	0.0151	0.48	1.13	1	6	0.01588907
	.25 - 1.00	11.64	9	0.289	0.48	1.13	1	6	2.73691786
	1.00 - 3.00	11.64	4	2.76	0.4	1.13	1	12	4.8403776
	3.00 + S	11.64		324	0.4	1.00	1	50	30.17088
	3.00 + R	11.64		0	0.3	1.00	1	50	0
								Total	37.7640645

	Size Class	Constant	N	D^5	S	A	C	NL	Tons/Acre
North	3 - .25	11.64	6	0.0151	0.48	1.13	1	6	0.09533439
	.25 - 1.00	11.64	11	0.289	0.48	1.13	1	6	3.34512182
	1.00 - 3.00	11.64	3	2.76	0.4	1.13	1	12	3.6302832
	3.00 + S	11.64		277	0.4	1.00	1	50	25.79424
	3.00 + R	11.64		0	0.3	1.00	1	50	0
								Total	32.8649794

Formation Type: I.B.2.N.g
Plot Number 1

Transect	Size Class	Constant	N	D^5	S	A	C	NL	Tons/Acre
East	3 - .25	11.64	7	0.0151	0.48	1.13	1	6	0.11122346
	.25 - 1.00	11.64	12	0.289	0.48	1.13	1	6	3.64922381
	1.00 - 3.00	11.64	2	2.76	0.4	1.13	1	12	2.4201888
	3.00 + S	11.64		338	0.4	1.00	1	50	31.47456
	3.00 + R	11.64		170	0.3	1.00	1	50	11.8728
								Total	49.5279961

	Size Class	Constant	N	D^5	S	A	C	NL	Tons/Acre
North	3 - .25	11.64	4	0.0151	0.48	1.13	1	6	0.06355626
	.25 - 1.00	11.64	4	0.289	0.48	1.13	1	6	1.21640794
	1.00 - 3.00	11.64	2	2.76	0.4	1.13	1	12	2.4201888
	3.00 + S	11.64		253	0.4	1.00	1	50	23.55936
	3.00 + R	11.64		113	0.3	1.00	1	50	7.89192
								Total	35.151433

Formation Type: I.B.2.N.e
Plot Number 18

Transect	Size Class	Constant	N	D^6	S	A	C	NL	Tons/Acre
East	4 - .25	11.64	11	0.0151	0.48	1.13	1	6	0.17477972
	.25 - 1.00	11.64	12	0.289	0.48	1.13	1	6	3.64922381
	1.00 - 3.00	11.64	0	2.76	0.4	1.13	1	12	0
	3.00 + S	11.64		348	0.4	1.00	1	50	32.40576
	3.00 + R	11.64		45.25	0.3	1.00	1	50	3.16026
								Total	39.3900235

	Size Class	Constant	N	D^6	S	A	C	NL	Tons/Acre
North	4 - .25	11.64	5	0.0151	0.48	1.13	1	6	0.07944533
	.25 - 1.00	11.64	10	0.289	0.48	1.13	1	6	3.04101984
	1.00 - 3.00	11.64	5	2.76	0.4	1.13	1	12	6.050472
	3.00 + S	11.64		1214.25	0.4	1.00	1	50	113.07096
	3.00 + R	11.64		160	0.3	1.00	1	50	11.1744
								Total	133.416297

Formation Type: I.A.8.N.b
Plot Number 26

Transect	Size Class	Constant	N	D^6	S	A	C	NL	Tons/Acre
East	4 - .25	11.64	9	0.0151	0.48	1.13	1	6	0.14300159
	.25 - 1.00	11.64	8	0.289	0.48	1.13	1	6	2.43281587
	1.00 - 3.00	11.64	3	2.76	0.4	1.13	1	12	3.6302832
	3.00 + S	11.64		98	0.4	1.00	1	50	9.12576
	3.00 + R	11.64		602	0.3	1.00	1	50	42.04368
								Total	57.3755407

	Size Class	Constant	N	D^6	S	A	C	NL	Tons/Acre
North	4 - .25	11.64	12	0.0151	0.48	1.13	1	6	0.19066879
	.25 - 1.00	11.64	8	0.289	0.48	1.13	1	6	2.43281587
	1.00 - 3.00	11.64	4	2.76	0.4	1.13	1	12	4.8403776
	3.00 + S	11.64		183	0.4	1.00	1	50	17.04096
	3.00 + R	11.64		137.25	0.3	1.00	1	50	9.58554
								Total	34.0903623

Formation Type: I.A.8.N.b
Plot Number 22

Transect	Size Class	Constant	N	D^7	S	A	C	NL	Tons/Acre
East	5 - .25	11.64	6	0.0151	0.48	1.13	1	6	0.09533439
	.25 - 1.00	11.64	6	0.289	0.48	1.13	1	6	1.8246119
	1.00 - 3.00	11.64	4	2.76	0.4	1.13	1	12	4.8403776
	3.00 + S	11.64		0	0.4	1.00	1	50	0
	3.00 + R	11.64		196	0.3	1.00	1	50	13.68864
								Total	20.4489639

	Size Class	Constant	N	D^7	S	A	C	NL	Tons/Acre
North	5 - .25	11.64	5	0.0151	0.48	1.13	1	6	0.07944533
	.25 - 1.00	11.64	10	0.289	0.48	1.13	1	6	3.04101984
	1.00 - 3.00	11.64	3	2.76	0.4	1.13	1	12	3.6302832
	3.00 + S	11.64		871	0.4	1.00	1	50	81.10752
	3.00 + R	11.64		694	0.3	1.00	1	50	48.46896
								Total	136.327228

Formation Type:	I.C.3.N.a								
Plot Number	13								
Transect	Size Class	Constant	N	D^7	S	A	C	NL	Tons/Acre
East	5 - .25	11.64	7	0.0151	0.48	1.13	1	6	0.11122346
	.25 - 1.00	11.64	11	0.289	0.48	1.13	1	6	3.34512182
	1.00 - 3.00	11.64	7	2.76	0.40	1.13	1	12	8.4706608
	3.00 + S	11.64		78.25	0.40	1.00	1	50	7.28664
	3.00 + R	11.64		0	0.30	1.00	1	50	0
								Total	19.2136461
	Size Class	Constant	N	D^7	S	A	C	NL	Tons/Acre
North	5 - .25	11.64	4	0.0151	0.48	1.13	1	6	0.06355626
	.25 - 1.00	11.64	5	0.289	0.48	1.13	1	6	1.52050992
	1.00 - 3.00	11.64	2	2.76	0.4	1.13	1	12	2.4201888
	3.00 + S	11.64		870.25	0.4	1.00	1	50	81.03768
	3.00 + R	11.64		115.25	0.3	1.00	1	50	8.04906
								Total	93.090995

Formation Type:	I.C.3.N.a								
Plot Number	25								
Transect	Size Class	Constant	N	D^8	S	A	C	NL	Tons/Acre
East	6 - .25	11.64	10	0.0151	0.48	1.13	1	6	0.15889066
	.25 - 1.00	11.64	12	0.289	0.48	1.13	1	6	3.64922381
	1.00 - 3.00	11.64	2	2.76	0.4	1.13	1	12	2.4201888
	3.00 + S	11.64		0	0.4	1.00	1	50	0
	3.00 + R	11.64		0	0.3	1.00	1	50	0
								Total	6.22830326
	Size Class	Constant	N	D^8	S	A	C	NL	Tons/Acre
North	6 - .25	11.64	12	0.0151	0.48	1.13	1	6	0.19066879
	.25 - 1.00	11.64	24	0.289	0.48	1.13	1	6	7.29844762
	1.00 - 3.00	11.64	1	2.76	0.4	1.13	1	12	1.2100944
	3.00 + S	11.64		81	0.4	1.00	1	50	7.54272
	3.00 + R	11.64		81	0.3	1.00	1	50	5.65704
								Total	21.8989708

Formation Type: I.A.8.N.b
Plot Number 19

Transect	Size Class	Constant	N	D^8	S	A	C	NL	Tons/Acre
East	6 - .25	11.64	9	0.0151	0.48	1.13	1	6	0.14300159
	.25 - 1.00	11.64	12	0.289	0.48	1.13	1	6	3.64922381
	1.00 - 3.00	11.64	5	2.76	0.4	1.13	1	12	6.050472
	3.00 + S	11.64		387	0.4	1.00	1	50	36.03744
	3.00 + R	11.64		9	0.3	1.00	1	50	0.62856
								Total	46.5086974

	Size Class	Constant	N	D^8	S	A	C	NL	Tons/Acre
North	6 - .25	11.64	9	0.0151	0.48	1.13	1	6	0.14300159
	.25 - 1.00	11.64	18	0.289	0.48	1.13	1	6	5.47383571
	1.00 - 3.00	11.64	1	2.76	0.4	1.13	1	12	1.2100944
	3.00 + S	11.64		43	0.4	1.00	1	50	4.00416
	3.00 + R	11.64		18	0.3	1.00	1	50	1.25712
								Total	12.0882117

Formation Type: I.B.2.N.a
Plot Number 14

Transect	Size Class	Constant	N	D^9	S	A	C	NL	Tons/Acre
East	7 - .25	11.64	13	0.0151	0.48	1.13	1	6	0.20655785
	.25 - 1.00	11.64	9	0.289	0.48	1.13	1	6	2.73691786
	1.00 - 3.00	11.64	1	2.76	0.4	1.13	1	12	1.2100944
	3.00 + S	11.64		374.25	0.4	1.00	1	50	34.85016
	3.00 + R	11.64		0	0.3	1.00	1	50	0
								Total	39.0037301

	Size Class	Constant	N	D^9	S	A	C	NL	Tons/Acre
North	7 - .25	11.64	6	0.0151	0.48	1.13	1	6	0.09533439
	.25 - 1.00	11.64	6	0.289	0.48	1.13	1	6	1.8246119
	1.00 - 3.00	11.64	2	2.76	0.4	1.13	1	12	2.4201888
	3.00 + S	11.64		16	0.4	1.00	1	50	1.48992
	3.00 + R	11.64		36	0.3	1.00	1	50	2.51424
								Total	8.3442951

Formation Type:	I.B.2.N.g								
Plot Number	2								
Transect	Size Class	Constant	N	D^9	S	A	C	NL	Tons/Acre
East	7 - .25	11.64	3	0.0151	0.48	1.13	1	6	0.0476672
	.25 - 1.00	11.64	7	0.289	0.48	1.13	1	6	2.12871389
	1.00 - 3.00	11.64	2	2.76	0.4	1.13	1	12	2.4201888
	3.00 + S	11.64		169	0.4	1.00	1	50	15.73728
	3.00 + R	11.64		0	0.3	1.00	1	50	0
								Total	20.3338499
	Size Class	Constant	N	D^9	S	A	C	NL	Tons/Acre
North	7 - .25	11.64	3	0.0151	0.48	1.13	1	6	0.0476672
	.25 - 1.00	11.64	1	0.289	0.48	1.13	1	6	0.30410198
	1.00 - 3.00	11.64	0	2.76	0.4	1.13	1	12	0
	3.00 + S	11.64		245	0.4	1.00	1	50	22.8144
	3.00 + R	11.64		0	0.3	1.00	1	50	0
								Total	23.1661692

Formation Type:	I.C.3.N.a								
Plot Number	29								
Transect	Size Class	Constant	N	D^9	S	A	C	NL	Tons/Acre
East	7 - .25	11.64	23	0.0151	0.48	1.13	1	6	0.36544851
	.25 - 1.00	11.64	10	0.289	0.48	1.13	1	6	3.04101984
	1.00 - 3.00	11.64	2	2.76	0.4	1.13	1	12	2.4201888
	3.00 + S	11.64		25	0.4	1.00	1	50	2.328
	3.00 + R	11.64		9	0.3	1.00	1	50	0.62856
								Total	8.78321715
	Size Class	Constant	N	D^9	S	A	C	NL	Tons/Acre
North	7 - .25	11.64	12	0.0151	0.48	1.13	1	6	0.19066879
	.25 - 1.00	11.64	13	0.289	0.48	1.13	1	6	3.95332579
	1.00 - 3.00	11.64	4	2.76	0.4	1.13	1	12	4.8403776
	3.00 + S	11.64		623.25	0.4	1.00	1	50	58.03704
	3.00 + R	11.64		0	0.3	1.00	1	50	0
								Total	67.0214122

Formation Type:	I.B.2.N.a								
Plot Number	8								
Transect	Size Class	Constant	N	D^10	S	A	C	NL	Tons/Acre
East	8 - .25	11.64	18	0.0151	0.48	1.13	1	6	0.28600318
	.25 - 1.00	11.64	15	0.289	0.48	1.13	1	6	4.56152976
	1.00 - 3.00	11.64	6	2.76	0.4	1.13	1	12	7.2605664
	3.00 + S	11.64		279.25	0.4	1.00	1	50	26.00376
	3.00 + R	11.64		247.25	0.3	1.00	1	50	17.26794
								Total	55.3797993
	Size Class	Constant	N	D^10	S	A	C	NL	Tons/Acre
North	8 - .25	11.64	11	0.0151	0.48	1.13	1	6	0.17477972
	.25 - 1.00	11.64	13	0.289	0.48	1.13	1	6	3.95332579
	1.00 - 3.00	11.64	2	2.76	0.4	1.13	1	12	2.4201888
	3.00 + S	11.64		571	0.4	1.00	1	50	53.17152
	3.00 + R	11.64		45	0.3	1.00	1	50	3.1428
								Total	62.8626143

Formation Type:	I.B.2.N.a								
Plot Number	10								
Transect	Size Class	Constant	N	D^10	S	A	C	NL	Tons/Acre
East	8 - .25	11.64	8	0.0151	0.48	1.13	1	6	0.12711252
	.25 - 1.00	11.64	8	0.289	0.48	1.13	1	6	2.43281587
	1.00 - 3.00	11.64	3	2.76	0.4	1.13	1	12	3.6302832
	3.00 + S	11.64		517	0.4	1.00	1	50	48.14304
	3.00 + R	11.64		134.25	0.3	1.00	1	50	9.37602
								Total	63.7092716
	Size Class	Constant	N	D^10	S	A	C	NL	Tons/Acre
North	8 - .25	11.64	11	0.0151	0.48	1.13	1	6	0.17477972
	.25 - 1.00	11.64	10	0.289	0.48	1.13	1	6	3.04101984
	1.00 - 3.00	11.64	4	2.76	0.4	1.13	1	12	4.8403776
	3.00 + S	11.64		699	0.4	1.00	1	50	65.09088
	3.00 + R	11.64		0	0.3	1.00	1	50	0
								Total	73.1470572

Formation Type:	I.B.2.N.d								
Plot Number	21								
Transect	Size Class	Constant	N	D^10	S	A	C	NL	Tons/Acre
East	8 - .25	11.64	8	0.0151	0.48	1.13	1	6	0.12711252
	.25 - 1.00	11.64	11	0.289	0.48	1.13	1	6	3.34512182
	1.00 - 3.00	11.64	6	2.76	0.4	1.13	1	12	7.2605664
	3.00 + S	11.64		488.25	0.4	1.00	1	50	45.46584
	3.00 + R	11.64		16	0.3	1.00	1	50	1.11744
								Total	57.3160807
	Size Class	Constant	N	D^10	S	A	C	NL	Tons/Acre
North	8 - .25	11.64	8	0.0151	0.48	1.13	1	6	0.12711252
	.25 - 1.00	11.64	8	0.289	0.48	1.13	1	6	2.43281587
	1.00 - 3.00	11.64	2	2.76	0.4	1.13	1	12	2.4201888
	3.00 + S	11.64		656	0.4	1.00	1	50	61.08672
	3.00 + R	11.64		0	0.3	1.00	1	50	0
								Total	66.0668372

Formation Type:	I.B.2.N.a								
Plot Number	5								
Transect	Size Class	Constant	N	D^11	S	A	C	NL	Tons/Acre
East	9 - .25	11.64	7	0.0151	0.48	1.13	1	6	0.11122346
	.25 - 1.00	11.64	9	0.289	0.48	1.13	1	6	2.73691786
	1.00 - 3.00	11.64	2	2.76	0.4	1.13	1	12	2.4201888
	3.00 + S	11.64		58	0.4	1.00	1	50	5.40096
	3.00 + R	11.64		0	0.3	1.00	1	50	0
								Total	10.6692901
	Size Class	Constant	N	D^11	S	A	C	NL	Tons/Acre
North	9 - .25	11.64	11	0.0151	0.48	1.13	1	6	0.17477972
	.25 - 1.00	11.64	10	0.289	0.48	1.13	1	6	3.04101984
	1.00 - 3.00	11.64	9	2.76	0.4	1.13	1	12	10.8908496
	3.00 + S	11.64		444	0.4	1.00	1	50	41.34528
	3.00 + R	11.64		162	0.3	1.00	1	50	11.31408
								Total	66.7660092

Formation Type:	I.C.3.N.a								
Plot Number	11								
Transect	Size Class	Constant	N	D^11	S	A	C	NL	Tons/Acre
East	9 - .25	11.64	10	0.0151	0.48	1.13	1	6	0.15889066
	.25 - 1.00	11.64	8	0.289	0.48	1.13	1	6	2.43281587
	1.00 - 3.00	11.64	0	2.76	0.4	1.13	1	12	0
	3.00 + S	11.64		256	0.4	1.00	1	50	23.83872
	3.00 + R	11.64		73	0.3	1.00	1	50	5.09832
								Total	31.5287465
	Size Class	Constant	N	D^11	S	A	C	NL	Tons/Acre
North	9 - .25	11.64	14	0.0151	0.48	1.13	1	6	0.22244692
	.25 - 1.00	11.64	8	0.289	0.48	1.13	1	6	2.43281587
	1.00 - 3.00	11.64	1	2.76	0.4	1.13	1	12	1.2100944
	3.00 + S	11.64		261	0.4	1.00	1	50	24.30432
	3.00 + R	11.64		0	0.3	1.00	1	50	0
								Total	28.1696772

Formation Type:	I.C.3.N.a								
Plot Number	20								
Transect	Size Class	Constant	N	D^11	S	A	C	NL	Tons/Acre
East	9 - .25	11.64	4	0.0151	0.48	1.13	1	6	0.06355626
	.25 - 1.00	11.64	11	0.289	0.48	1.13	1	6	3.34512182
	1.00 - 3.00	11.64	1	2.76	0.4	1.13	1	12	1.2100944
	3.00 + S	11.64		0	0.4	1.00	1	50	0
	3.00 + R	11.64		64	0.3	1.00	1	50	4.46976
								Total	9.08853249
	Size Class	Constant	N	D^11	S	A	C	NL	Tons/Acre
North	9 - .25	11.64	9	0.0151	0.48	1.13	1	6	0.14300159
	.25 - 1.00	11.64	9	0.289	0.48	1.13	1	6	2.73691786
	1.00 - 3.00	11.64	2	2.76	0.4	1.13	1	12	2.4201888
	3.00 + S	11.64		1565	0.4	1.00	1	50	145.7328
	3.00 + R	11.64		181.25	0.3	1.00	1	50	12.6585
								Total	163.691408

Formation Type: I.A.8.N.b
Plot Number 24

Transect	Size Class	Constant	N	D^12	S	A	C	NL	Tons/Acre
East	10 - .25	11.64	14	0.0151	0.48	1.13	1	6	0.22244692
	.25 - 1.00	11.64	13	0.289	0.48	1.13	1	6	3.95332579
	1.00 - 3.00	11.64	4	2.76	0.4	1.13	1	12	4.8403776
	3.00 + S	11.64		449.25	0.4	1.00	1	50	41.83416
	3.00 + R	11.64		0	0.3	1.00	1	50	0
								Total	50.8503103

	Size Class	Constant	N	D^12	S	A	C	NL	Tons/Acre
North	10 - .25	11.64	14	0.0151	0.48	1.13	1	6	0.22244692
	.25 - 1.00	11.64	14	0.289	0.48	1.13	1	6	4.25742778
	1.00 - 3.00	11.64	2	2.76	0.4	1.13	1	12	2.4201888
	3.00 + S	11.64		658.25	0.4	1.00	1	50	61.29624
	3.00 + R	11.64		20.25	0.3	1.00	1	50	1.41426
								Total	69.6105635

Formation Type: I.B.2.N.d
Plot Number 16

Transect	Size Class	Constant	N	D^12	S	A	C	NL	Tons/Acre
East	10 - .25	11.64	0	0.0151	0.48	1.13	1	6	0
	.25 - 1.00	11.64	7	0.289	0.48	1.13	1	6	2.12871389
	1.00 - 3.00	11.64	3	2.76	0.4	1.13	1	12	3.6302832
	3.00 + S	11.64		576	0.4	1.00	1	50	53.63712
	3.00 + R	11.64		25	0.3	1.00	1	50	1.746
								Total	61.1421171

	Size Class	Constant	N	D^12	S	A	C	NL	Tons/Acre
North	10 - .25	11.64	5	0.0151	0.48	1.13	1	6	0.07944533
	.25 - 1.00	11.64	11	0.289	0.48	1.13	1	6	3.34512182
	1.00 - 3.00	11.64	4	2.76	0.4	1.13	1	12	4.8403776
	3.00 + S	11.64		0	0.4	1.00	1	50	0
	3.00 + R	11.64		25	0.3	1.00	1	50	1.746
								Total	10.0109448

Appendix D. PETE updated fuel model spatial dataset

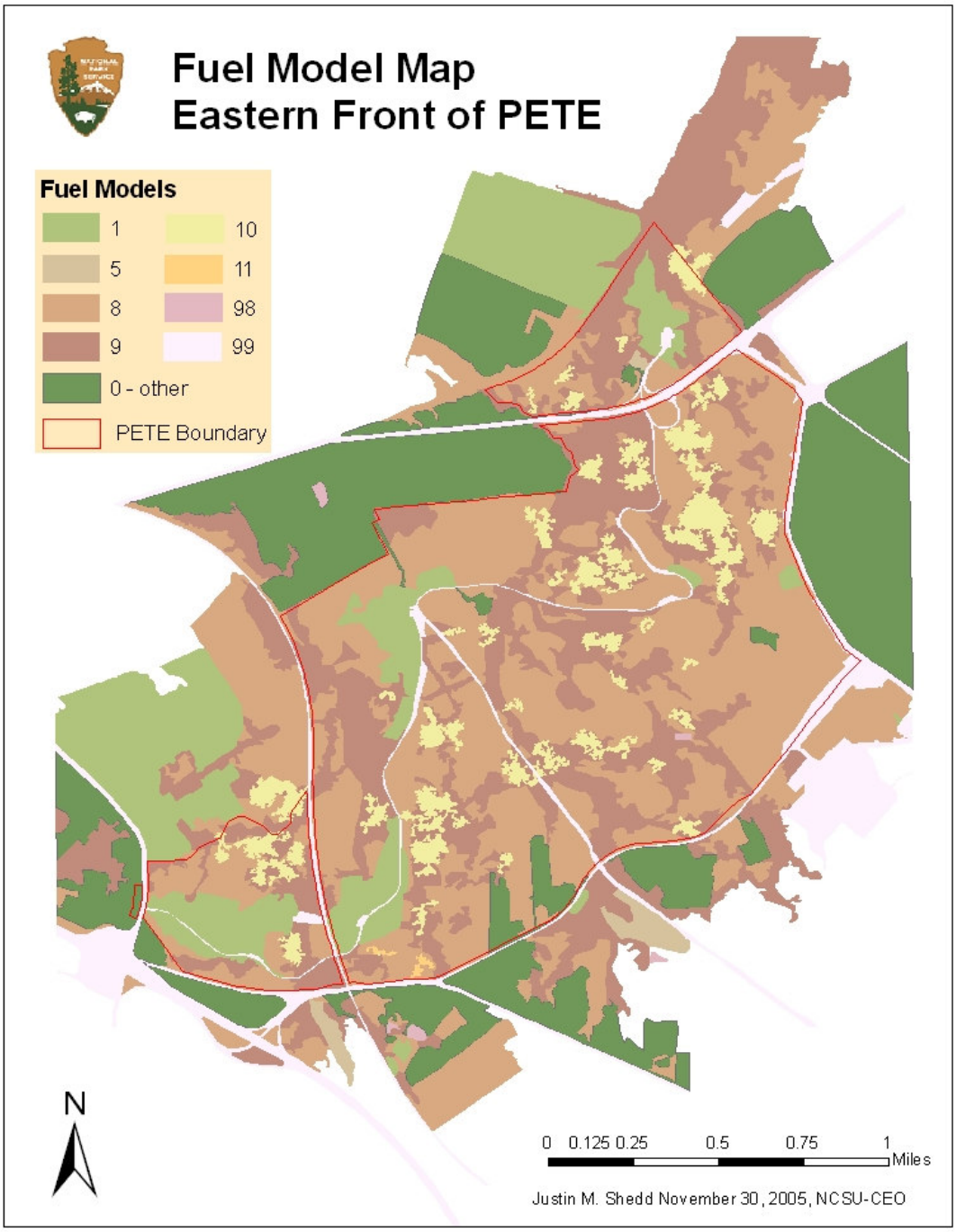

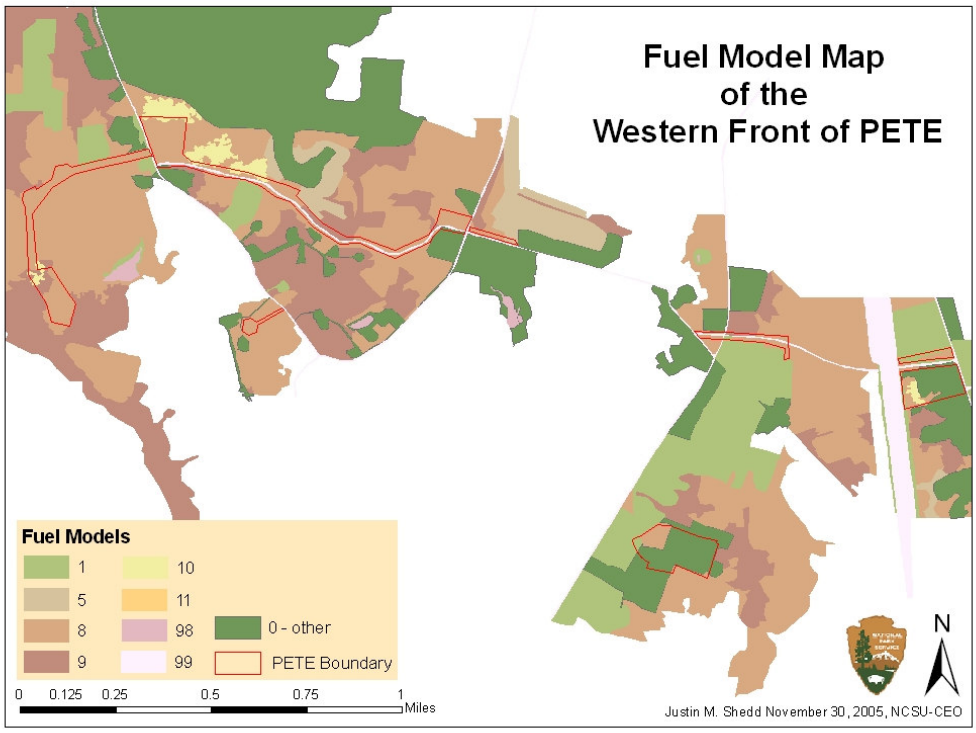
Fuel Model Map
of the
Western Front of PETE
Fuel Models
1
5
8
9
10
11
98
99
0 - other
PETE Boundary
0 0.125 0.25 0.5 0.75 1
Miles
N
Justin M. Shedd November 30, 2005, NCSU-CEO

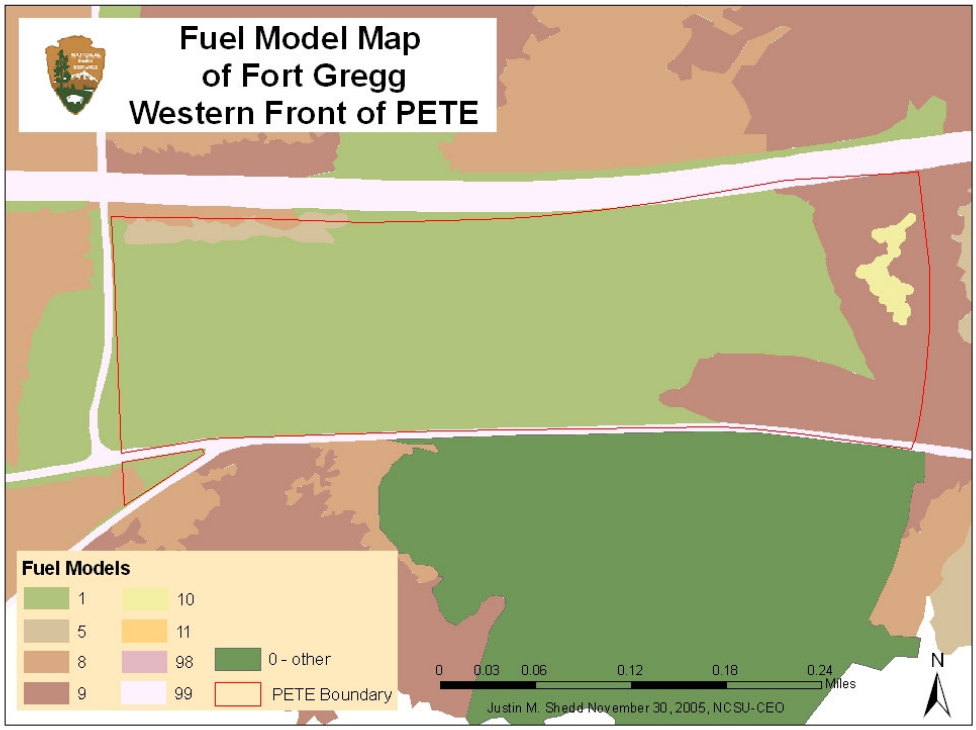
Fuel Model Map
of Fort Gregg
Western Front of PETE
Fuel Models
1
5
8
9
10
11
98
99
0 - other
PETE Boundary
0 0.03 0.06 0.12 0.18 0.24
Miles
N
Justin M. Shedd November 30, 2005, NCSU-CEO

Appendix E. Updated Vegetation Spatial Dataset of PETE

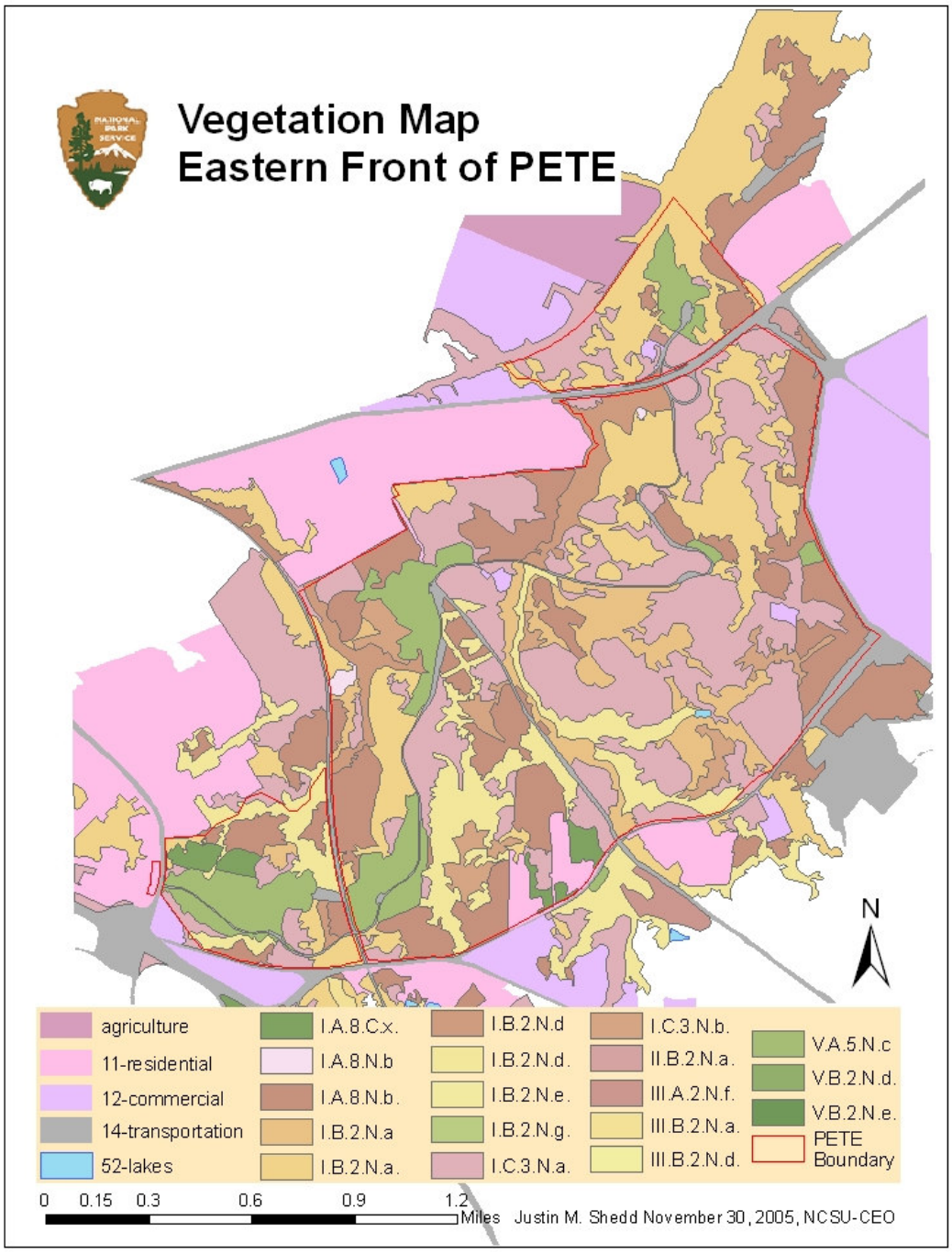

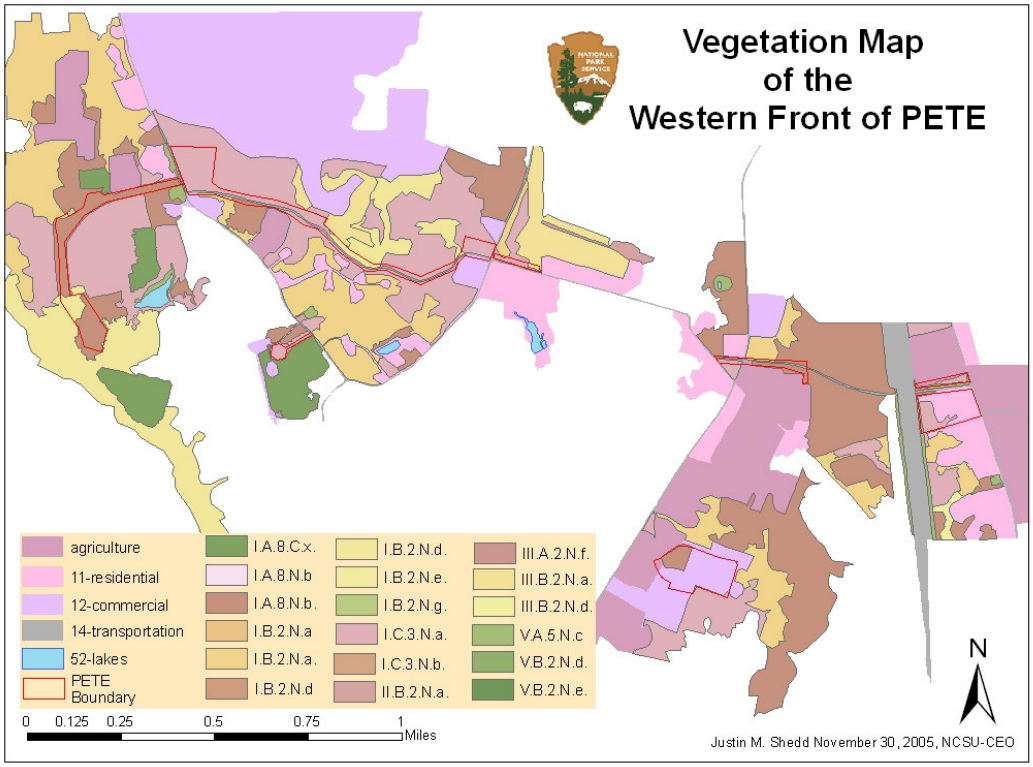
Vegetation Map
of the
Western Front of PETE
agriculture
11-residential
12-commercial
14-transportation
52-lakes
PETE Boundary
I.A.8.C.x.
I.A.8.N.b
I.A.8.N.b.
I.B.2.N.a
I.B.2.N.a.
I.B.2.N.d
I.B.2.N.d.
I.B.2.N.e.
I.B.2.N.g.
I.C.3.N.a.
I.C.3.N.b.
II.B.2.N.a.
III.A.2.N.f.
III.B.2.N.a.
III.B.2.N.d.
V.A.5.N.c
V.B.2.N.d.
V.B.2.N.e.
0 0.125 0.25 0.5 0.75 1
Miles
N
Justin M. Shedd November 30, 2005, NCSU-CEO

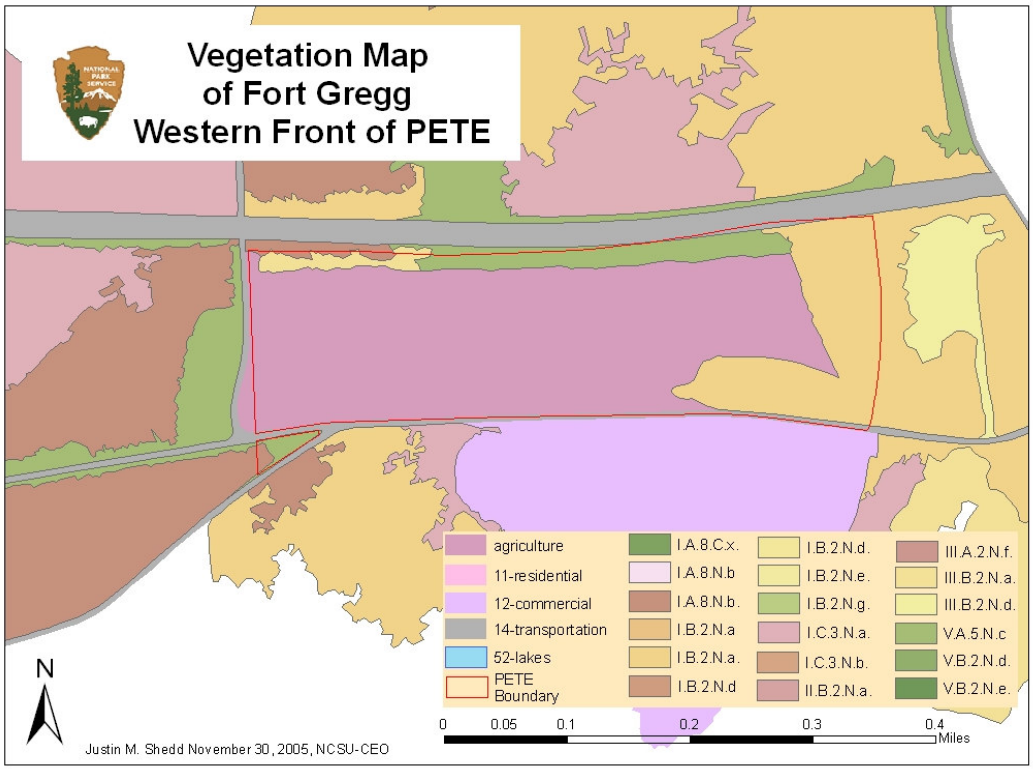
Vegetation Map
of Fort Gregg
Western Front of PETE
agriculture
11-residential
12-commercial
14-transportation
52-lakes
PETE Boundary
I.A.8.C.x.
I.A.8.N.b
I.A.8.N.b.
I.B.2.N.a
I.B.2.N.a.
I.B.2.N.d
I.B.2.N.d.
I.B.2.N.e.
I.B.2.N.g.
I.C.3.N.a.
I.C.3.N.b.
II.B.2.N.a.
III.A.2.N.f.
III.B.2.N.a.
III.B.2.N.d.
V.A.5.N.c
V.B.2.N.d.
V.B.2.N.e.
0 0.05 0.1 0.2 0.3 0.4
Miles
N
Justin M. Shedd November 30, 2005, NCSU-CEO

Appendix F. NDVI Classification of the Rocky Top Fire

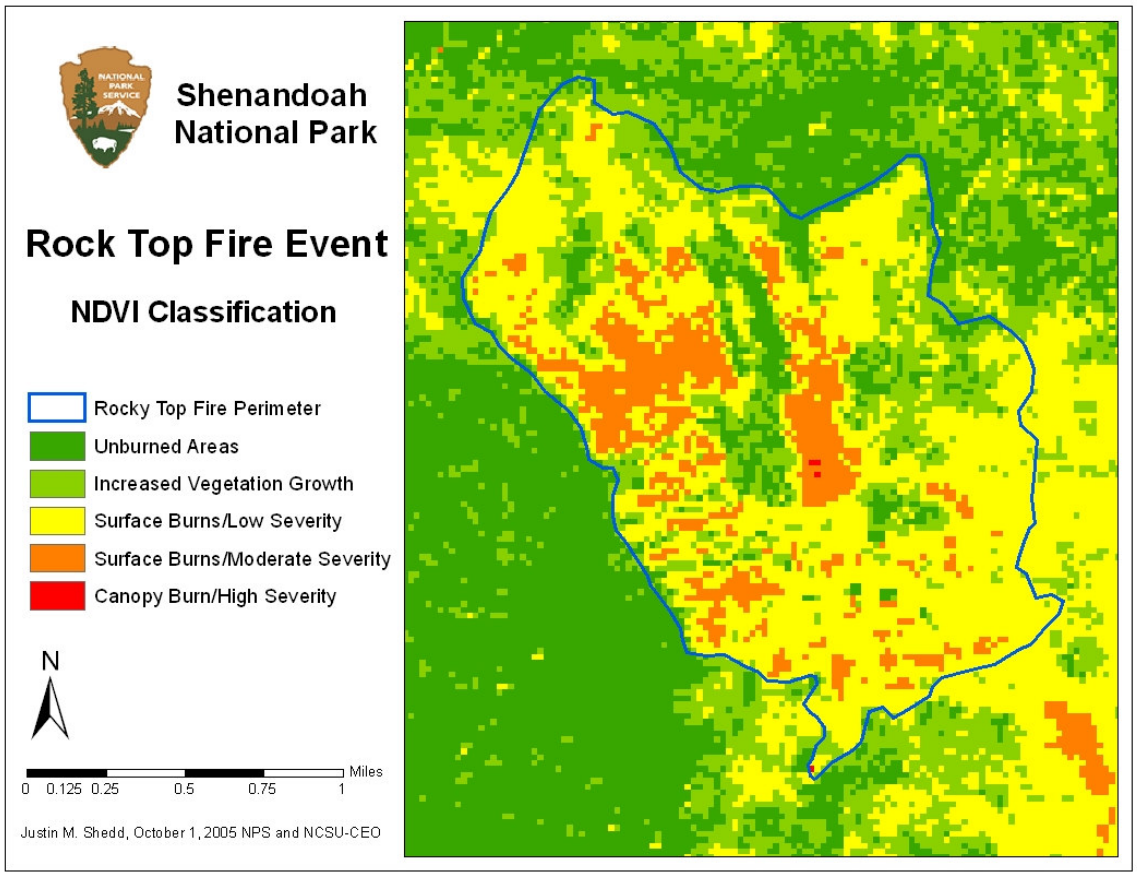

Appendix G. Tasseled Cap Classification of Rocky Top Fire

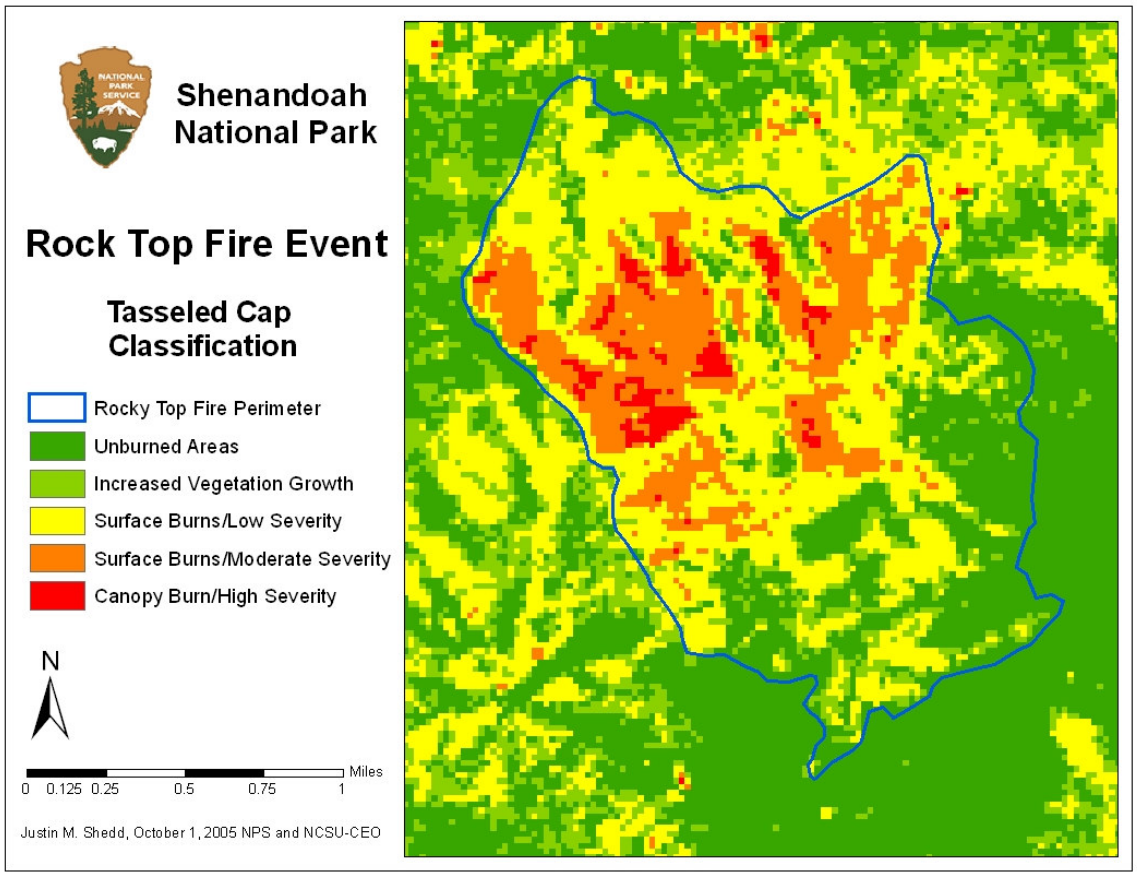

Appendix H. dNBR classification of the Rocky Top Fire

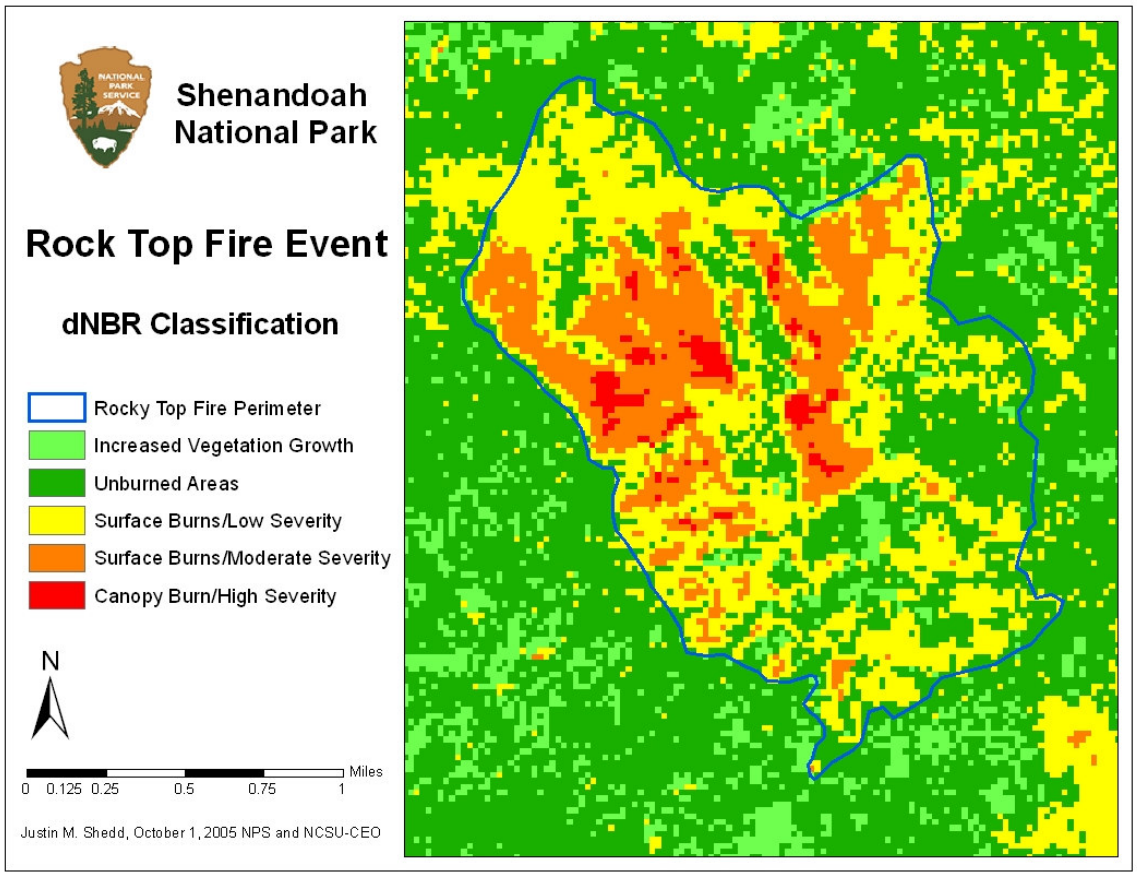

Appendix I. SHEN fuel calculations used to determine fuel loading

Formation Type:	III.A.2.N.a								
Plot Number	45								
Transect	Size Class	Constant	N	D^2	S	A	C	NL	Tons/Acre
East	0 - .25	11.64	4	0.0151	0.48	1.13	1	6	0.06356
	.25 - 1.00	11.64	1	0.289	0.48	1.13	1	6	0.3041
	1.00 - 3.00	11.64	2	2.76	0.40	1.13	1	12	2.42019
	3.00 + S	11.64		0	0.40	1.00	1	50	0
	3.00 + R	11.64		0	0.30	1.00	1	50	0
								Total	2.78785
	Size Class	Constant	N	D^2	S	A	C	NL	Tons/Acre
North	0 - .25	11.64	1	0.0151	0.48	1.13	1	6	0.01589
	.25 - 1.00	11.64	1	0.289	0.48	1.13	1	6	0.3041
	1.00 - 3.00	11.64	0	2.76	0.40	1.13	1	12	0
	3.00 + S	11.64		0	0.40	1.00	1	50	0
	3.00 + R	11.64		1	0.30	1.00	1	50	0.06984
								Total	0.38983

Formation Type:	I.B.2.N.a								
Plot Number	13								
Transect	Size Class	Constant	N	D^3	S	A	C	NL	Tons/Acre
East	1 - .25	11.64	1	0.0151	0.48	1.13	1	6	0.01589
	.25 - 1.00	11.64	3	0.289	0.48	1.13	1	6	0.91231
	1.00 - 3.00	11.64	0	2.76	0.40	1.13	1	12	0
	3.00 + S	11.64		0	0.40	1.00	1	50	0
	3.00 + R	11.64		4	0.30	1.00	1	50	0.27936
								Total	1.20756
	Size Class	Constant	N	D^3	S	A	C	NL	Tons/Acre
North	0 - .25	11.64	3	0.0151	0.48	1.13	1	6	0.04767
	.25 - 1.00	11.64	2	0.289	0.48	1.13	1	6	0.6082
	1.00 - 3.00	11.64	1	2.76	0.40	1.13	1	12	1.21009
	3.00 + S	11.64		0	0.40	1.00	1	50	0
	3.00 + R	11.64		25	0.30	1.00	1	50	1.746
								Total	3.61197

Formation Type:	III.B.2.N.a								
Plot Number	1								
Transect	Size Class	Constant	N	D^3	S	A	C	NL	Tons/Acre
East	1 - .25	11.64	4	0.0151	0.48	1.13	1	6	0.06356
	.25 - 1.00	11.64	0	0.289	0.48	1.13	1	6	0
	1.00 - 3.00	11.64	1	2.76	0.4	1.13	1	12	1.21009
	3.00 + S	11.64		0	0.4	1.00	1	50	0
	3.00 + R	11.64		4	0.3	1.00	1	50	0.27936
								Total	1.55301
	Size Class	Constant	N	D^3	S	A	C	NL	Tons/Acre
North	1 - .25	11.64	4	0.0151	0.48	1.13	1	6	0.06356
	.25 - 1.00	11.64	0	0.289	0.48	1.13	1	6	0
	1.00 - 3.00	11.64	2	2.76	0.4	1.13	1	12	2.42019
	3.00 + S	11.64		0	0.4	1.00	1	50	0
	3.00 + R	11.64		0	0.3	1.00	1	50	0
								Total	2.48375

Formation Type:	I.B.2.N.a								
Plot Number	26								
Transect	Size Class	Constant	N	D^4	S	A	C	NL	Tons/Acre
East	2 - .25	11.64	5	0.0151	0.48	1.13	1	6	0.07945
	.25 - 1.00	11.64	0	0.289	0.48	1.13	1	6	0
	1.00 - 3.00	11.64	1	2.76	0.4	1.13	1	12	1.21009
	3.00 + S	11.64		0	0.4	1.00	1	50	0
	3.00 + R	11.64		16	0.3	1.00	1	50	1.11744
								Total	2.40698
	Size Class	Constant	N	D^4	S	A	C	NL	Tons/Acre
North	2 - .25	11.64	1	0.0151	0.48	1.13	1	6	0.01589
	.25 - 1.00	11.64	3	0.289	0.48	1.13	1	6	0.91231
	1.00 - 3.00	11.64	1	2.76	0.4	1.13	1	12	1.21009
	3.00 + S	11.64		0	0.4	1.00	1	50	0
	3.00 + R	11.64		36	0.3	1.00	1	50	2.51424
								Total	4.65253

Formation Type:	I.B.2.N.a								
Plot Number	25								
Transect	Size Class	Constant	N	D^4	S	A	C	NL	Tons/Acre
East	2 - .25	11.64	4	0.0151	0.48	1.13	1	6	0.06356
	.25 - 1.00	11.64	5	0.289	0.48	1.13	1	6	1.52051
	1.00 - 3.00	11.64	2	2.76	0.4	1.13	1	12	2.42019
	3.00 + S	11.64		1	0.4	1.00	1	50	0.09312
	3.00 + R	11.64		0	0.3	1.00	1	50	0
								Total	4.09737
	Size Class	Constant	N	D^4	S	A	C	NL	Tons/Acre
North	2 - .25	11.64	5	0.0151	0.48	1.13	1	6	0.07945
	.25 - 1.00	11.64	8	0.289	0.48	1.13	1	6	2.43282
	1.00 - 3.00	11.64	2	2.76	0.4	1.13	1	12	2.42019
	3.00 + S	11.64		1	0.4	1.00	1	50	0.09312
	3.00 + R	11.64		1	0.3	1.00	1	50	0.06984
								Total	5.09541

Formation Type:	I.B.2.N.a								
Plot Number	21								
Transect	Size Class	Constant	N	D^5	S	A	C	NL	Tons/Acre
East	3 - .25	11.64	5	0.0151	0.48	1.13	1	6	0.07945
	.25 - 1.00	11.64	5	0.289	0.48	1.13	1	6	1.52051
	1.00 - 3.00	11.64	0	2.76	0.4	1.13	1	12	0
	3.00 + S	11.64		0	0.4	1.00	1	50	0
	3.00 + R	11.64		0	0.3	1.00	1	50	0
								Total	1.59996
	Size Class	Constant	N	D^5	S	A	C	NL	Tons/Acre
North	3 - .25	11.64	12	0.0151	0.48	1.13	1	6	0.19067
	.25 - 1.00	11.64	5	0.289	0.48	1.13	1	6	1.52051
	1.00 - 3.00	11.64	1	2.76	0.4	1.13	1	12	1.21009
	3.00 + S	11.64		9	0.4	1.00	1	50	0.83808
	3.00 + R	11.64		1	0.3	1.00	1	50	0.06984
								Total	3.82919

Formation Type: I.B.2.N.a

Plot Number 35

Transect	Size Class	Constant	N	D^5	S	A	C	NL	Tons/Acre
East	3 - .25	11.64	2	0.0151	0.48	1.13	1	6	0.03178
	.25 - 1.00	11.64	3	0.289	0.48	1.13	1	6	0.91231
	1.00 - 3.00	11.64	2	2.76	0.4	1.13	1	12	2.42019
	3.00 + S	11.64		4	0.4	1.00	1	50	0.37248
	3.00 + R	11.64		0	0.3	1.00	1	50	0
								Total	3.73675

	Size Class	Constant	N	D^5	S	A	C	NL	Tons/Acre
North	3 - .25	11.64	9	0.0151	0.48	1.13	1	6	0.143
	.25 - 1.00	11.64	7	0.289	0.48	1.13	1	6	2.12871
	1.00 - 3.00	11.64	2	2.76	0.4	1.13	1	12	2.42019
	3.00 + S	11.64		1	0.4	1.00	1	50	0.09312
	3.00 + R	11.64		0	0.3	1.00	1	50	0
								Total	4.78502

Formation Type: III.A.2.N.f

Plot Number 11

Transect	Size Class	Constant	N	D^6	S	A	C	NL	Tons/Acre
East	4 - .25	11.64	7	0.0151	0.48	1.13	1	6	0.11122
	.25 - 1.00	11.64	6	0.289	0.48	1.13	1	6	1.82461
	1.00 - 3.00	11.64	0	2.76	0.4	1.13	1	12	0
	3.00 + S	11.64		1	0.4	1.00	1	50	0.09312
	3.00 + R	11.64		1	0.3	1.00	1	50	0.06984
								Total	2.0988

	Size Class	Constant	N	D^6	S	A	C	NL	Tons/Acre
North	4 - .25	11.64	12	0.0151	0.48	1.13	1	6	0.19067
	.25 - 1.00	11.64	8	0.289	0.48	1.13	1	6	2.43282
	1.00 - 3.00	11.64	1	2.76	0.4	1.13	1	12	1.21009
	3.00 + S	11.64		1	0.4	1.00	1	50	0.09312
	3.00 + R	11.64		4	0.3	1.00	1	50	0.27936
								Total	4.20606

Formation Type:	I.B.2.N.a								
Plot Number	33								
Transect	Size Class	Constant	N	D^7	S	A	C	NL	Tons/Acre
East	5 - .25	11.64	15	0.0151	0.48	1.13	1	6	0.23834
	.25 - 1.00	11.64	14	0.289	0.48	1.13	1	6	4.25743
	1.00 - 3.00	11.64	3	2.76	0.4	1.13	1	12	3.63028
	3.00 + S	11.64		9	0.4	1.00	1	50	0.83808
	3.00 + R	11.64		1	0.3	1.00	1	50	0.06984
								Total	9.03397
	Size Class	Constant	N	D^7	S	A	C	NL	Tons/Acre
North	5 - .25	11.64	9	0.0151	0.48	1.13	1	6	0.143
	.25 - 1.00	11.64	16	0.289	0.48	1.13	1	6	4.86563
	1.00 - 3.00	11.64	0	2.76	0.4	1.13	1	12	0
	3.00 + S	11.64		4	0.4	1.00	1	50	0.37248
	3.00 + R	11.64		0	0.3	1.00	1	50	0
								Total	5.38111

Formation Type:	III.B.2.N.a								
Plot Number	42								
Transect	Size Class	Constant	N	D^7	S	A	C	NL	Tons/Acre
East	5 - .25	11.64	8	0.0151	0.48	1.13	1	6	0.12711
	.25 - 1.00	11.64	8	0.289	0.48	1.13	1	6	2.43282
	1.00 - 3.00	11.64	1	2.76	0.40	1.13	1	12	1.21009
	3.00 + S	11.64		4	0.40	1.00	1	50	0.37248
	3.00 + R	11.64		0	0.30	1.00	1	50	0
								Total	4.1425
	Size Class	Constant	N	D^7	S	A	C	NL	Tons/Acre
North	5 - .25	11.64	7	0.0151	0.48	1.13	1	6	0.11122
	.25 - 1.00	11.64	3	0.289	0.48	1.13	1	6	0.91231
	1.00 - 3.00	11.64	2	2.76	0.4	1.13	1	12	2.42019
	3.00 + S	11.64		1	0.4	1.00	1	50	0.09312
	3.00 + R	11.64		0	0.3	1.00	1	50	0
								Total	3.53684

Formation Type:	I.B.2.N.a								
Plot Number	17								
Transect	Size Class	Constant	N	D^8	S	A	C	NL	Tons/Acre
East	6 - .25	11.64	9	0.0151	0.48	1.13	1	6	0.143
	.25 - 1.00	11.64	6	0.289	0.48	1.13	1	6	1.82461
	1.00 - 3.00	11.64	3	2.76	0.4	1.13	1	12	3.63028
	3.00 + S	11.64		4	0.4	1.00	1	50	0.37248
	3.00 + R	11.64		0	0.3	1.00	1	50	0
								Total	5.97038
	Size Class	Constant	N	D^8	S	A	C	NL	Tons/Acre
North	6 - .25	11.64	12	0.0151	0.48	1.13	1	6	0.19067
	.25 - 1.00	11.64	5	0.289	0.48	1.13	1	6	1.52051
	1.00 - 3.00	11.64	3	2.76	0.4	1.13	1	12	3.63028
	3.00 + S	11.64		1	0.4	1.00	1	50	0.09312
	3.00 + R	11.64		0	0.3	1.00	1	50	0
								Total	5.43458

Formation Type:	I.B.2.N.a								
Plot Number	19								
Transect	Size Class	Constant	N	D^8	S	A	C	NL	Tons/Acre
East	6 - .25	11.64	14	0.0151	0.48	1.13	1	6	0.22245
	.25 - 1.00	11.64	5	0.289	0.48	1.13	1	6	1.52051
	1.00 - 3.00	11.64	0	2.76	0.4	1.13	1	12	0
	3.00 + S	11.64		4	0.4	1.00	1	50	0.37248
	3.00 + R	11.64		0	0.3	1.00	1	50	0
								Total	2.11544
	Size Class	Constant	N	D^8	S	A	C	NL	Tons/Acre
North	6 - .25	11.64	10	0.0151	0.48	1.13	1	6	0.15889
	.25 - 1.00	11.64	5	0.289	0.48	1.13	1	6	1.52051
	1.00 - 3.00	11.64	1	2.76	0.4	1.13	1	12	1.21009
	3.00 + S	11.64		1	0.4	1.00	1	50	0.09312
	3.00 + R	11.64		1	0.3	1.00	1	50	0.06984
								Total	3.05245

Formation Type:	I.B.2.N.a								
Plot Number	4								
Transect	Size Class	Constant	N	D^9	S	A	C	NL	Tons/Acre
East	7 - .25	11.64	10	0.0151	0.48	1.13	1	6	0.15889
	.25 - 1.00	11.64	2	0.289	0.48	1.13	1	6	0.6082
	1.00 - 3.00	11.64	0	2.76	0.4	1.13	1	12	0
	3.00 + S	11.64		0	0.4	1.00	1	50	0
	3.00 + R	11.64		0	0.3	1.00	1	50	0
								Total	0.76709
	Size Class	Constant	N	D^9	S	A	C	NL	Tons/Acre
North	7 - .25	11.64	9	0.0151	0.48	1.13	1	6	0.143
	.25 - 1.00	11.64	7	0.289	0.48	1.13	1	6	2.12871
	1.00 - 3.00	11.64	3	2.76	0.4	1.13	1	12	3.63028
	3.00 + S	11.64		0	0.4	1.00	1	50	0
	3.00 + R	11.64		0	0.3	1.00	1	50	0
								Total	5.902

Formation Type:	I.B.2.N.a								
Plot Number	7								
Transect	Size Class	Constant	N	D^9	S	A	C	NL	Tons/Acre
East	7 - .25	11.64	5	0.0151	0.48	1.13	1	6	0.07945
	.25 - 1.00	11.64	4	0.289	0.48	1.13	1	6	1.21641
	1.00 - 3.00	11.64	0	2.76	0.4	1.13	1	12	0
	3.00 + S	11.64		0	0.4	1.00	1	50	0
	3.00 + R	11.64		0	0.3	1.00	1	50	0
								Total	1.29585
	Size Class	Constant	N	D^9	S	A	C	NL	Tons/Acre
North	7 - .25	11.64	6	0.0151	0.48	1.13	1	6	0.09533
	.25 - 1.00	11.64	4	0.289	0.48	1.13	1	6	1.21641
	1.00 - 3.00	11.64	0	2.76	0.4	1.13	1	12	0
	3.00 + S	11.64		0	0.4	1.00	1	50	0
	3.00 + R	11.64		0	0.3	1.00	1	50	0
								Total	1.31174

Formation Type:	III.B.2.N.a								
Plot Number	2								
Transect	Size Class	Constant	N	D^9	S	A	C	NL	Tons/Acre
East	7 - .25	11.64	3	0.0151	0.48	1.13	1	6	0.04767
	.25 - 1.00	11.64	7	0.289	0.48	1.13	1	6	2.12871
	1.00 - 3.00	11.64	1	2.76	0.4	1.13	1	12	1.21009
	3.00 + S	11.64		0	0.4	1.00	1	50	0
	3.00 + R	11.64		1	0.3	1.00	1	50	0.06984
								Total	3.45632
	Size Class	Constant	N	D^9	S	A	C	NL	Tons/Acre
North	7 - .25	11.64	5	0.0151	0.48	1.13	1	6	0.07945
	.25 - 1.00	11.64	3	0.289	0.48	1.13	1	6	0.91231
	1.00 - 3.00	11.64	1	2.76	0.4	1.13	1	12	1.21009
	3.00 + S	11.64		0	0.4	1.00	1	50	0
	3.00 + R	11.64		1	0.3	1.00	1	50	0.06984
								Total	2.27169

Formation Type:	I.B.2.N.a								
Plot Number	44								
Transect	Size Class	Constant	N	D^10	S	A	C	NL	Tons/Acre
East	8 - .25	11.64	11	0.0151	0.48	1.13	1	6	0.17478
	.25 - 1.00	11.64	8	0.289	0.48	1.13	1	6	2.43282
	1.00 - 3.00	11.64	0	2.76	0.4	1.13	1	12	0
	3.00 + S	11.64		1	0.4	1.00	1	50	0.09312
	3.00 + R	11.64		1	0.3	1.00	1	50	0.06984
								Total	2.77056
	Size Class	Constant	N	D^10	S	A	C	NL	Tons/Acre
North	8 - .25	11.64	12	0.0151	0.48	1.13	1	6	0.19067
	.25 - 1.00	11.64	5	0.289	0.48	1.13	1	6	1.52051
	1.00 - 3.00	11.64	3	2.76	0.4	1.13	1	12	3.63028
	3.00 + S	11.64		0	0.4	1.00	1	50	0
	3.00 + R	11.64		1	0.3	1.00	1	50	0.06984
								Total	5.4113

Formation Type:	I.B.2.N.a								
Plot Number	8								
Transect	Size Class	Constant	N	D^10	S	A	C	NL	Tons/Acre
East	8 - .25	11.64	5	0.0151	0.48	1.13	1	6	0.07945
	.25 - 1.00	11.64	5	0.289	0.48	1.13	1	6	1.52051
	1.00 - 3.00	11.64	2	2.76	0.4	1.13	1	12	2.42019
	3.00 + S	11.64		1	0.4	1.00	1	50	0.09312
	3.00 + R	11.64		1	0.3	1.00	1	50	0.06984
								Total	4.1831
	Size Class	Constant	N	D^10	S	A	C	NL	Tons/Acre
North	8 - .25	11.64	8	0.0151	0.48	1.13	1	6	0.12711
	.25 - 1.00	11.64	4	0.289	0.48	1.13	1	6	1.21641
	1.00 - 3.00	11.64	4	2.76	0.4	1.13	1	12	4.84038
	3.00 + S	11.64		0	0.4	1.00	1	50	0
	3.00 + R	11.64		1	0.3	1.00	1	50	0.06984
								Total	6.25374

Appendix J. 1-, 10-, 100-Hour Fuel Loading and Fuel Bed Depth of SHEN plots

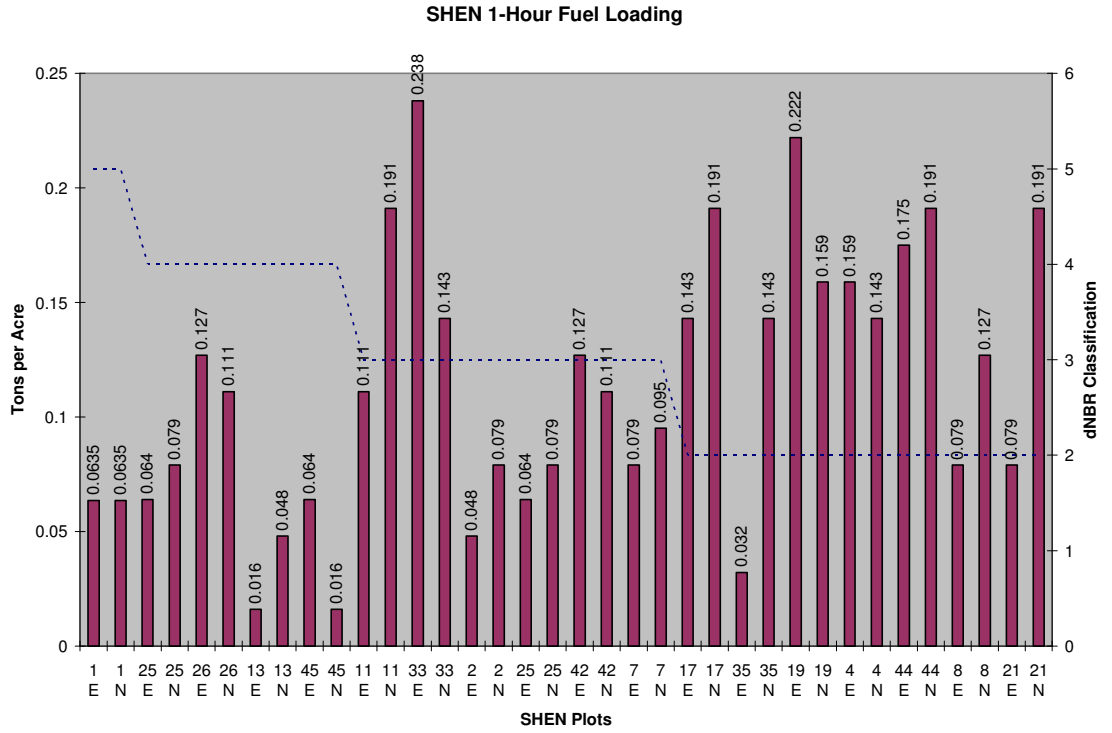

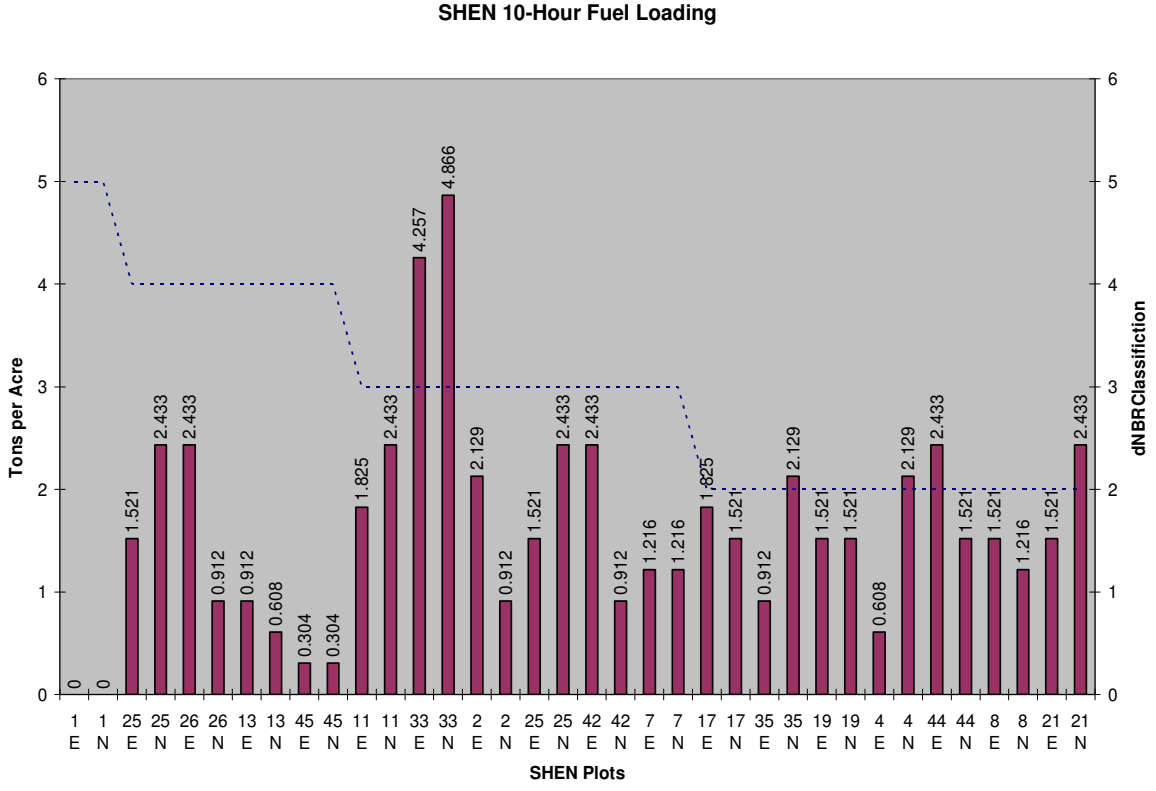

SHEN 100-Hour Fuel Loading

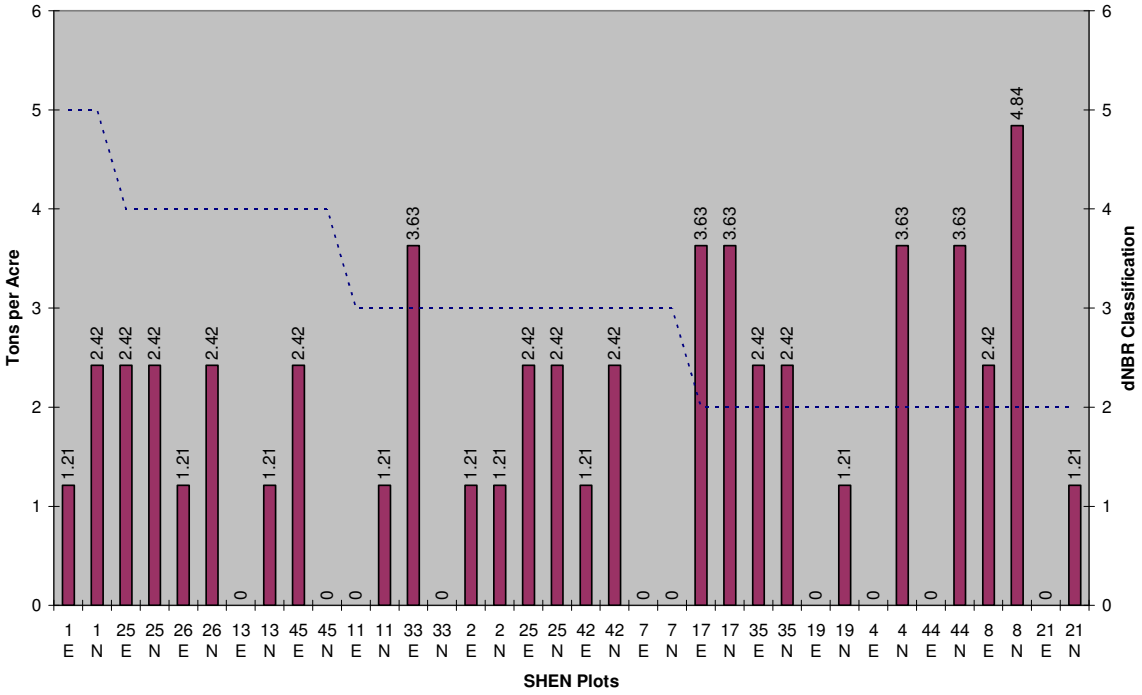

SHEN Fuel Bed Depth

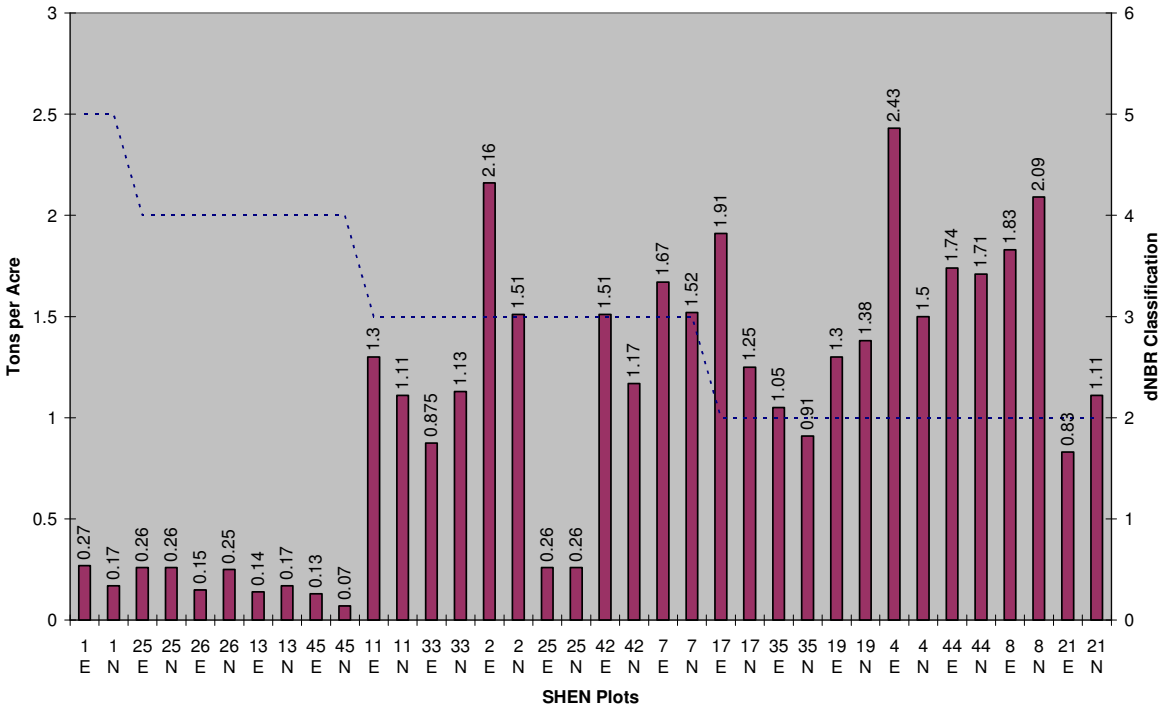

Appendix K. Updated Fuel Model Spatial Dataset of Shenandoah National Park.

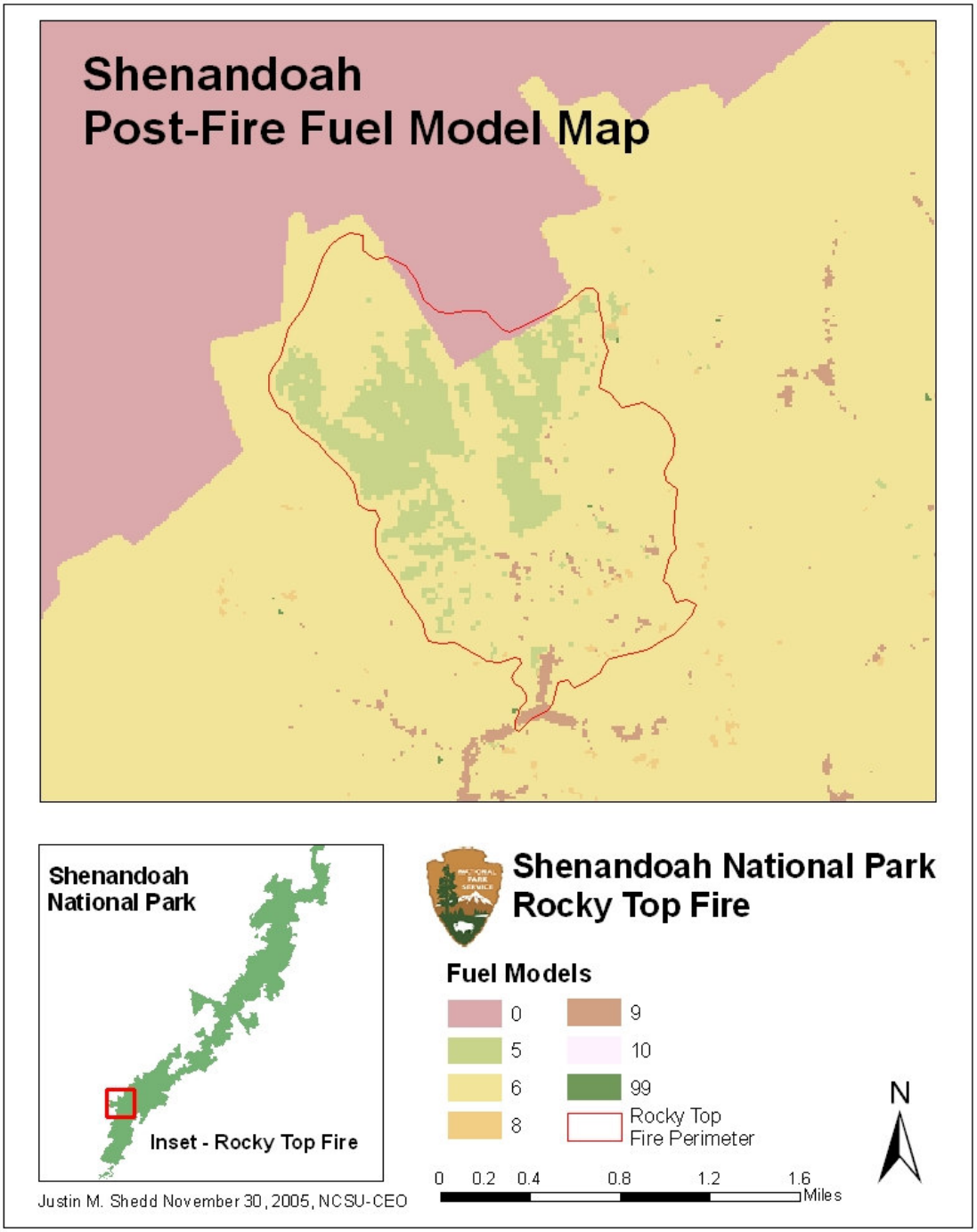

Appendix L. Updated Vegetation Spatial Dataset of Shenandoah National Park.